

,

# Large-angle production of charged pions with 3-12.9 GeV/ $c$ incident protons on nuclear targets

M.G. Catanesi,<sup>1</sup> E. Radicioni,<sup>1</sup> R. Edgecock,<sup>2</sup> M. Ellis,<sup>2,\*</sup> F.J.P. Soler,<sup>2</sup> C. Gößling,<sup>3</sup> S. Bunyatov,<sup>4</sup> A. Krasnoperov,<sup>4</sup> B. Popov,<sup>4,†</sup> V. Serdiouk,<sup>4</sup> V. Tereschenko,<sup>4</sup> E. Di Capua,<sup>5</sup> G. Vidal-Sitjes,<sup>5,‡</sup> A. Artamonov,<sup>6,§</sup> S. Giani,<sup>6</sup> S. Gilardoni,<sup>6</sup> P. Gorbunov,<sup>6,§</sup> A. Grant,<sup>6</sup> A. Grossheim,<sup>6,¶</sup> A. Ivanchenko,<sup>6,\*\*</sup> V. Ivanchenko,<sup>6,††</sup> A. Kayis-Topaksu,<sup>6,††</sup> J. Panman,<sup>6</sup> I. Papadopoulos,<sup>6</sup> E. Tcherniaev,<sup>6</sup> I. Tsukerman,<sup>6,§</sup> R. Veenhof,<sup>6</sup> C. Wiebusch,<sup>6,§§</sup> P. Zucchelli,<sup>6,¶¶</sup> A. Blondel,<sup>7</sup> S. Borghi,<sup>7</sup> M.C. Morone,<sup>7,\*\*\*</sup> G. Prior,<sup>7,†††</sup> R. Schroeter,<sup>7</sup> C. Meurer,<sup>8</sup> U. Gastaldi,<sup>9</sup> G. B. Mills,<sup>10,†††</sup> J.S. Graulich,<sup>11,§§§</sup> G. Grégoire,<sup>11</sup> M. Bonesini,<sup>12,¶¶¶</sup> F. Ferri,<sup>12</sup> M. Kirsanov,<sup>13</sup> A. Bagulya,<sup>14</sup> V. Grichine,<sup>14</sup> N. Polukhina,<sup>14</sup> V. Palladino,<sup>15</sup> L. Coney,<sup>16,†††</sup> D. Schmitz,<sup>16,†††</sup> G. Barr,<sup>17</sup> A. De Santo,<sup>17</sup> F. Bobisut<sup>a,b,18</sup> D. Gibin<sup>a,b,18</sup> A. Guglielmi<sup>b,18</sup> M. Mezzetto<sup>b,18</sup> J. Dumarchez,<sup>19</sup> U. Dore,<sup>20</sup> D. Orestano<sup>c,d,21</sup> F. Pastore<sup>c,d,21</sup> A. Tonazzo<sup>c,d,21</sup> L. Tortora<sup>d,21</sup> C. Booth,<sup>22</sup> L. Howlett,<sup>22</sup> G. Skoro,<sup>22</sup> M. Bogomilov,<sup>23</sup> M. Chizhov,<sup>23</sup> D. Kolev,<sup>23</sup> R. Tsenov,<sup>23</sup> S. Piperov,<sup>24</sup> P. Temnikov,<sup>24</sup> M. Apollonio,<sup>25</sup> P. Chimenti,<sup>25</sup> G. Giannini,<sup>25</sup> J. Burguet-Castell,<sup>26</sup> A. Cervera-Villanueva,<sup>26</sup> J.J. Gómez-Cadenas,<sup>26</sup> J. Martín-Albo,<sup>26</sup> P. Novella,<sup>26</sup> M. Sorel,<sup>26</sup> and A. Tornero<sup>26</sup>

(HARP Collaboration)

<sup>1</sup>Sezione INFN, Bari, Italy

<sup>2</sup>Rutherford Appleton Laboratory, Chilton, Didcot, UK

<sup>3</sup>Institut für Physik, Universität Dortmund, Germany

<sup>4</sup>Joint Institute for Nuclear Research, JINR Dubna, Russia

<sup>5</sup>Università degli Studi e Sezione INFN, Ferrara, Italy

<sup>6</sup>CERN, Geneva, Switzerland

<sup>7</sup>Section de Physique, Université de Genève, Switzerland

<sup>8</sup>Institut für Physik, Forschungszentrum Karlsruhe, Germany

<sup>9</sup>Laboratori Nazionali di Legnaro dell' INFN, Legnaro, Italy

<sup>10</sup>Los Alamos National Laboratory, Los Alamos, USA

<sup>11</sup>Institut de Physique Nucléaire, UCL, Louvain-la-Neuve, Belgium

<sup>12</sup>Sezione INFN Milano Bicocca, Milano, Italy

<sup>13</sup>Institute for Nuclear Research, Moscow, Russia

<sup>14</sup>P. N. Lebedev Institute of Physics (FIAN), Russian Academy of Sciences, Moscow, Russia

<sup>15</sup>Università "Federico II" e Sezione INFN, Napoli, Italy

<sup>16</sup>Columbia University, New York, USA

<sup>17</sup>Nuclear and Astrophysics Laboratory, University of Oxford, UK

<sup>18</sup>Università degli Studi<sup>a</sup> e Sezione INFN<sup>b</sup>, Padova, Italy

<sup>19</sup>LPNHE, Universités de Paris VI et VII, Paris, France

<sup>20</sup>Università "La Sapienza" e Sezione INFN Roma I, Roma, Italy

<sup>21</sup>Università degli Studi<sup>c</sup> e Sezione INFN Roma Tre<sup>d</sup>, Roma, Italy

<sup>22</sup>Dept. of Physics, University of Sheffield, UK

<sup>23</sup> Faculty of Physics, St. Kliment Ohridski University, Sofia, Bulgaria

<sup>24</sup> Institute for Nuclear Research and Nuclear Energy, Academy of Sciences, Sofia, Bulgaria

<sup>25</sup> Università degli Studi e Sezione INFN, Trieste, Italy

<sup>26</sup> Instituto de Física Corpuscular, IFIC, CSIC and Universidad de Valencia, Spain

(Dated: October 24, 2018)

Measurements of the double-differential  $\pi^\pm$  production cross-section in the range of momentum  $100 \text{ MeV}/c \leq p \leq 800 \text{ MeV}/c$  and angle  $0.35 \text{ rad} \leq \theta \leq 2.15 \text{ rad}$  in proton–beryllium, proton–carbon, proton–aluminium, proton–copper, proton–tin, proton–tantalum and proton–lead collisions are presented. The data were taken with the large acceptance HARP detector in the T9 beam line of the CERN PS. The pions were produced by proton beams in a momentum range from  $3 \text{ GeV}/c$  to  $12.9 \text{ GeV}/c$  hitting a target with a thickness of 5% of a nuclear interaction length. The tracking and identification of the produced particles was performed using a small-radius cylindrical time projection chamber (TPC) placed inside a solenoidal magnet. Incident particles were identified by an elaborate system of beam detectors. Results are obtained for the double-differential cross-sections  $d^2\sigma/dpd\theta$  at six incident proton beam momenta ( $3 \text{ GeV}/c$ ,  $5 \text{ GeV}/c$ ,  $8 \text{ GeV}/c$ ,  $8.9 \text{ GeV}/c$  (Be only),  $12 \text{ GeV}/c$  and  $12.9 \text{ GeV}/c$  (Al only)). They are based on a complete correction of static and dynamic distortions of tracks in the HARP TPC which allows the complete statistics of collected data set to be used. The results include and supersede our previously published results and are compatible with these. Results are compared with the GEANT4 and MARS MonteCarlo simulation.

PACS numbers: 13.75Cs, 13.85Ni

## I. INTRODUCTION

The HARP experiment [1] makes use of a large-acceptance spectrometer for a systematic study of hadron production on a large range of target nuclei for beam momenta from  $1.5 \text{ GeV}/c$  to  $15 \text{ GeV}/c$ . This corresponds to a proton momentum region of great interest for neutrino beams and far from coverage by earlier dedicated hadroproduction experiments [2], [3].

The main motivations are to measure pion yields for a quantitative design of the proton driver of a future neutrino factory [4], to provide measurements to allow substantially improved calculations of the atmospheric neutrino flux [5, 6, 7, 8, 9] to be made and to measure particle yields as input for the flux calculation of accelerator neutrino experiments [10], such as K2K [11, 12], MiniBooNE [13] and SciBooNE [14].

This paper presents our final measurements of the double-differential cross-section,  $d^2\sigma^\pi/dpd\theta$  for  $\pi^\pm$  production at large angles by protons of  $3 \text{ GeV}/c$ ,  $5 \text{ GeV}/c$ ,  $8 \text{ GeV}/c$ ,  $8.9 \text{ GeV}/c$  (Be only),  $12 \text{ GeV}/c$

\*Now at FNAL, Batavia, Illinois, USA.

†Also supported by LPNHE, Paris, France.

‡Now at Imperial College, University of London, UK.

§ITEP, Moscow, Russian Federation.

¶Now at TRIUMF, Vancouver, Canada.

\*\*On leave from Novosibirsk University, Russia.

††On leave from Ecoanalitica, Moscow State University, Moscow, Russia.

‡‡Now at Çukurova University, Adana, Turkey.

§§Now at III Phys. Inst. B, RWTH Aachen, Germany.

¶¶Now at SpinX Technologies, Geneva, Switzerland;

on leave from INFN, Sezione di Ferrara, Italy.

\*\*\*Now at University of Rome Tor Vergata, Italy.

†††Now at LBL, Berkeley, California, USA.

‡‡‡MiniBooNE Collaboration.

§§§Now at Section de Physique, Université de Genève, Switzerland.

¶¶¶Electronic address: maurizio.bonesini@mib.infn.it

and  $12.9 \text{ GeV}/c$  (Al only) momentum impinging on a thin beryllium, carbon, aluminium, copper, tin, tantalum or lead target of 5% nuclear interaction length. A first set of results on the production of pions at large angles have been published by the HARP Collaboration in references [15, 16, 17], based on the analysis of the data in the beginning of each accelerator spill. The reduction of the data set was necessary to avoid problems in the TPC detector responsible for dynamic distortions to the image of the particle trajectories as the ion charge was building up during each spill. Corrections that allow the use of the full statistics to be made, correcting for such distortions, have been developed in [29] and are fully applied in this analysis. The obtained results are fully compatible within the statistical errors and differential systematic uncertainties with those previously published. The increase of statistics is particularly useful in the  $3 \text{ GeV}/c$  data sets. Comparisons with MonteCarlo models are then shown for a light and a heavy target.

This paper, covering an extended range of solid targets in the same experiment, makes it possible to perform systematic comparison of hadron production models with measurements at different incoming beam momenta over a large range of target atomic number  $A$ . Results for pion production in the forward direction are the subject of other HARP publications [18, 19, 20].

Pion production data at low momenta ( $\simeq 200 \text{ MeV}/c$ ) are extremely scarce and HARP is the first experiment to provide a large data set, taken with many different targets, full particle identification and large detector acceptance. In addition, the acceptance of the large-angle detector of the HARP experiment matches well the required phase space region of pions relevant to the production of  $\mu$ 's in a neutrino factory (NF). It covers the large majority of the pions accepted in the focussing system of a typical design. For the optimization of the NF target, data were taken with high- $Z$  nuclear targets such as tantalum and lead.

Data were taken in the T9 beam of the CERN PS. The collected statistics, for the different nuclear targets, are reported in table I.

The analysis proceeds by selecting tracks in the Time Projection Chamber (TPC), after corrections for static and dynamic distortions (see later for details), in events with incident beam of protons. Momentum and polar angle measurements and particle identification are based on the measurements of track position and energy deposition in the TPC. An unfolding method is used to correct for experimental resolution, efficiency and acceptance and to obtain the double-differential pion production cross-sections. The method allows a full error evaluation to be made. A comparison with available data is presented. The analysis follows the same methods as used for the determination of  $\pi^\pm$  production by protons on a tantalum target which are described in Ref. [15] and will be only briefly outlined here.

## II. EXPERIMENTAL APPARATUS AND DATA SELECTION.

The HARP detector is shown in Fig. 1 and is fully described in reference [21]. The forward spectrometer, mainly used in the analysis for the conventional neutrino beams and atmospheric neutrino flux, comprises of a dipole magnet, large planar drift chambers (NDC) [22], a time-of-flight wall (TOFW) [23], a threshold Cerenkov counter (CHE) and an electromagnetic calorimeter (ECAL). In the large-angle region a cylindrical TPC with a radius of 408 mm is positioned inside a solenoidal magnet with a field of 0.7 T. The TPC detector was designed to measure and identify tracks in the angular region from 0.25 rad to 2.5 rad with respect to the beam axis. The target is placed inside the inner field cage (IFC) of the TPC such that, in addition to particles produced in the forward direction, backward-going tracks can be measured. The TPC is used for tracking, momentum determination and measurement of the energy deposition  $dE/dx$  for particle identification [24]. A set of resistive plate chambers (RPC) form a barrel inside the solenoid around the TPC to measure the arrival time of the secondary particles [25]. Charged particle identification (PID) can be achieved by measuring the ionization per unit length in the gas ( $dE/dx$ ) as a function of the total momentum of the particle. Additional PID can be performed through a time-of-flight measurement with the RPCs.

The momentum of the T9 beam is known with a precision of the order of 1% [26]. The absolute normalization of the number of incident protons was performed using a total of 1,148,120 incident proton triggers. These are triggers where the same selection on the beam particle was applied but no selection on the interaction was performed. The rate of this trigger was down-scaled by a factor 64. A cross-check

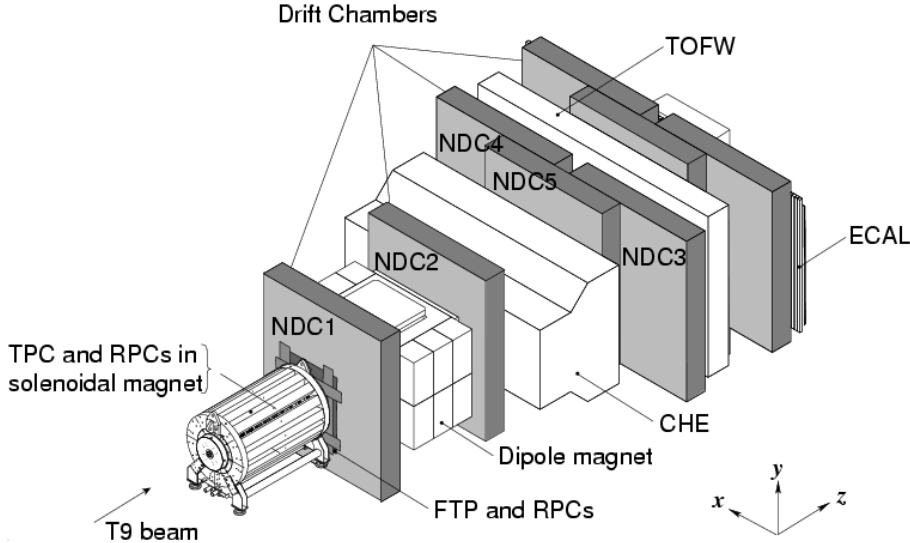


FIG. 1: Schematic layout of the HARP detector. The convention for the coordinate system is shown in the lower-right corner. The three most downstream (unlabelled) drift chamber modules are only partly equipped with electronics and are not used for tracking. The detector covers a total length of 13.5 m along the beam axis and has a maximum width of 6.5 m perpendicular to the beam.

of the absolute normalization was provided by counting tracks in the forward spectrometer.

Beam instrumentation provides identification of the incoming particle, the determination of the time when it hits the target, and the impact point and direction of the beam particle on the target. It is based on a set of four multi-wire proportional chambers (MWPC) to measure position and direction of the incoming beam particles and time-of-flight detectors and  $N_2$ -filled Cherenkov counters to identify incoming particles. Several trigger detectors are installed to select events with an interaction and to define the normalization.

Besides the usual need for calibration of the detector, a number of hardware shortfalls, discovered mainly after the end of data-taking, had to be overcome to use the TPC data reliably in the analysis. The TPC is affected by a relatively large number of dead or noisy pads and static and dynamic distortions of the reconstructed trajectories. The applied corrections are briefly resumed in the next section.

The beam of positive particles used for this measurement contains mainly positrons, pions and protons, with small components of kaons and deuterons and heavier ions. Its composition depends on the selected beam momentum. The proton fraction in the incoming beam varies from 35% at 3 GeV/c to 92% at 12 GeV/c.

At momenta higher than 5 GeV/c protons are selected by rejecting particles with a measured signal in either of the beam Cherenkov detectors. At 3 GeV/c the time-of-flight measurement allows the selection of pions from protons to be made at more than  $5\sigma$ . Deuterons (and heavier ions) are removed by TOF measurements. The selection of protons for the beam momenta with the Cherenkov detectors has been described in detail in Ref [18]. More details on the beam particle selection can be found in Ref. [21]. The purity of the selection of protons is higher than 99% at all momenta. A set of MWPCs is used to select events with only one beam particle for which the trajectory extrapolates to the target. An identical beam particle selection was performed for events triggered with the incident-proton trigger in order to provide an absolute normalization of the incoming protons. This trigger selected every 64<sup>th</sup> beam particle coincidence outside the dead-time of the data acquisition system.

The length of the accelerator spill is 400 ms with a typical intensity of 15 000 beam particles per spill. The average number of events recorded by the data acquisition ranges from 300 to 350 per spill for the different beam momenta. The analysis proceeds by first selecting a beam proton hitting the target, not accompanied by other tracks. Then an event is required to give a large angle interaction (LAI) trigger to be retained. After the event selection the sample of tracks to be used for analysis is defined. Table I

shows the number of events and the number of  $\pi^\pm$  selected in the analysis. The large difference between the first and second set of rows (“total events taken by the DAQ” and “Accepted protons with Large Angle Interaction”) is due to the relatively large fraction of pions in the beam and to the larger number of triggers taken for the measurements with the forward dipole spectrometer.

TABLE I: Total number of events and tracks used in the various nuclear 5%  $\lambda_I$  target data sets and the number of protons on target as calculated from the pre-scaled incident proton triggers.

<b>Data set (GeV/c)</b>	<b>3</b>	<b>5</b>	<b>8</b>	<b>8.9</b>	<b>12</b>	<b>12.9</b>
Total DAQ events	(Be) 1399714	1473815	1102415	7236396	1211220	–
	(C) 1345461	2628362	1878590	–	1855615	–
	(Al) 1586331	1787620	1706919	–	619021	5401701
	(Cu) 623965	2089292	2613229	–	748443	–
	(Sn) 1652751	2827934	2422110	–	1803035	–
	(Ta) 2202760	2094286	2045631	–	886307	–
	(Pb) 1299264	2110904	2314552	–	486875	–
Acc. protons with LAI	(Be) 76694	157625	200352	1267418	282272	–
	(C) 58421	228490	337150	–	504945	–
	(Al) 69794	195912	341687	–	169151	1391159
	(Cu) 38290	229316	544615	–	226245	–
	(Sn) 84330	304949	523432	–	558306	–
	(Ta) 97732	218293	442625	–	269927	–
	(Pb) 79188	194064	491672	–	145843	–
Fraction of triggers used	(Be) 79%	75%	83%	94%	79%	–
	(C) 95%	90%	83%	–	84%	–
	(Al) 78%	80%	63%	–	96%	72%
	(Cu) 91%	76%	66%	–	76%	–
	(Sn) 97%	73%	67%	–	76%	–
	(Ta) 86%	81%	69%	–	76%	–
	(Pb) 74%	56%	69%	–	50%	–
$\pi^-$ selected with PID	(Be) 6553	20020	32078	231278	47608	–
	(C) 4831	33436	52105	–	72307	–
	(Al) 5496	26502	45442	–	37812	250037
	(Cu) 3065	28395	79497	–	46153	–
	(Sn) 7146	38337	89799	–	124925	–
	(Ta) 6758	27767	74977	–	63349	–
	(Pb) 4408	17766	81821	–	25050	–
$\pi^+$ selected with PID	(Be) 11245	27796	41683	294594	58882	–
	(C) 9944	52633	73157	–	95151	–
	(Al) 9519	38657	59345	–	47609	314552
	(Cu) 4976	39823	102797	–	56665	–
	(Sn) 10179	48820	104239	–	145923	–
	(Ta) 9270	33985	87226	–	72275	–
	(Pb) 6160	21074	92913	–	27085	–

### A. Corrections for distortion of tracks in the TPC

The TPC contains a relatively large number of dead or noisy pads. Noisy pads were considered equivalent to dead channels in this analysis. The large number of dead pads ( $\simeq 15\%$ ) in the experimental data taking required a day-by-day determination of the dead channel map. The same map was used in the simulation to provide a description of the TPC performances on a short term scale. A method based on tracks

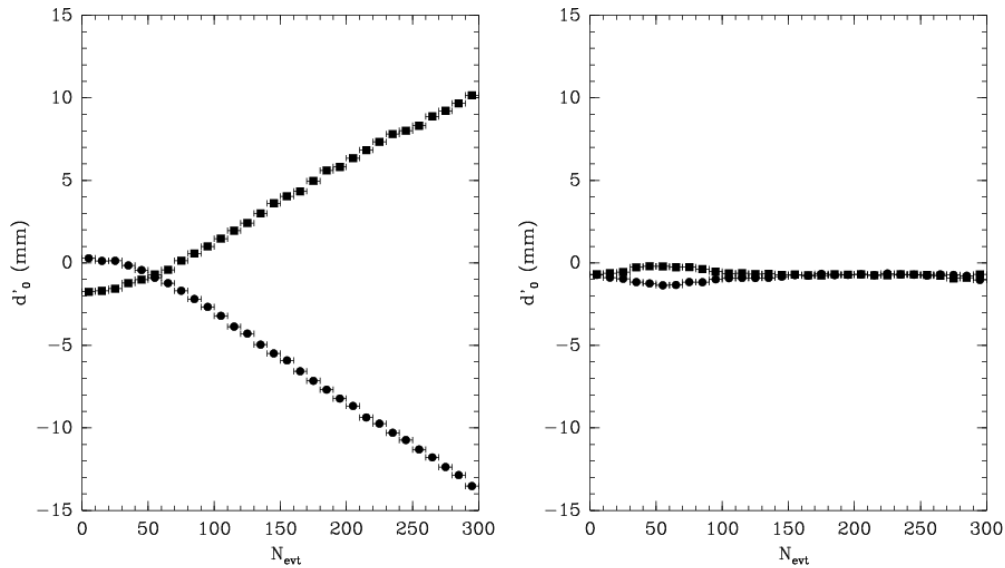


FIG. 2: Effect of dynamic distortions on a track in the HARP TPC for a p–Be interactions sample at 5 GeV/c, as a function of the event number in the spill. Left panel: before corrections, right panel: after dynamic distortion corrections. The symbols show the average extrapolated distance from the incoming beam particle trajectory for  $\pi^-$  (filled squares),  $\pi^+$  (filled circles)

accumulated during the data taking was used to measure the gain variations of each pad, see Ref. [21] for details. It is used to reduce the fluctuations in response between different pads down to a 3% level.

Static distortions on reconstructed tracks are caused by the inhomogeneity of the electric field, due to an accidental mismatch between the inner and outer field cage (powered by two distinct HV supplies). The day–by–day variations of this mismatch are consistent with the specifications of the stability and reproducibility of the power supplies. A specific calibration for each setting has been made.

Dynamic distortions are caused instead by the build-up of ion-charge density in the drift volume during the 400 ms long beam spill. All these effects were fully studied and available corrections are described in detail in Ref. [15, 29]. In our earlier published analyses a practical approach has been followed. Only the events corresponding to the early part of the spill, where the effects of the dynamic distortions are still small, have been used (this translates into a cut on the maximum number of events ( $N_{\text{evt}} \simeq 100$ ) to be retained). The time interval between spills is large enough to drain all charges in the TPC related to the effect of the beam. The combined effect of the distortions on the kinematic quantities used in the analysis has been studied in detail and only that part of the data for which the systematic errors can be assessed with physical benchmarks was used, as fully explained in [15]. More than 30 – 40% of the recorded data were thus used in the published analyses. The influence of distortions was monitored taking the average value of the extrapolated minimum distance of the secondary tracks from the incoming beam particle trajectory  $\langle d'_0 \rangle$ . An example of the result of the corrections for one setting is shown in Fig. 2.

In the presented analysis, instead, the TPC track dynamic distortions are corrected on an event–by–event basis, as outlined in [29]. A direct measurement of the distortions as a function of the radius  $R$  and time–in–spill was performed using the prediction of the trajectory of the recoil proton in elastic scattering events on a liquid hydrogen target. The measurement of the direction of the forward scattered proton determined the kinematics and predicts the trajectory of the recoil proton. The actual measurements in the chamber are then compared with the prediction as a function of time. In addition to this direct measurement also a model of ion charges and their effect was developed.

The strength of the effect depends on many parameters such as the beam intensity, the momentum and the target. An iterative procedure is applied to find the value of the strength parameter until  $\langle d'_0 \rangle$  is flattened down to  $\pm 2$  mm, by using the empirical model described below to shape the corrections. Taking into account the beam intensity, the data acquisition rate and the target thickness, the HARP experiment was operated in conditions of  $\approx 95\%$  deadtime. The electrons are normally multiplied near the TPC plane

with a multiplication factor  $\sim 10^5$ , producing an equivalent number of Ar ions. Any inefficiency of the gating grid at the  $10^{-4} - 10^{-5}$  level would give an overwhelming number of ions drifting in the TPC gas volume. The phenomenological model is based on the fact that the field which is responsible for the force acting on each drift electron is equivalent to:

- a field system where ions, in a given angular section at  $R$  values internal to the drift electron position contribute to attract the drift electrons inwards;
- a field system where ions, in a given angular section at  $R$  values external to the drift electron position, contribute to attract the drift electrons outwards.

This model makes it possible to understand all the peculiar features of the TPC dynamic distortions:

- the dependence of the distortion on the event number in the spill,
- the dependence of the distortion on tracks generated at different longitudinal coordinate  $Z$  in the TPC. In particular tracks produced at increasingly larger  $Z$  exhibit the distortion saturation at increasingly later times and the distortions tend to zero at  $Z$  values already passed by the ion packet;
- the dependence of the distortion of cosmic-ray tracks collected out of the spill as a function of time and  $Z$ , with the non-trivial fact that cosmic-rays just after the spill are more distorted than the cosmic-rays taken later;
- the  $R-\phi$  dependence as measured with elastic scattering. The distortions have a peculiar behaviour as a function of the TPC pad rows: from the  $E \times B$  calculation it follows that the inner rows are distorted by a radial electric field pointing inwards; there exists a pad row around the middle of the chamber where the radial electric field vanishes.

The corrections, provided by the model, calibrated on a run-by-run basis allow a full control of the TPC response along the spill. In figure 3 the  $Q/p_T$  spectrum for p–Be interactions at 8.9 GeV/c is shown separately for the first 50 events in the spill, the next 50 and so on up to the last 50, before and after the dynamic distortion correction. After the correction, the curves are compatible within the statistical errors, indicating that the correction is adequate.

The main point, using beginning of spill data or full spill data, is the presence of possible residual momentum bias in the TPC measurement due to the dynamic distortions. A dedicated paper [29] addresses this point and shows that our estimation of momentum bias is below 3%, although the systematics can in principle be different in the uncorrected begin-of-spill data and the fully corrected data. From the studies made we conclude that the data of the full spill can be used for the analysis once the corrections for dynamic distortions have been applied. In a small number of data sets the distortions in the last part of the spill are too large to be reliably corrected. These are mainly high  $A$ , high beam momentum settings, where sufficient statistics are available even without this part of the spill. The reliability of the correction has been checked by observing the stability as a function of the event number in the spill of the average momentum of protons in a small window of large  $dE/dx$ . An additional benchmark assesses the stability of the momentum measurement inside a spill after the dynamic distortion correction for the TPC tracks. The dependence of the average momentum for four different track samples as a function of  $N_{\text{evt}}$  is shown in Fig. 4. The range of  $p_T$  tested by this benchmark covers nearly the full range used in the analysis.

The stability of the TPC  $dE/dx$  and momentum calibration over the collected data sets is shown in Fig. 5. The  $X$ -axis runs over all settings starting at low  $A$  (Be) up to high  $A$  such (Pb) and all used beam momenta from 3 GeV/c to 12.9 GeV/c.

### III. DATA ANALYSIS

Only a short outline of the data analysis procedure is presented here, for further details see Ref. [15]. The most relevant difference is the use of the full spill statistics by means of a correction of the dynamic

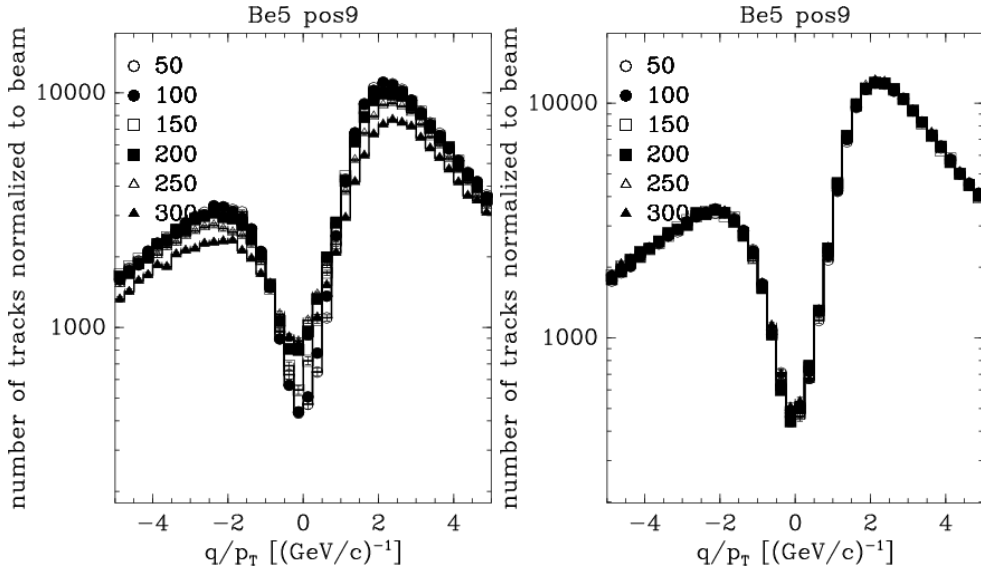


FIG. 3: Full spill analysis of  $Q/p_T$  for the highest statistics data sample: p-Be at 8.9 GeV/c. Left panel: before corrections, right panel: after corrections. Six curves are drawn, each for the next 50 events in the spill. One notices that the distributions in the right panel are not distinguishable.

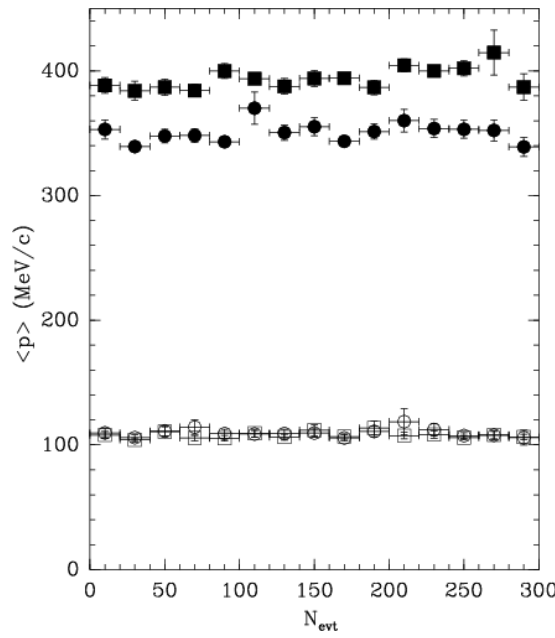


FIG. 4: As a momentum benchmark, after the dynamic distortion correction, the closed box shows the average momentum observed for protons selected using their range (reaching the second RPC) and  $dE/dx$ . Closed circles show protons selected within a high  $dE/dx$  region; open circles:  $\pi^-$  selected with  $dE/dx$ ; open boxes:  $\pi^+$  selected with  $dE/dx$ . The angle of the particles is restricted in a range with  $\sin \theta \approx 0.9$ . The variation in the uncorrected sample was  $\approx 5\%$  for the high  $p_T$  samples. The corrected data stay stable well within 3%. The low  $p_T$  data remain stable with or without correction.

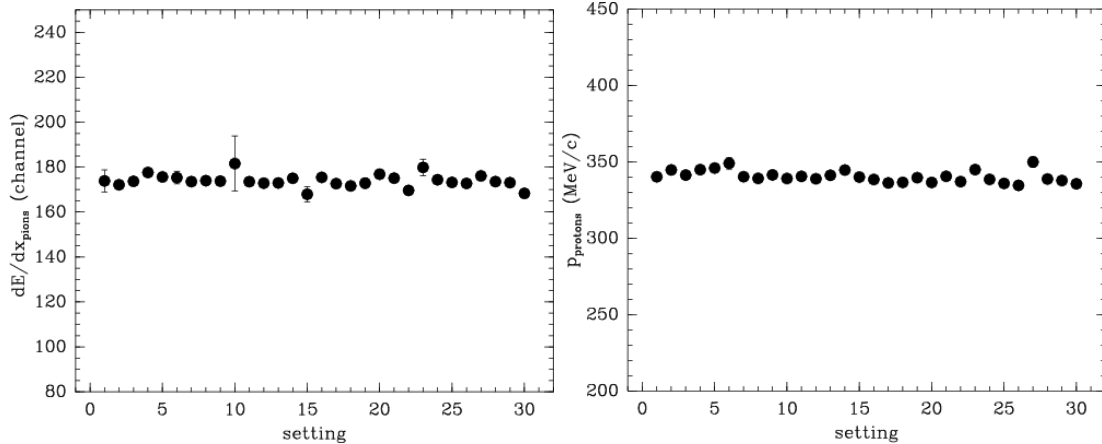


FIG. 5: Stability of the TPC calibration. Left panel:  $dE/dx$  versus settings for pions with  $300 \leq p \leq 500$  MeV/c. Right panel: mean momentum for protons with a  $dE/dx$  between 7 and 8 MIP versus setting, Settings go from low  $A$  to high  $A$  including beam momenta from  $3$  GeV/c to  $12.9$  GeV/c.

distortions in the TPC tracks, as outlined before.

The double-differential cross-section for the production of a particle of type  $\alpha$  can be expressed in the laboratory system as:

$$\frac{d^2\sigma_\alpha}{dp_i d\theta_j} = \frac{1}{N_{\text{pot}}} \frac{A}{N_A \rho t} \frac{1}{\Delta p_j \Delta \theta_j} \sum_{i', j', \alpha'} M_{ij\alpha i' j' \alpha'}^{-1} \cdot N_{i' j'}^{\alpha'} \quad (1)$$

where  $\frac{d^2\sigma_\alpha}{dp_i d\theta_j}$  is expressed in bins of true momentum ( $p_i$ ), angle ( $\theta_j$ ) and particle type ( $\alpha$ ).  $\Delta p_J$  and  $\Delta \theta_j$  are the bin sizes in momentum and angle, respectively.

The ‘raw yield’  $N_{i' j'}^{\alpha'}$  is the number of particles of observed type  $\alpha'$  in bins of reconstructed momentum ( $p_{i'}$ ) and angle ( $\theta_{j'}$ ). These particles must satisfy the event, track and PID selection criteria. Although, owing to the stringent PID selection, the background from misidentified protons in the pion sample is small, the pion and proton raw yields ( $N_{i' j'}^{\alpha'}$ , for  $\alpha' = \pi^-, \pi^+, p$ ) have been measured simultaneously. It is thus possible to correct for the small remaining proton background in the pion data without prior assumptions concerning the proton production cross-section.

The matrix  $M_{ij\alpha i' j' \alpha'}^{-1}$  corrects for the efficiency and the resolution of the detector. It unfolds the true variables  $ij\alpha$  from the reconstructed variables  $i' j' \alpha'$  with a Bayesian technique [27] and corrects the observed number of particles to take into account effects such as trigger efficiency, reconstruction efficiency, acceptance, absorption, pion decay, tertiary production, PID efficiency, PID misidentification and electron background. The method used to correct for the various effects is described in more detail in Ref. [15].

In order to predict the population of the migration matrix element  $M_{ij\alpha i' j' \alpha'}$ , the resolution, efficiency and acceptance of the detector are obtained from the MonteCarlo. This is accurate provided the MonteCarlo simulation describes these quantities correctly. Where some deviations from the control samples measured from the data are found, the data are used to introduce (small) *ad hoc* corrections to the MonteCarlo. Using the unfolding approach, possible known biases in the measurements are taken into account automatically as long as they are described by the MonteCarlo. In the experiment simulation, which is based on the GEANT4 toolkit [28], the materials in the beam-line and the detector are accurately described as well as the relevant features of the detector response and the digitization process. In general, the MonteCarlo simulation compares well with the data, as shown in Ref. [15]. For all important issues physical benchmarks have been used to validate the analysis. The absolute efficiency and the measurement of the angle and momentum was determined with elastic scattering. The momentum and angular resolution was determined exploiting the two halves of cosmic-ray tracks crossing the TPC

volume. The efficiency of the particle identification was checked using two independent detector systems. Only the latter needs a small *ad hoc* correction compared to the simulation.

The factor  $\frac{A}{N_A \rho t}$  in Eq. 1 is the inverse of the number of target nuclei per unit area ( $A$  is the atomic mass,  $N_A$  is the Avogadro number,  $\rho$  and  $t$  are the target density and thickness) [43]. The result is normalized to the number of incident protons on the target  $N_{\text{pot}}$ . The absolute normalization of the result is calculated in the first instance relative to the number of incident beam particles accepted by the selection. After unfolding, the factor  $\frac{A}{N_A \rho t}$  is applied. The beam normalization using down-scaled incident proton triggers has uncertainties smaller than 2% for all beam momentum settings.

The background due to interactions of the primary protons outside the target (called ‘Empty target background’) is measured using data taken without the target mounted in the target holder. Owing to the selection criteria which only accept events from the target region and the good definition of the interaction point this background is negligible ( $< 10^{-5}$ ).

The effects of the systematic uncertainties on the final results are estimated by repeating the analysis with the relevant input modified within the estimated uncertainty intervals. In many cases this procedure requires the construction of a set of different migration matrices. The correlations of the variations between the cross-section bins are evaluated and expressed in the covariance matrix. Each systematic error source is represented by its own covariance matrix. The sum of these matrices describes the total systematic error. The magnitude of the systematic errors and their dependence on momentum and angle will be shown in Section IV.

#### IV. EXPERIMENTAL RESULTS

The measured double-differential cross-sections for the production of  $\pi^+$  and  $\pi^-$  in the laboratory system as a function of the momentum and the polar angle for each incident beam momentum are shown in Figures 6 to 12 for targets from Be to Pb. The error bars shown are the square-roots of the diagonal elements in the covariance matrix, where statistical and systematic uncertainties are combined in quadrature. The correlation of the statistical errors (introduced by the unfolding procedure) are typically smaller than 20% for adjacent momentum bins and even smaller for adjacent angular bins. The correlations of the systematic errors are larger, typically 80% for adjacent bins. The overall scale error ( $< 2\%$ ) is not shown. The results of this analysis are also tabulated in Appendix A.

These results are in agreement with what was previously found using only the first part of the spill and using no dynamic distortions corrections. Figures 13 to 16 show the ratio of the cross sections without and with the correction factor for dynamic distortions in 8.9 GeV/c Beryllium data (as an example of light target), where the statistics is bigger and in 8 GeV/c Tantalum data (as an example of heavy target). The error band in the ratio takes into account the usual estimate of momentum error and the error on efficiency, the other errors are correlated. The agreement is within  $1\sigma$  for most of the points.

The dependence of the averaged pion yields on the incident beam momentum is shown in Fig. 17. The  $\pi^+$  and  $\pi^-$  yields are averaged over the region  $0.35 \text{ rad} \leq \theta < 1.55 \text{ rad}$  and  $100 \text{ MeV}/c \leq p < 700 \text{ MeV}/c$  (pions produced in the forward direction only). Whereas the beam energy dependence of the yields in the p–Be, p–C data differs clearly from the dependence in the p–Ta, p–Pb data one can observe that the p–Al, p–Cu and p–Sn data display a smooth transition between them. The dependence in the p–Be, p–C data is much more flat with a saturation of the yield between 8 GeV/c and 12 GeV/c with the p–Al, p–Cu and p–Sn showing an intermediate behaviour.

The integrated  $\pi^-/\pi^+$  ratio in the forward direction is displayed in Fig. 18 as a function of the secondary momentum. In the covered part of the momentum range in most bins more  $\pi^+$ ’s are produced than  $\pi^-$ ’s. In the p–Ta and p–Pb data the ratio is closer to unity than for the p–Be, p–C and p–Al data. The  $\pi^-/\pi^+$  ratio is larger for higher incoming beam momenta than for lower momenta.

In the tantalum and lead data, the number of  $\pi^+$ ’s produced is smaller than the number of  $\pi^-$ ’s in the lowest momentum bin (100 MeV/c–150 MeV/c) for the 8 GeV/c and 12 GeV/c incoming beam momenta. A similar effect was seen by E910 in their p–Au data [30]. Lighter targets do not show this behaviour.

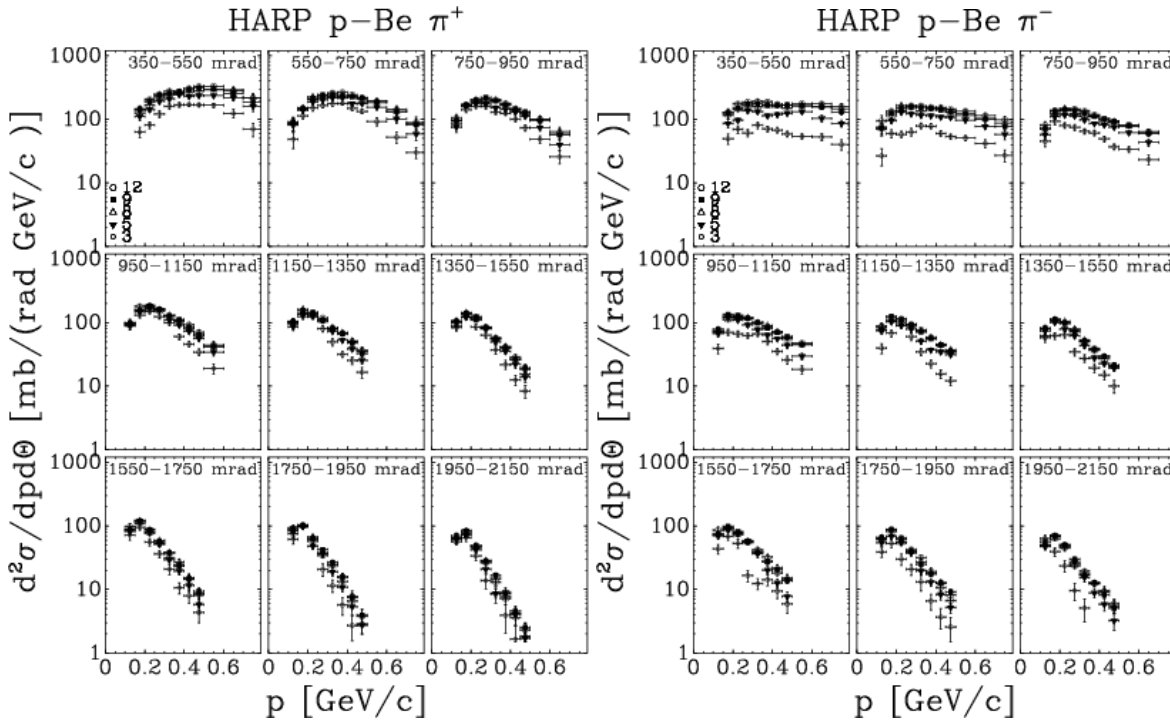


FIG. 6: Double-differential cross-sections for  $\pi^+$  production (left) and  $\pi^-$  production (right) in p-Be interactions as a function of momentum displayed in different angular bins (shown in mrad in the panels). In the figure, the symbol legend 9 refers to 8.9 GeV/c nominal beam momentum. The error bars represent the combination of statistical and systematic uncertainties.

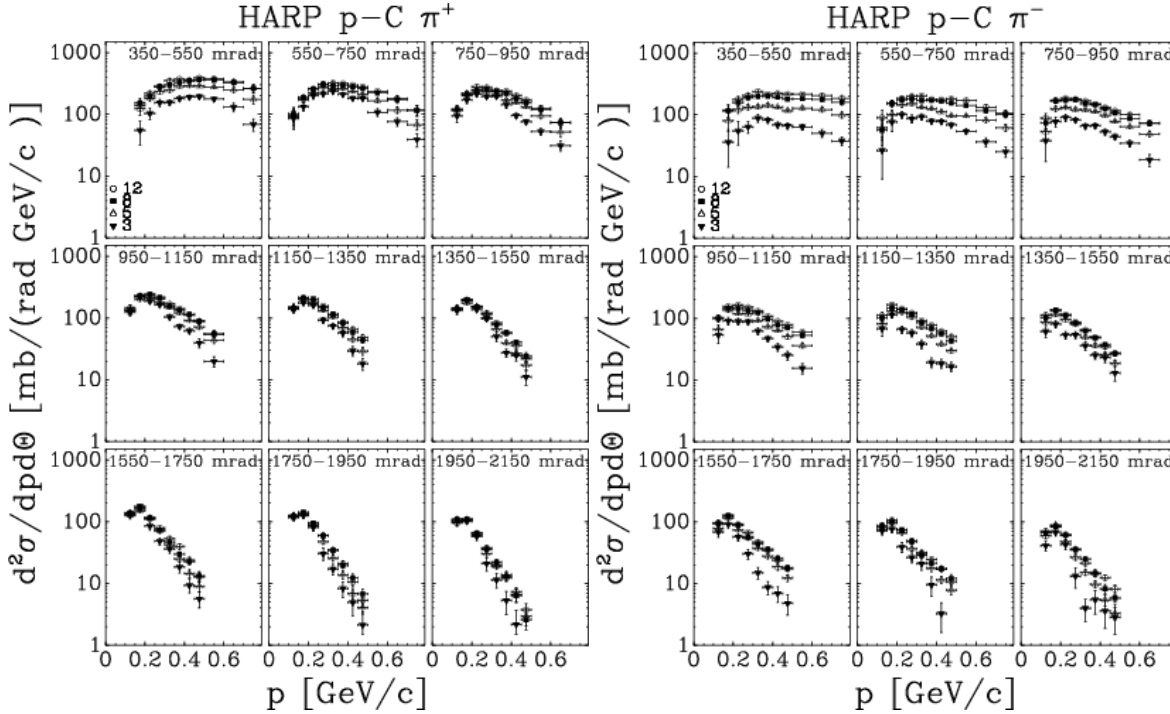


FIG. 7: Double-differential cross-sections for  $\pi^+$  production (left) and  $\pi^-$  production (right) in p-C interactions as a function of momentum displayed in different angular bins (shown in mrad in the panels). The error bars represent the combination of statistical and systematic uncertainties.

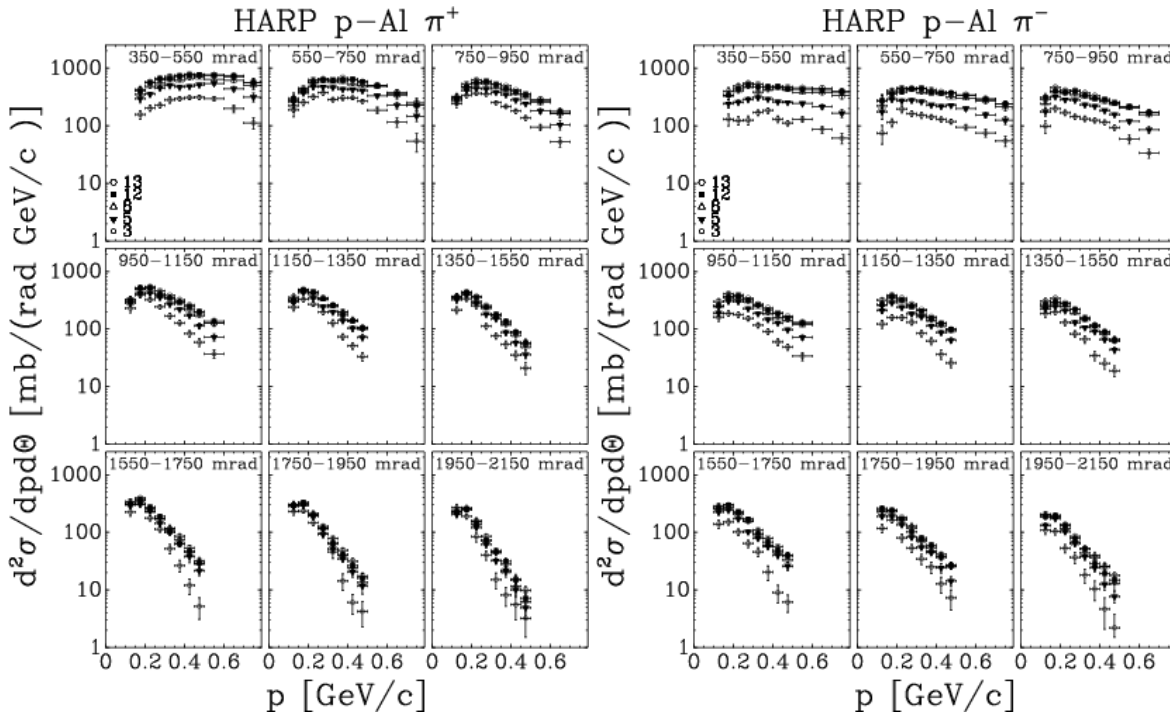


FIG. 8: Double-differential cross-sections for  $\pi^+$  production (left) and  $\pi^-$  production (right) in p-Al interactions as a function of momentum displayed in different angular bins (shown in mrad in the panels). In the figure, the symbol legend 13 refers to 12.9 GeV/c nominal beam momentum. The error bars represent the combination of statistical and systematic uncertainties.

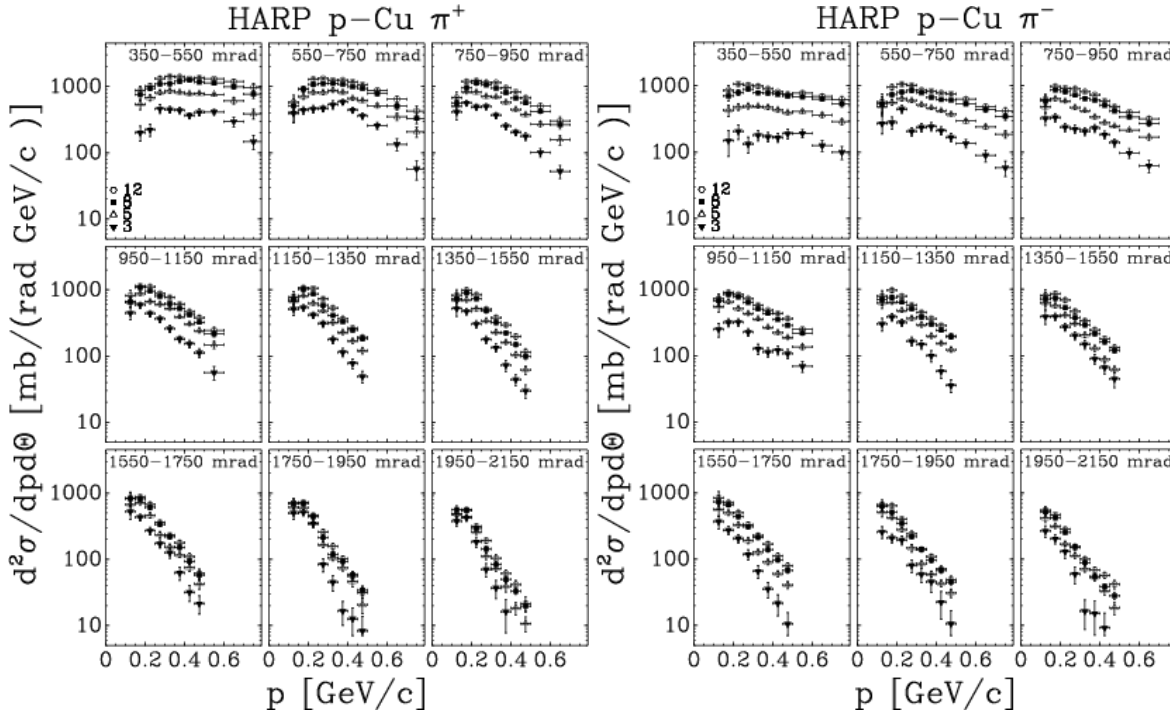


FIG. 9: Double-differential cross-sections for  $\pi^+$  production (left) and  $\pi^-$  production (right) in p-Cu interactions as a function of momentum displayed in different angular bins (shown in mrad in the panels). The error bars represent the combination of statistical and systematic uncertainties.

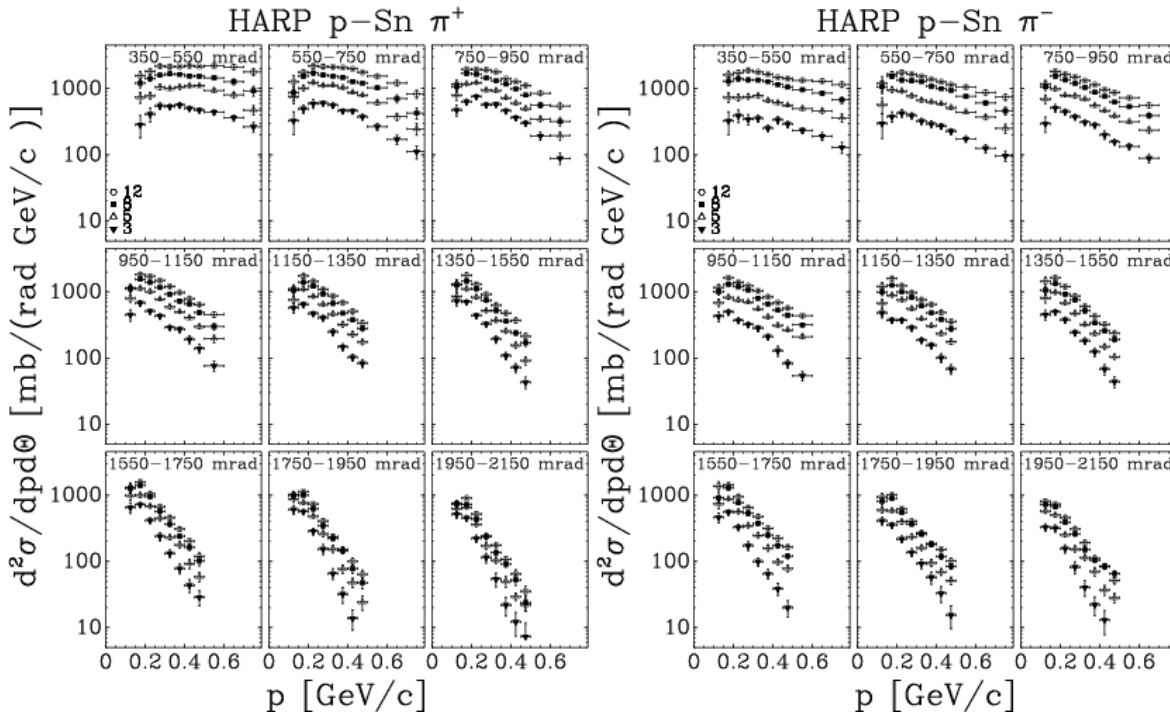


FIG. 10: Double-differential cross-sections for  $\pi^+$  production (left) and  $\pi^-$  production (right) in p-Sn interactions as a function of momentum displayed in different angular bins (shown in mrad in the panels). The error bars represent the combination of statistical and systematic uncertainties.

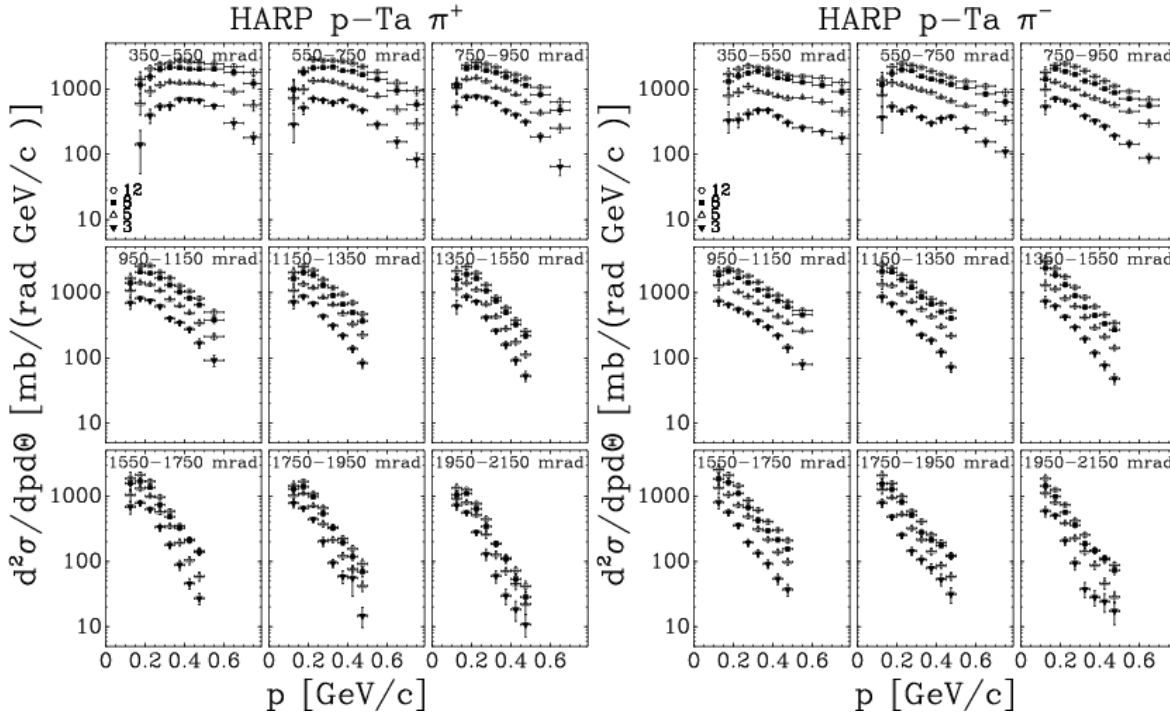


FIG. 11: Double-differential cross-sections for  $\pi^+$  production (left) and  $\pi^-$  production (right) in p-Ta interactions as a function of momentum displayed in different angular bins (shown in mrad in the panels). The error bars represent the combination of statistical and systematic uncertainties.

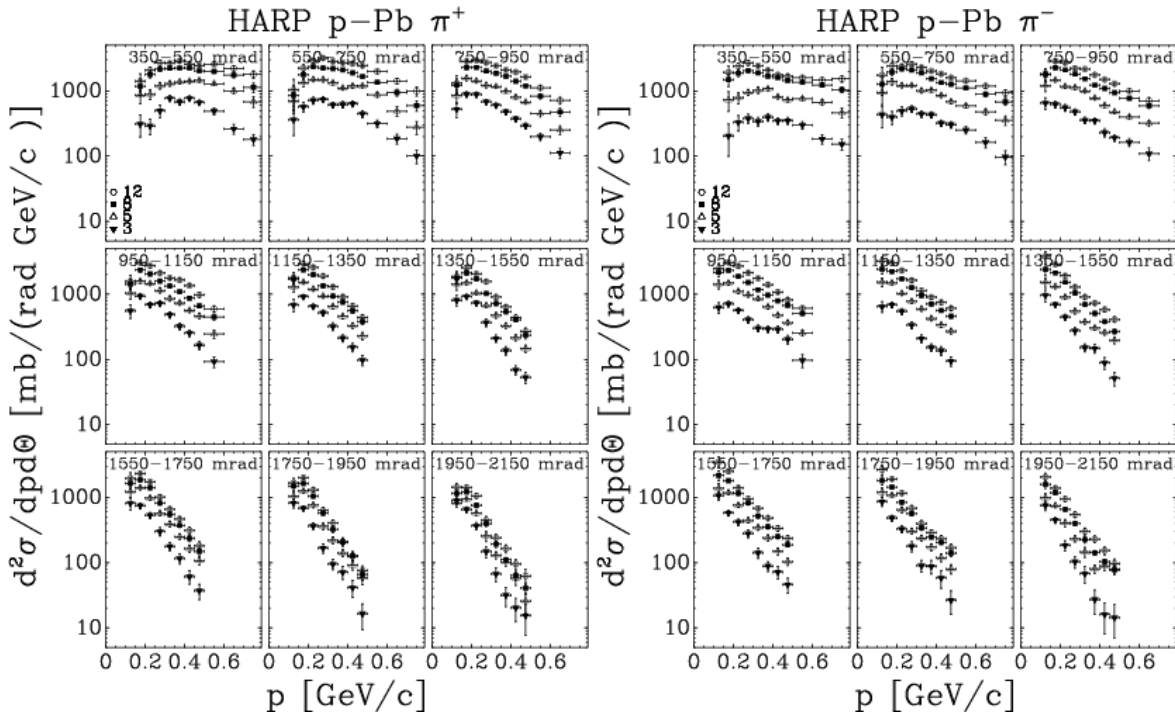


FIG. 12: Double-differential cross-sections for  $\pi^+$  production (left) and  $\pi^-$  production (right) in p-Pb interactions as a function of momentum displayed in different angular bins (shown in mrad in the panels). The error bars represent the combination of statistical and systematic uncertainties.

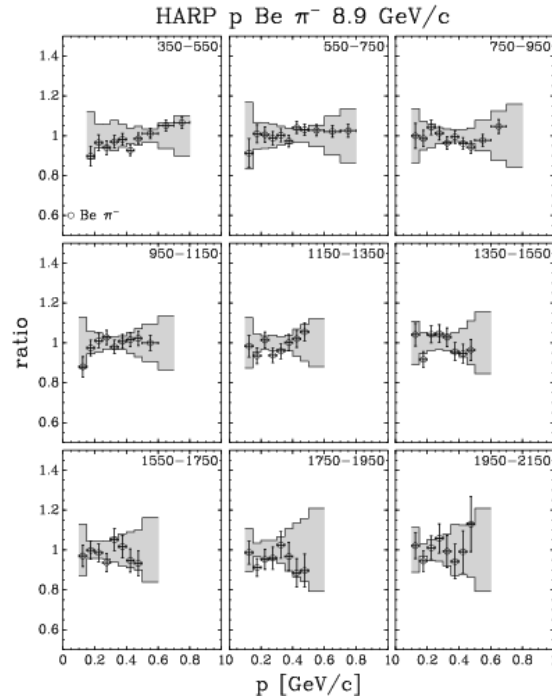


FIG. 13: Ratio of the  $\pi^-$  production cross-sections measured without and with corrections for dynamic distortions in p-Be interactions at 8.9 GeV/c, as a function of momentum for different angular bins (shown in mrad in the panels). The error band in the ratio takes into account momentum error and the error on the efficiency, the other errors being correlated. The errors on the data points are statistical.

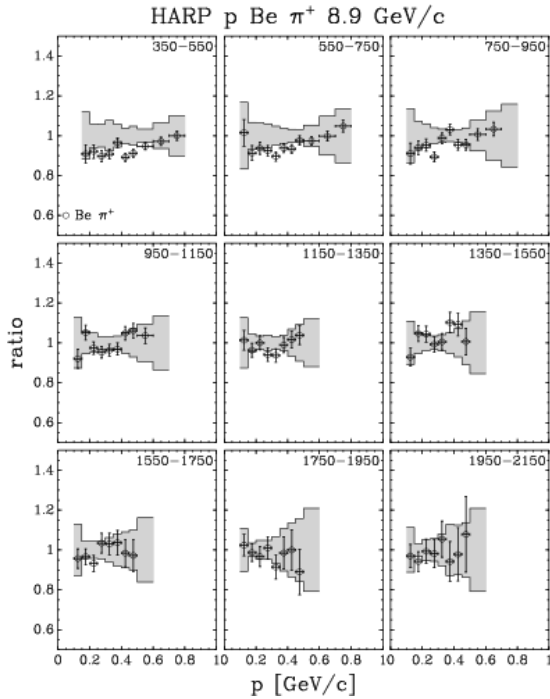


FIG. 14: Ratio of the  $\pi^+$  production cross-sections measured without and with corrections for dynamic distortions in p–Be interactions at 8.9 GeV/c, as a function of momentum for different angular bins (shown in mrad in the panels). The error band in the ratio takes into account momentum error and the error on the efficiency, the other errors being correlated. The errors on the data points are statistical.

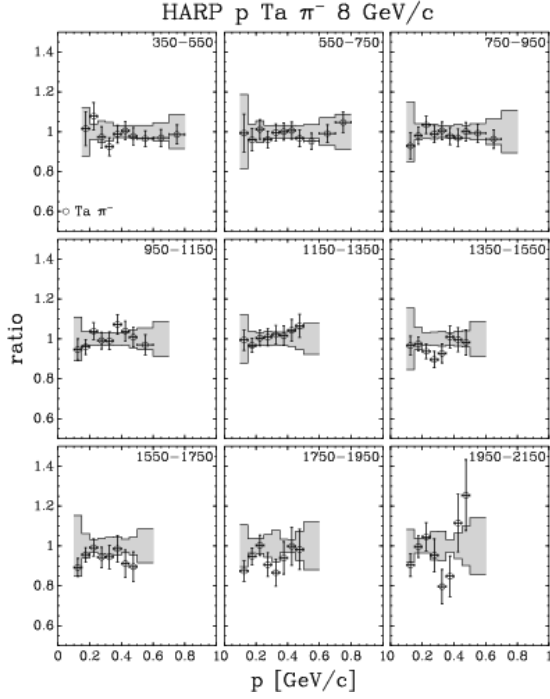


FIG. 15: Ratio of the  $\pi^-$  production cross-sections measured without and with corrections for dynamic distortions in p–Ta interactions at 8 GeV/c, as a function of momentum for different angular bins (shown in mrad in the panels). The error band in the ratio takes into account momentum error and the error on the efficiency, the other errors being correlated. The errors on the data points are statistical.

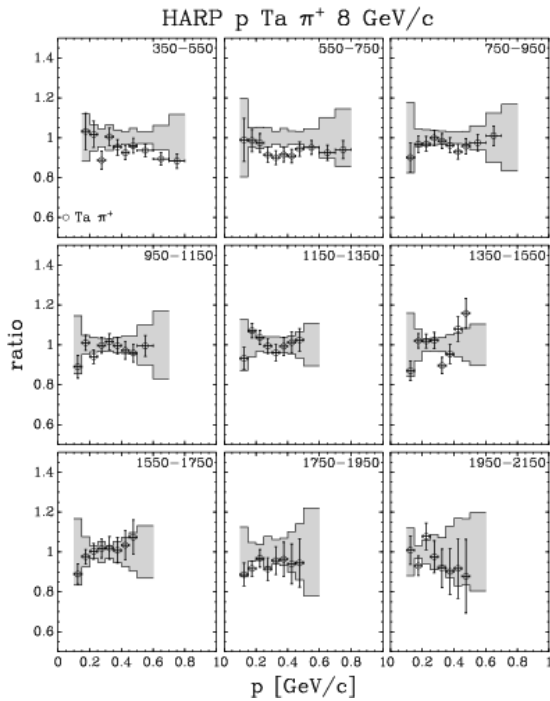


FIG. 16: Ratio of the  $\pi^+$  production cross-sections measured without and with corrections for dynamic distortions in p-Ta interactions at 8 GeV/c, as a function of momentum for different angular bins (shown in mrad in the panels). The error band in the ratio takes into account momentum error and the error on the efficiency, the other errors being correlated. The errors on the data points are statistical.

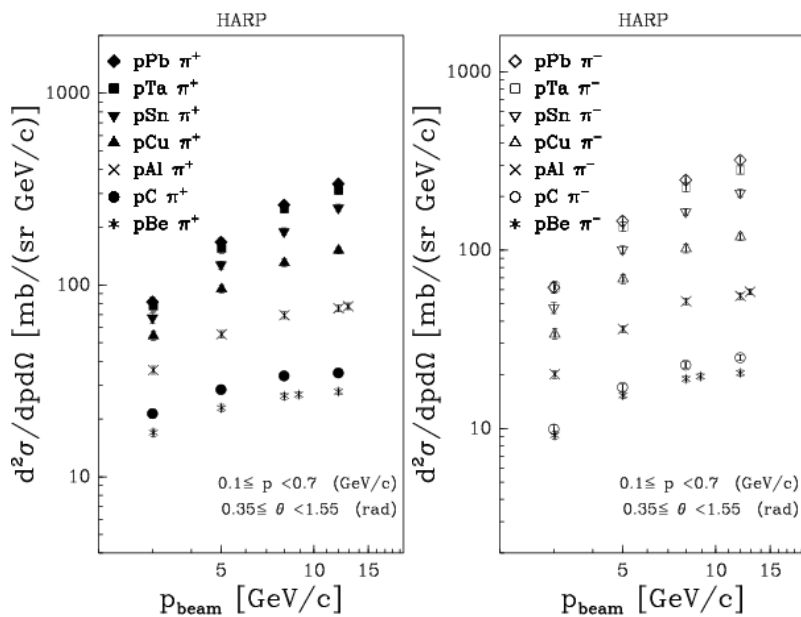


FIG. 17: The dependence on the beam momentum of the  $\pi^-$  (right) and  $\pi^+$  (left) production yields in p-Be, p-C, p-Al, p-Cu, p-Sn, p-Ta, p-Pb interactions averaged over the forward angular region ( $0.350 \text{ rad} \leq \theta < 1.550 \text{ rad}$ ) and momentum region  $100 \text{ MeV}/c \leq p < 700 \text{ MeV}/c$ . The results are given in arbitrary units, with a consistent scale between the left and right panel. Data points for different target nuclei and equal momenta are slightly shifted horizontally with respect to each other to increase the visibility.

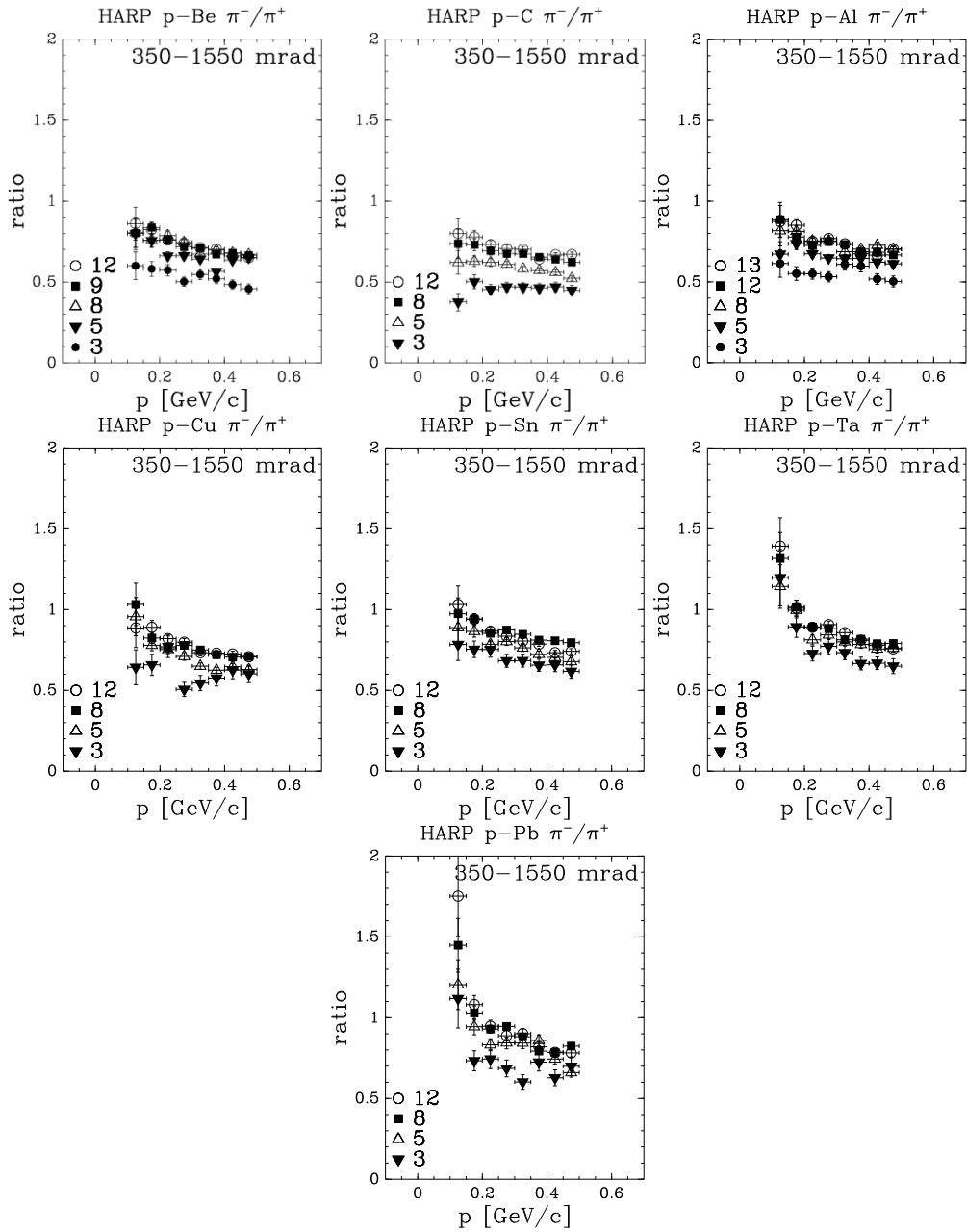


FIG. 18: From top-left panel to bottom-right panel, the ratio of the differential cross-sections for  $\pi^-$  and  $\pi^+$  production in p-Be, p-C, p-Al, p-Cu, p-Sn, p-Ta and p-Pb interactions as a function of the secondary momentum integrated over the forward angular region (shown in mrad). In the figure, the symbol legends 13 and 9 refer to 12.9 and 8.9 GeV/c nominal beam momentum, respectively.

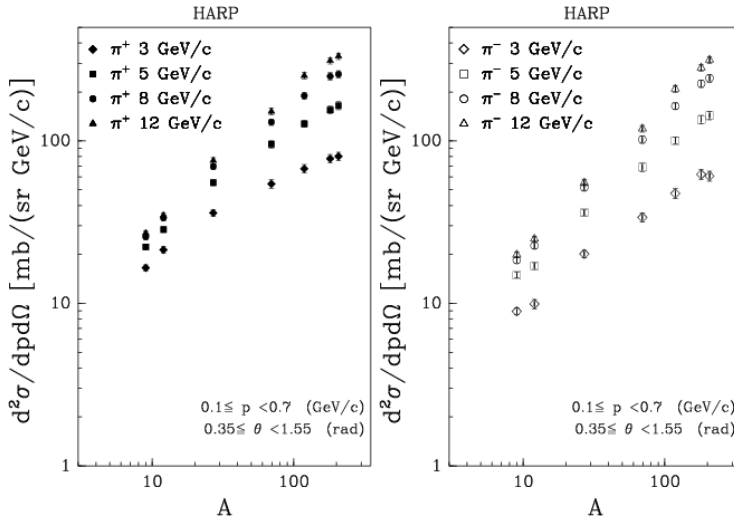


FIG. 19: The dependence on the atomic number  $A$  of the pion production yields in p–Be, p–Al, p–C, p–Cu, p–Sn, p–Ta, p–Pb interactions averaged over the forward angular region ( $0.35 \text{ rad} \leq \theta < 1.55 \text{ rad}$ ) and momentum region  $100 \text{ MeV}/c \leq p < 700 \text{ MeV}/c$ . The results are given in arbitrary units, with a consistent scale between the left and right panel. The vertical scale used in this figure is consistent with the one in Fig. 17.

The dependence of the averaged pion yields on the atomic number  $A$  is shown in Fig. 19. The  $\pi^+$  yields averaged over the region  $0.350 \text{ rad} \leq \theta < 1.550 \text{ rad}$  and  $100 \text{ MeV}/c \leq p < 700 \text{ MeV}/c$  are shown in the left panel and the  $\pi^-$  data averaged over the same region in the right panel for four different beam momenta. One observes a smooth behaviour of the averaged yields. The  $A$ -dependence is slightly different for  $\pi^-$  and  $\pi^+$  production, the latter saturating earlier towards higher  $A$ , especially at lower beam momenta.

The analysis reported here (for p–Ta and p–Pb interactions) covers the major part of pions produced in the target and accepted by the focusing system of the input stage of a neutrino factory [31]. The effective coverage of the kinematic range can be defined as the fraction of the number of muons transported by the input stage of a neutrino factory design originating from decays for which the pion production cross-section is within the kinematic range measured by the present experiment. As an example, this effective coverage was evaluated for the “International scoping study of a Neutrino Factory and super-beam facility” (ISS) input stage [31] to be 69% for  $\pi^+$  and 72% for  $\pi^-$ , respectively [32], using a particular model for pion production at an incoming beam momentum of  $10.9 \text{ GeV}/c$  [33]. Since the data covers already a large fraction of the relevant phase-space, one would expect that the extrapolation to the full region with hadronic production models can be done reliably, once these models are adjusted to reproduce this data set in the region covered. Such tuning of models can also profit from the additional data provided with the HARP forward spectrometer.

As an indication of the overall pion yield as a function of incoming beam momentum, the  $\pi^+$  and  $\pi^-$  production cross-sections were averaged over the full HARP kinematic range in the forward hemisphere ( $100 \text{ MeV}/c < p < 700 \text{ MeV}/c$  and  $0.35 < \theta < 1.55$ ). The results are shown in Fig. 20. The integrated yields are shown in the left panel and the integrated yields normalized to the kinetic energy of the incoming beam particles are shown in the right panel. The outer error bars indicate the total statistical and systematic errors. If one compares the  $\pi^+$  and  $\pi^-$  rates for a given beam momentum or if one compares the rates at a different beam momentum the relative systematic error is reduced by about a factor of two. The relative uncertainties are shown as inner error bar. It is shown that the pion yield increases with momentum and that in our kinematic coverage the optimum yield is between  $5 \text{ GeV}/c$  and  $8 \text{ GeV}/c$ .

However, these calculations should be completed with more realistic kinematical cuts in the integration. To show the trend the rates within restricted ranges are also given: a restricted angular range ( $0.35 < \theta < 0.95$ ) and a range further restricted in momentum ( $250 \text{ MeV}/c < p < 500 \text{ MeV}/c$ ). The latter range may be most representative for the neutrino factory.

Of course this analysis only gives a simplified picture of the results. One should note that the best result

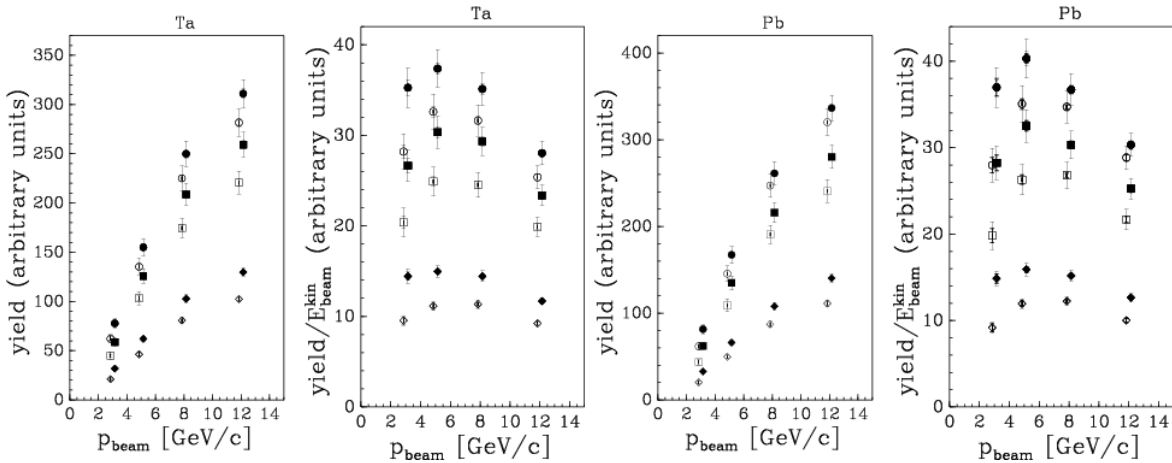


FIG. 20: Predictions of the  $\pi^+$  (closed symbols) and  $\pi^-$  (open symbols) yields for different design of the NF focussing stage. Integrated yields (left) and the integrated yields normalized to the kinetic energy of the proton (right) for p-Ta and p-Pb interactions. The circles indicate the integral over the full HARP acceptance ( $100 \text{ MeV}/c < p < 700 \text{ MeV}/c$  and  $0.35 \text{ rad} < \theta < 1.55 \text{ rad}$ ), the squares are integrated over  $0.35 \text{ rad} < \theta < 0.95 \text{ rad}$ , while the diamonds are calculated for the smaller angular range and  $250 \text{ MeV}/c < p < 500 \text{ MeV}/c$ . Although the units are indicated as “arbitrary”, for the largest region the yield is expressed as  $d^2\sigma/dpd\Omega$  in  $\text{mb}/(\text{GeV}/c \text{ sr})$ . For the other regions the same normalization is chosen, but now scaled with the relative bin size to show visually the correct ratio of number of pions produced in these kinematic regions. The full error bar shows the overall (systematic and statistical) error, while the inner error bar shows the error relevant for the point-to-point comparison. For the latter error only the uncorrelated systematic uncertainties were added to the statistical error.

can be obtained by using the full information of the double-differential cross-section and by developing designs optimized specifically for each single beam momentum. Then these optimized designs can be compared.

The experimental uncertainties are summarized for  $\pi^+$  in Table II for all used targets and shown for two typical targets (one light and one heavy) in Figure 21. They are very similar for  $\pi^-$  and at the other beam energies: 3, 5, 8, 12 and  $12.9 \text{ GeV}/c$ . Going from lighter (Be, C) to heavier targets (Ta, Pb) the corrections for  $\pi^0$  (conversion) and absorption/tertiaries are bigger.

One observes that only for the  $3 \text{ GeV}/c$  beam is the statistical error similar in magnitude to the systematic error, while the statistical error is negligible for the  $8 \text{ GeV}/c$  and  $12 \text{ GeV}/c$  beam settings. The statistical error is calculated by error propagation as part of the unfolding procedure. It takes into account that the unfolding matrix is obtained from the data themselves [44] and hence contributes also to the statistical error. This procedure almost doubles the statistical error, but avoids an important systematic error which would otherwise be introduced by assuming a cross-section model *a priori* to calculate the corrections.

The largest systematic error corresponds to the uncertainty in the absolute momentum scale, which was estimated to be around 3% using elastic scattering [15]. Although the corrections for the dynamic distortions have been applied in this analysis, contrary to the previously published ones, the systematic error has not been reduced. This is due to the fact that now the full statistics has been used introducing data with larger distortions. The benefit of the introduction of the larger statistics is evident mainly at low incident beam momenta ( $3 \text{ GeV}/c$ ), in the bins with higher secondary momenta and larger scattering angle. At low momentum in the relatively small angle forward direction the uncertainty in the subtraction of the electron and positron background due to  $\pi^0$  production is dominant ( $\sim 6 - 10\%$ ). This uncertainty is split between the variation in the shape of the  $\pi^0$  spectrum and the normalization using the recognized electrons. The target region definition and the uncertainty in the PID efficiency and background from tertiaries (particles produced in secondary interactions) are of similar size and are not negligible ( $\sim 2 - 3\%$ ). Relatively small errors are introduced by the uncertainties in the absorption correction, absolute knowledge of the angular and the momentum resolution. The correction for tertiaries is relatively large at low momenta and large angles ( $\sim 3 - 5\%$ ). As expected, this region is most affected by this component. The errors are quoted for the positive pion data. Owing to the similarity of the spectra the errors are

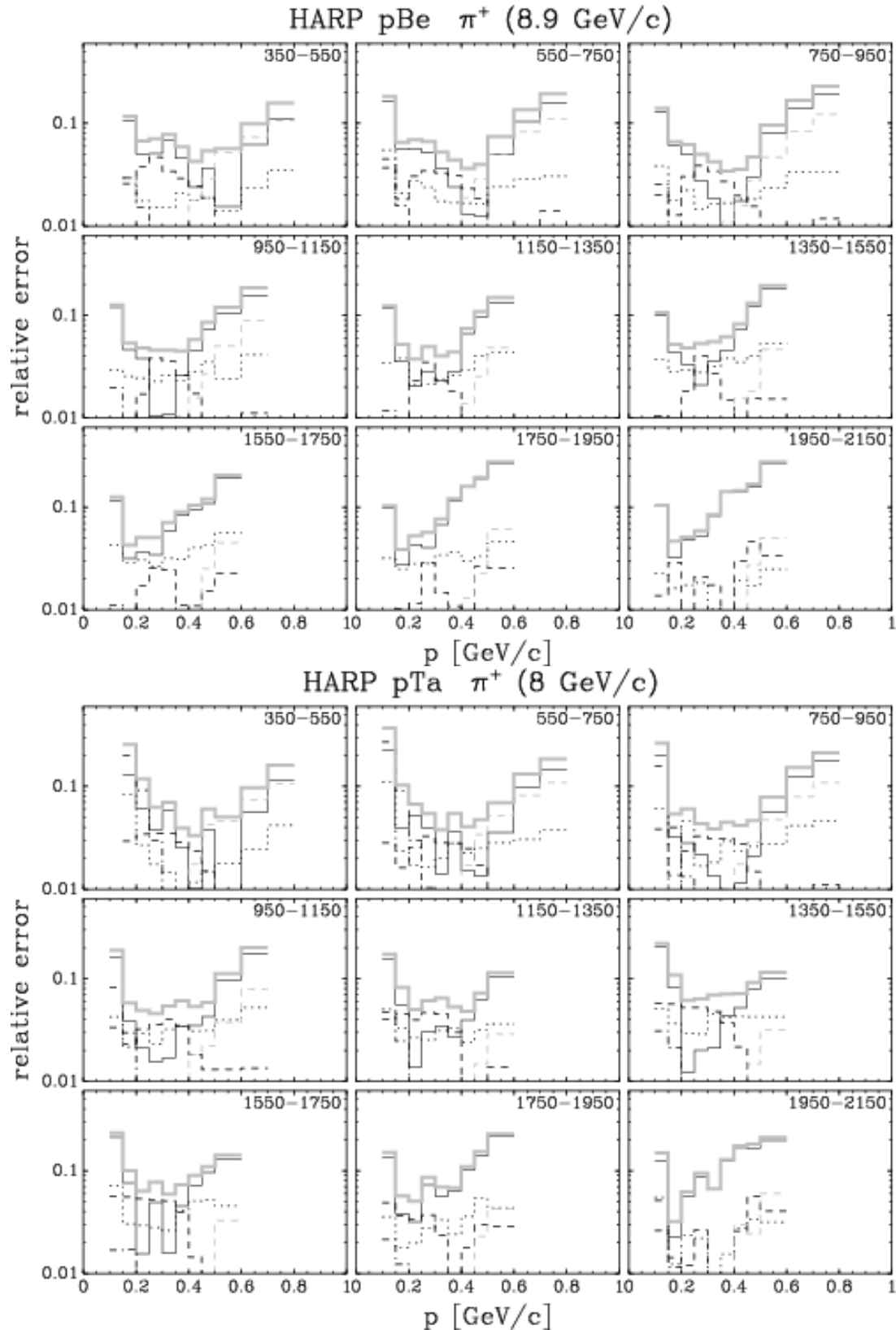


FIG. 21: Total systematic error (grey solid line) and main components: black short-dashed line for absorption+tertiaries interactions, black dotted line for track efficiency and target pointing efficiency, black dot-dashed line for  $\pi^0$  subtraction, black solid line for momentum scale+resolution and angle scale, grey short-dashed line for PID for two typical targets (Be and Ta)

very similar for the negative pions.

As already mentioned above, the overall normalization has an uncertainty of 2%, and is not reported in the table. It is mainly due to the uncertainty in the efficiency that beam protons counted in the normalization actually hit the target, with smaller components from the target density and beam particle counting procedure.

TABLE II: Experimental uncertainties for the analysis of the data taken with beryllium, carbon, aluminium, copper, tin and lead targets at 3, 5, 8, 8.9, 12 and 12.9 GeV/c. The numbers represent the uncertainty in percent of the cross-section integrated over the angle and momentum region indicated.

<b>p (GeV/c)</b>		0.1 – 0.3			0.3 – 0.5			0.5 – 0.7	
<b>Angle (mrad)</b>		350–950	950–1550	1550–2150	350–950	950–1550	1550–2150	350–950	950–1550
<b>3 GeV/c</b>									
<b>Total syst.</b>	(Be)	8.2	4.7	3.5	3.9	6.3	8.9	9.5	14.9
	(C)	13.2	5.2	3.2	3.8	6.9	10.1	9.5	16.5
	(Al)	9.3	4.8	3.5	3.8	7.2	13.1	10.0	13.6
	(Cu)	10.0	7.7	6.7	3.7	5.4	9.0	9.0	12.6
	(Sn)	14.2	6.7	5.1	3.4	6.5	9.8	8.1	14.2
	(Ta)	13.7	8.1	7.5	3.8	6.0	6.0	9.9	13.9
	(Pb)	13.2	7.5	6.7	3.7	5.7	7.8	9.5	14.1
<b>Statistics</b>	(Be)	2.8	2.6	3.6	2.2	3.7	9.0	2.9	6.8
	(C)	3.2	2.6	3.3	2.4	3.8	8.9	3.1	7.5
	(Al)	3.0	2.5	3.2	2.4	3.9	8.2	3.2	7.0
	(Cu)	4.4	3.8	4.6	3.6	5.4	11.2	4.7	9.7
	(Sn)	3.1	2.5	2.9	2.5	3.6	6.9	3.3	6.3
	(Ta)	3.3	2.6	3.1	2.5	3.5	6.5	3.4	6.2
	(Pb)	4.2	3.1	3.7	3.2	4.5	8.5	4.4	8.2
<b>5 GeV/c</b>									
<b>Total syst.</b>	(Be)	9.0	4.8	3.2	4.2	5.1	10.0	7.9	13.8
	(C)	11.1	5.0	3.2	3.9	5.3	8.0	6.9	11.7
	(Al)	9.5	5.0	3.3	3.9	4.8	8.9	7.8	12.7
	(Cu)	10.6	8.1	7.0	3.7	5.2	6.7	7.1	12.8
	(Sn)	10.1	6.2	5.1	3.5	5.2	8.0	7.3	11.6
	(Ta)	12.5	8.1	7.7	3.7	5.2	7.7	7.1	10.7
	(Pb)	12.6	7.6	6.6	3.7	5.6	6.5	7.3	11.5
<b>Statistics</b>	(Be)	1.7	1.6	2.1	1.3	2.1	4.3	1.5	3.3
	(C)	1.6	1.3	1.6	1.0	1.5	2.9	1.1	2.3
	(Al)	1.5	1.3	1.7	1.1	1.7	3.2	1.4	2.7
	(Cu)	1.6	1.4	1.7	1.2	1.7	3.1	1.4	2.6
	(Sn)	1.5	1.3	1.5	1.1	1.6	2.8	1.4	2.4
	(Ta)	1.7	1.4	1.7	1.3	1.7	3.0	1.5	2.5
	(Pb)	2.2	1.8	2.1	1.7	2.2	3.9	2.0	3.4
<b>8 GeV/c</b>									
<b>Total syst.</b>	(Be)	8.6	4.7	3.1	4.0	4.5	7.5	7.2	12.0
	(C)	10.4	4.8	3.1	3.7	3.8	7.0	6.6	11.8
	(Al)	9.4	5.0	3.5	3.8	4.3	7.5	7.2	11.2
	(Cu)	10.1	7.8	7.1	3.6	4.3	6.3	6.5	10.8
	(Sn)	9.1	6.2	5.3	3.3	5.0	6.9	7.1	11.2
	(Ta)	11.5	8.2	7.6	3.7	5.0	5.9	7.1	10.4
	(Pb)	11.2	7.5	6.5	3.5	4.9	6.9	6.4	9.9
<b>Statistics</b>	(Be)	1.4	1.3	1.7	1.0	1.6	3.1	1.2	2.4
	(C)	1.3	1.0	1.3	0.7	1.1	2.1	0.8	1.6
	(Al)	1.2	1.1	1.4	0.9	1.3	2.5	1.0	1.9
	(Cu)	1.0	0.9	1.1	0.7	1.0	1.8	0.8	1.4
	(Sn)	1.0	0.9	1.1	0.7	1.0	1.8	0.9	1.5
	(Ta)	1.1	0.9	1.2	0.8	1.1	1.9	0.9	1.6
	(Pb)	1.1	0.9	1.0	0.7	1.0	1.8	0.9	1.5

<b>p (GeV/c)</b>		0.1 – 0.3			0.3 – 0.5			0.5 – 0.7	
<b>Angle (mrad)</b>		350–950	950–1550	1550–2150	350–950	950–1550	1550–2150	350–950	950–1550
<b>8.9 GeV/c</b>									
<b>Total syst.</b>	(Be)	8.8	4.7	3.1	4.2	4.4	7.7	7.9	12.4
<b>Statistics</b>	(Be)	0.5	0.5	0.6	0.4	0.6	1.1	0.4	0.9
<b>12 GeV/c</b>									
<b>Total syst.</b>	(Be)	9.0	4.8	3.3	3.8	4.1	7.3	7.3	12.1
	(C)	9.8	5.8	4.1	3.9	4.5	6.8	7.5	10.8
	(Al)	9.6	5.4	3.9	3.5	4.0	7.6	7.6	11.7
	(Cu)	10.1	7.8	7.1	2.9	4.3	6.3	6.7	11.2
	(Sn)	10.0	6.7	5.7	2.9	4.7	6.6	6.1	9.6
	(Ta)	11.4	7.2	6.8	2.3	4.4	5.9	6.6	9.4
	(Pb)	10.8	7.1	6.7	2.9	4.4	5.6	7.1	9.1
<b>Statistics</b>	(Be)	1.1	1.1	1.5	0.8	1.3	2.6	0.9	2.0
	(C)	1.9	1.9	2.4	1.5	2.2	4.4	1.6	3.2
	(Al)	1.3	1.2	1.5	0.9	1.5	2.8	1.1	2.1
	(Cu)	1.2	1.2	1.5	0.9	1.3	2.5	1.0	1.9
	(Sn)	0.8	0.8	0.9	0.6	0.9	1.5	0.7	1.2
	(Ta)	1.1	1.0	1.2	0.8	1.2	2.1	1.0	1.7
	(Pb)	1.8	1.6	2.0	1.4	1.9	3.5	1.6	2.7
<b>12.9 GeV/c</b>									
<b>Total syst.</b>	(Al)	9.6	5.2	3.7	3.5	4.1	6.8	7.4	11.7
<b>Statistics</b>	(Al)	0.5	0.5	0.6	0.4	0.6	1.1	0.4	0.8

### A. Comparisons with MC predictions

As our final results, obtained with a full correction of the distortions of TPC tracks (static+dynamic), are compatible with our preliminary ones published in [15, 16, 17], we refer to these papers for a comparison with published data. We only stress here that previous data sets are scarce, with big total errors and cover only a limited region of the phase space covered by the HARP experiment.

In the following we will show only some comparisons with publicly available MonteCarlo simulations: GEANT4 [28] and MARS [40], using different models. We stress that no tuning to our data has been done by the GEANT4 or MARS teams. The comparison will be shown for a limited set of plots and only for the C and Ta targets, as examples of a light and a heavy target nucleus, in figures 22 to 33.

At intermediate energies (up to 5-10 GeV), GEANT4 uses two types of intra-nuclear cascade models: the Bertini model [36, 37] (valid up to  $\sim 10$  GeV) and the binary model [35] (valid up to  $\sim 3$  GeV). Both models treat the target nucleus in detail, taking into account density variations and tracking in the nuclear field. The binary model is based on hadron collisions with nucleons, giving resonances that decay according to their quantum numbers. The Bertini model is based on the cascade code reported in [38] and hadron collisions are assumed to proceed according to free-space partial cross sections and final state distributions measured for the incident particle types.

At higher energies, instead, two parton string models, the quark-gluon string (QGS) model [36, 39] and the Fritiof (FTP) model [39] are used, in addition to a High Energy Parametrized model (HEP) derived from the high energy part of the Gheisha code used inside GEANT3 [42].

The parametrized models of GEANT4 (HEP and LEP) are intended to be fast, but conserve energy and momentum on average and not event by event.

A realistic GEANT4 simulation is built by combining models and physics processes into what is called a “physics list”. In high energy calorimetry the two most commonly used are the QGSP physics list, based on the QGS model, the pre-compound nucleus model and some of the Low Energy Parametrized (LEP)

model (that has its root in the GHEISHA code inside GEANT3) and the LHEP physics list [34] based on the parametrized LEP model and HEP models.

The MARS code system [40] uses as basic model an inclusive approach multiparticle production originated by R. Feynman. Above 3 GeV/c phenomenological particle production models are used. Below 5 GeV/c a cascade-exciton model [41] combined with the Fermi break-up model, the coalescence model, an evaporation model and a multifragmentation extension is used instead.

None of the considered models describe fully our data. However, backward or central region production seems to be described better than relatively more forward production, especially at higher incident momenta. In our data, the lowest angular bin corresponds to a transition region from forward to central production, that is more difficult to describe by MC models.

In general,  $\pi^+$  production is better described than  $\pi^-$  production. At higher energies the FTP model (from GEANT4) and the MARS model describe better the data, while at the lowest energies the Bertini and binary cascade models (from GEANT4) seem more appropriate. Parametrized models, as LHEP from GEANT4, show relevant discrepancies: up to a factor three in the forward region at low energies.

The comparison, just outlined in our paper, between data and models shows that the full set of HARP data, taken with targets spanning the full periodic table of elements, with small total errors and large coverage of the solid angle with a single detector, may greatly help the tuning of models used in hadronic simulations in the difficult energy range between 3 GeV/c and 15 GeV/c of incident momentum.

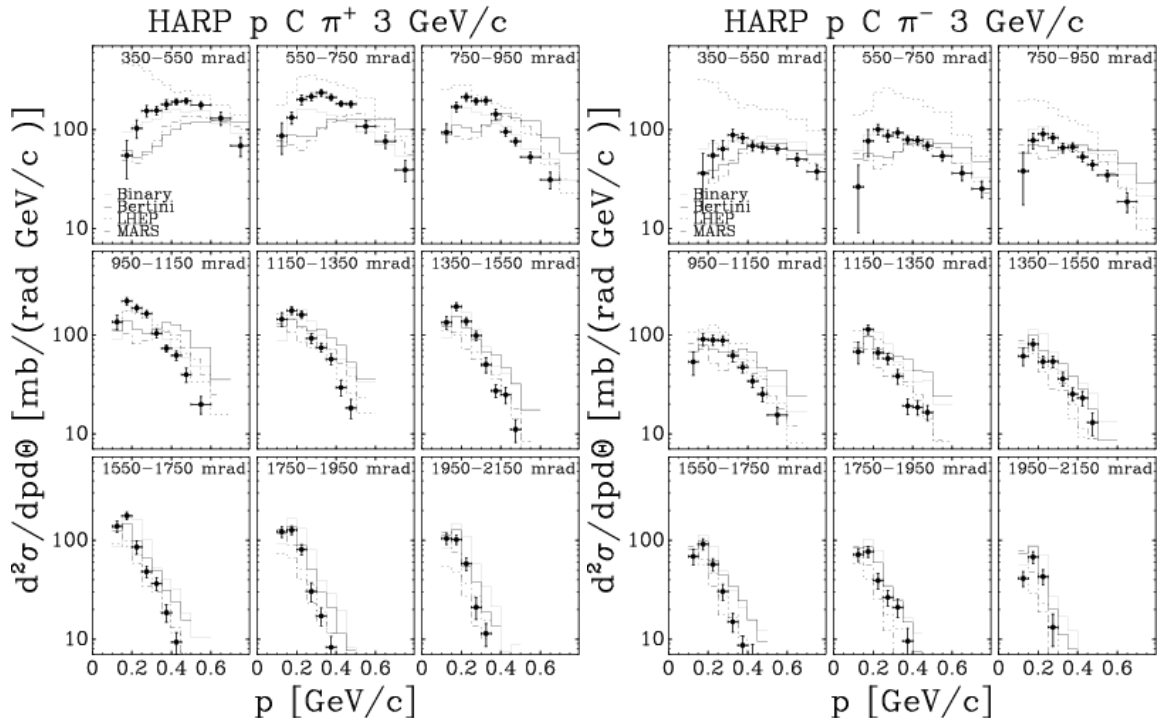


FIG. 22: Comparison of HARP double-differential  $\pi^+$  ( $\pi^-$ ) cross sections for p-C at 3 GeV/c with GEANT4 and MARS MC predictions, using several generator models (see text for details).

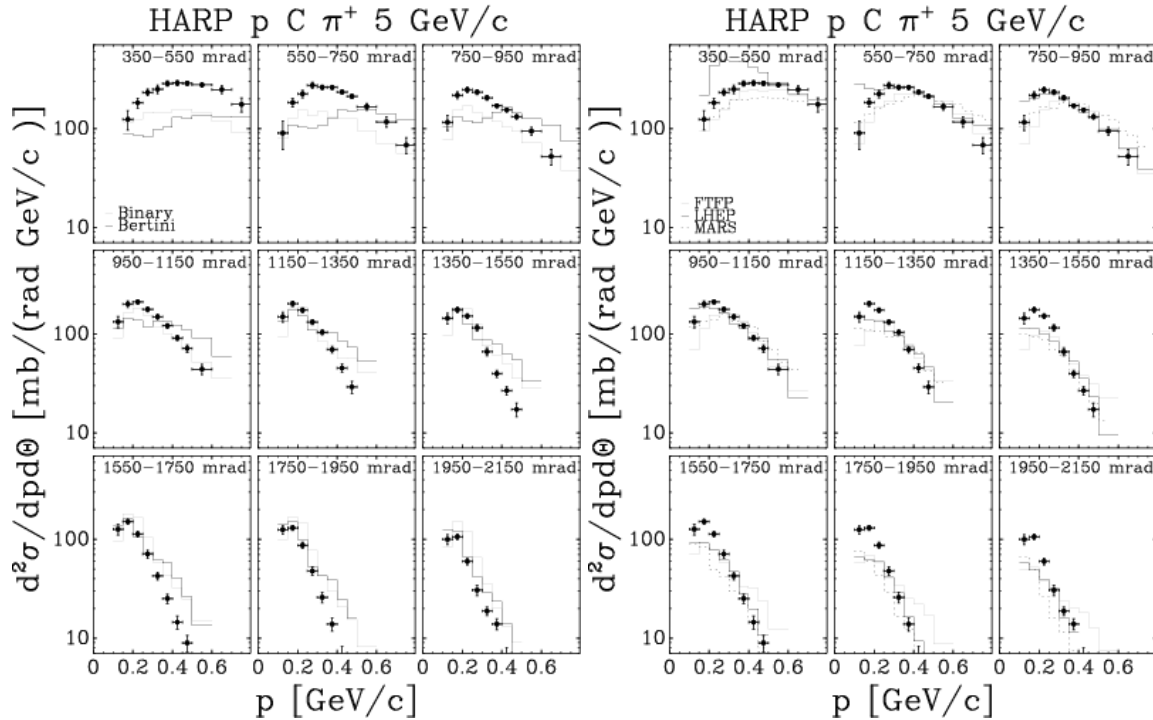


FIG. 23: Comparison of HARP double-differential  $\pi^+$  cross sections for p-C at 5 GeV/c with GEANT4 and MARS MC predictions, using several generator models (see text for details).

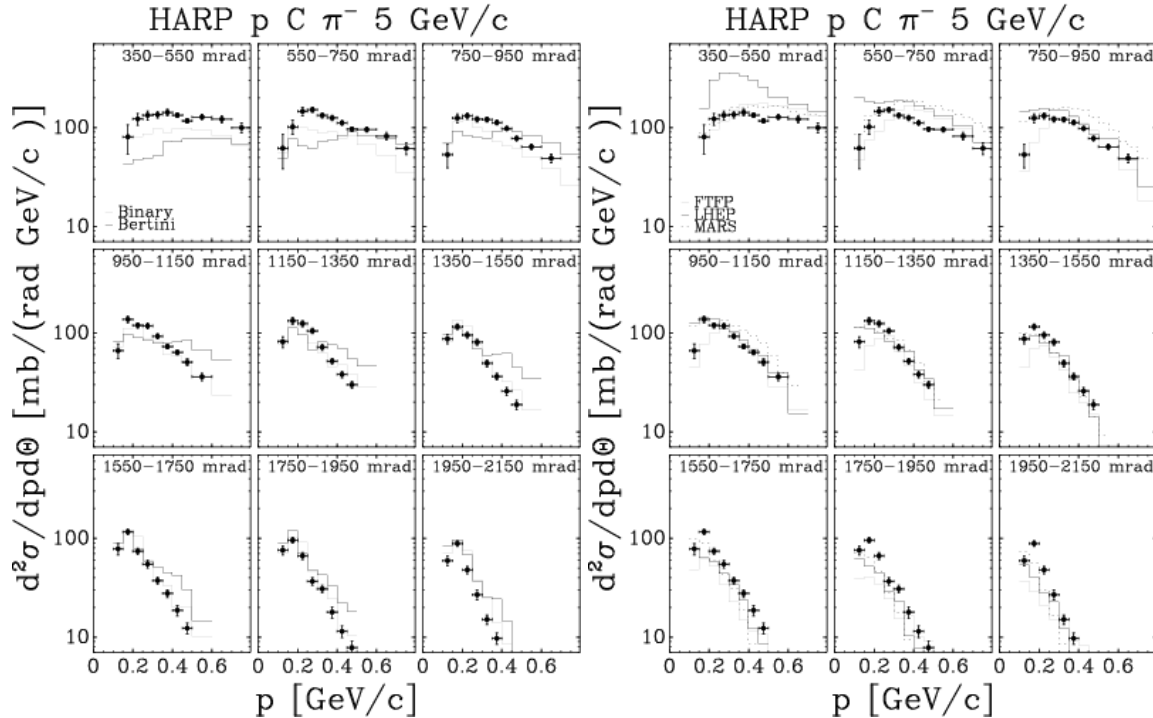


FIG. 24: Comparison of HARP double-differential  $\pi^-$  cross sections for p-C at 5 GeV/c with GEANT4 MC predictions, using several generator models (see text for details).

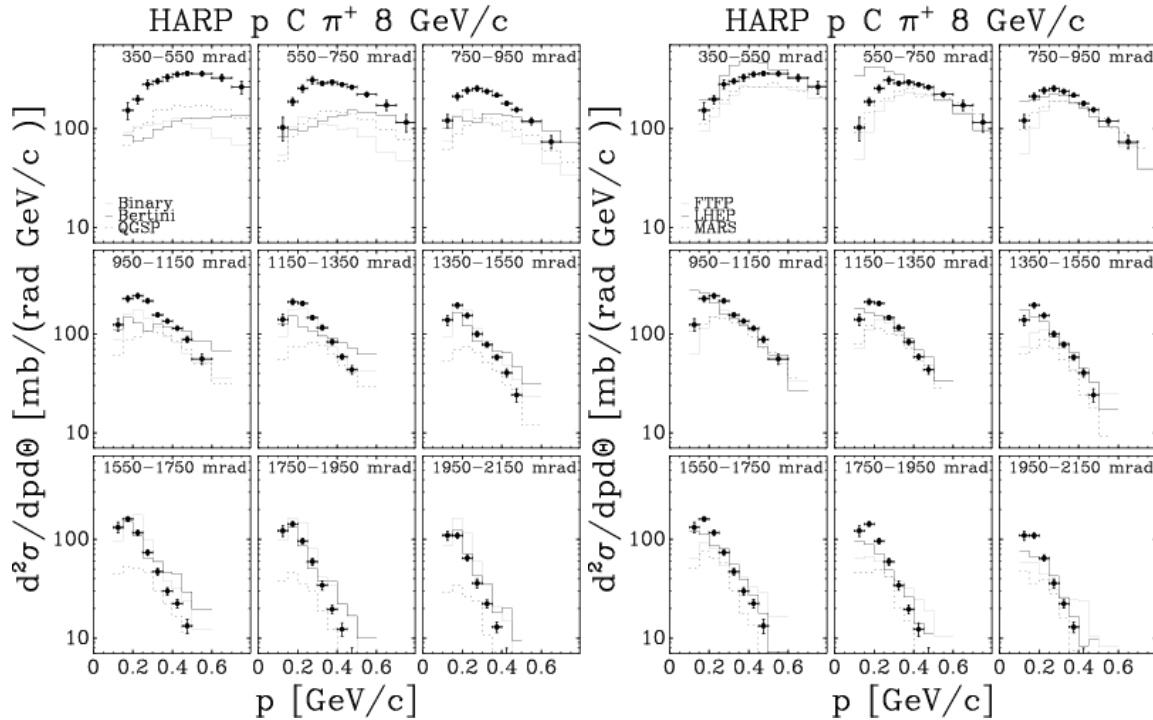


FIG. 25: Comparison of HARP double-differential  $\pi^+$  cross sections for p-C at 8 GeV/c with GEANT4 and MARS MC predictions, using several generator models (see text for details).

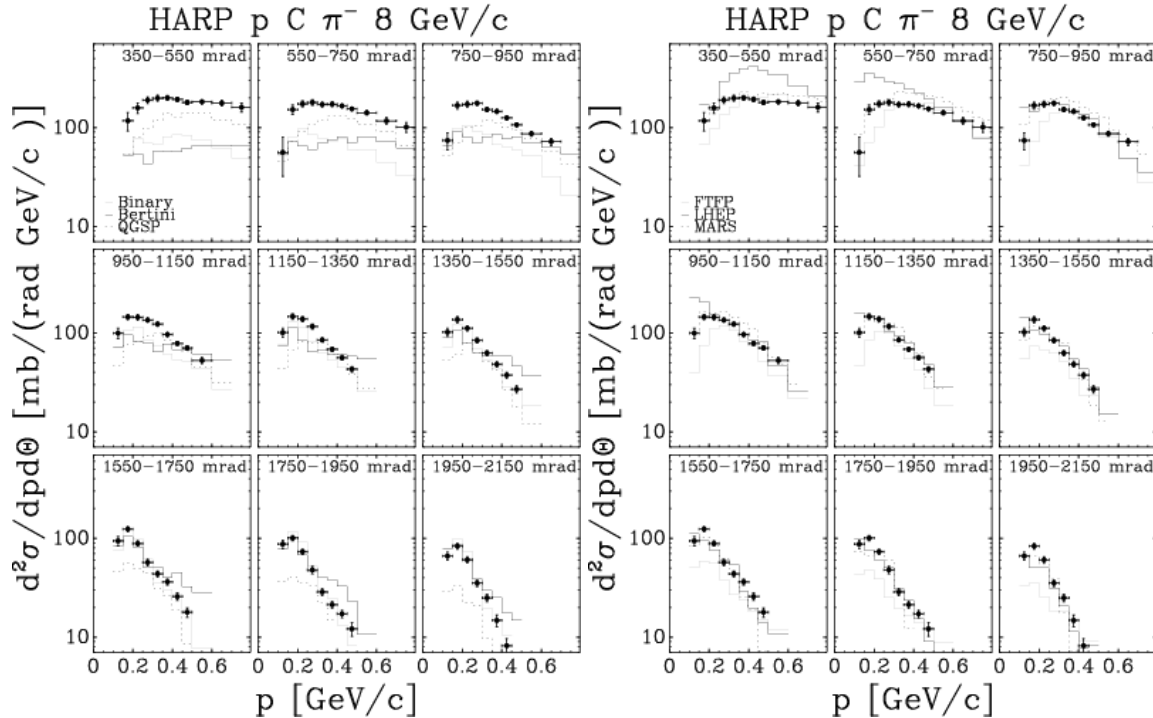


FIG. 26: Comparison of HARP double-differential  $\pi^-$  cross sections for p-C at 8 GeV/c with GEANT4 and MARS MC predictions, using several generator models (see text for details).

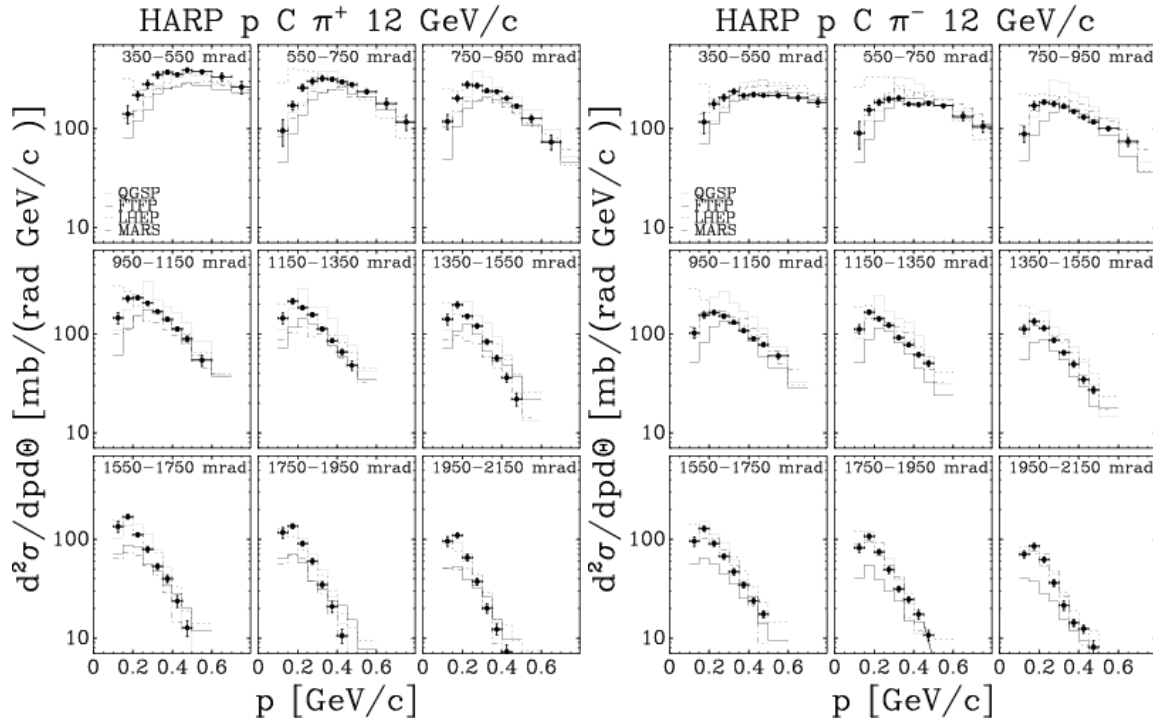


FIG. 27: Comparison of HARP double-differential  $\pi^\pm$  cross sections for p-C at 12 GeV/c with GEANT4 and MARS MC predictions, using several generator models (see text for details).

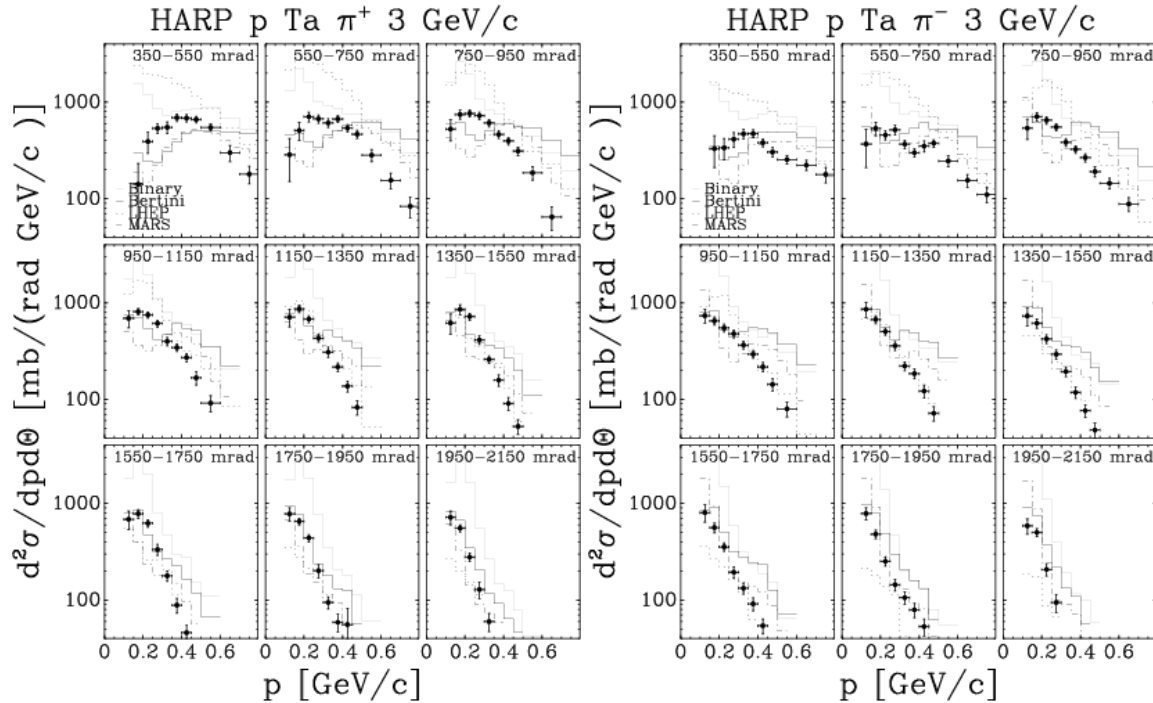


FIG. 28: Comparison of HARP double-differential  $\pi^\pm$  cross sections for p-Ta at 3 GeV/c with GEANT4 and MARS MC predictions, using several generator models (see text for details).

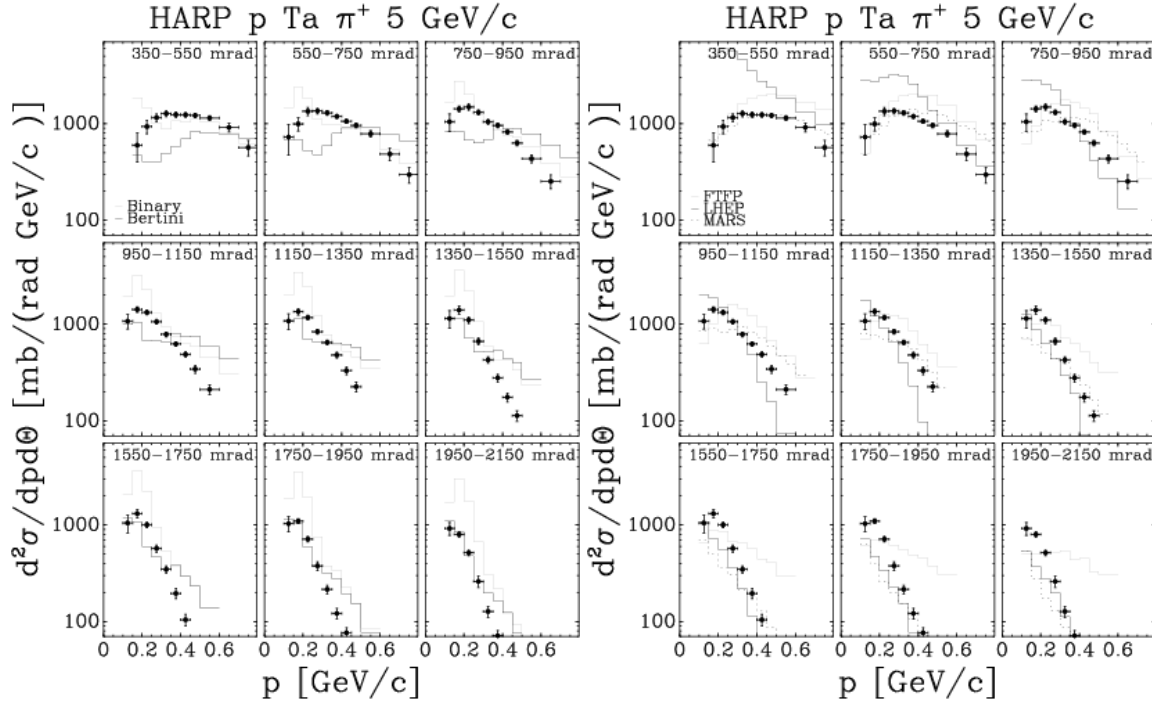


FIG. 29: Comparison of HARP double-differential  $\pi^+$  cross sections for p-Ta at 5 GeV/c with GEANT4 and MARS MC predictions, using several generator models (see text for details).

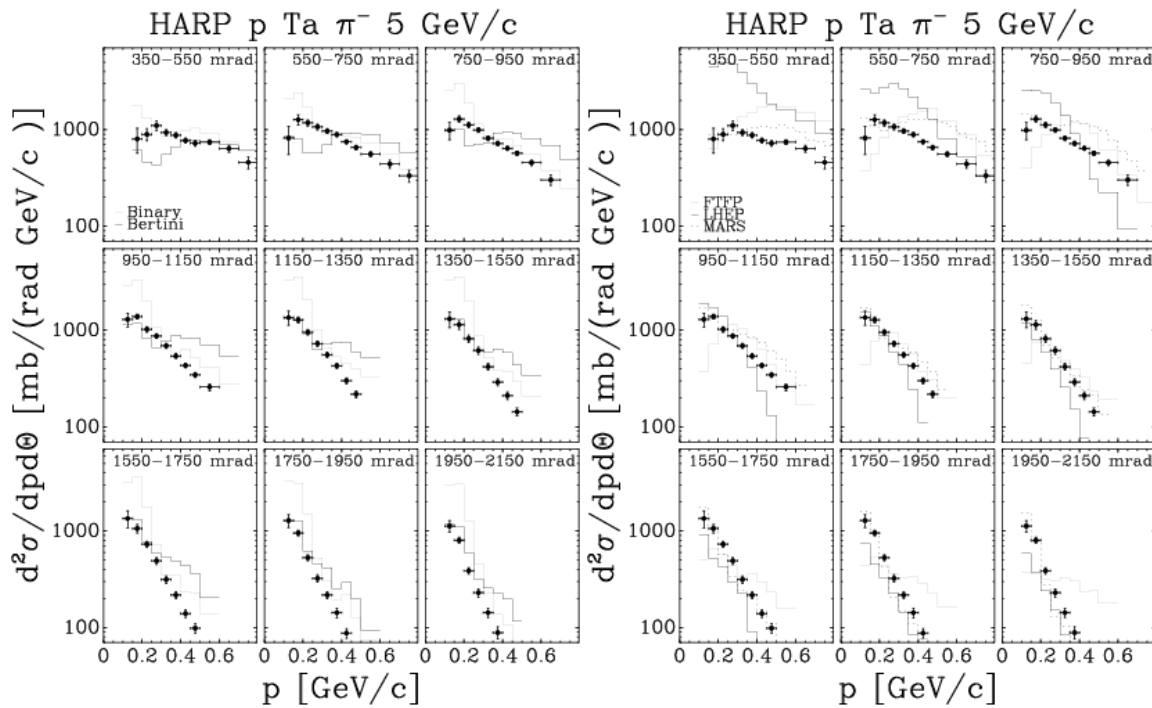


FIG. 30: Comparison of HARP double-differential  $\pi^-$  cross sections for p-Ta at 5 GeV/c with GEANT4 and MARS MC predictions, using several generator models (see text for details).

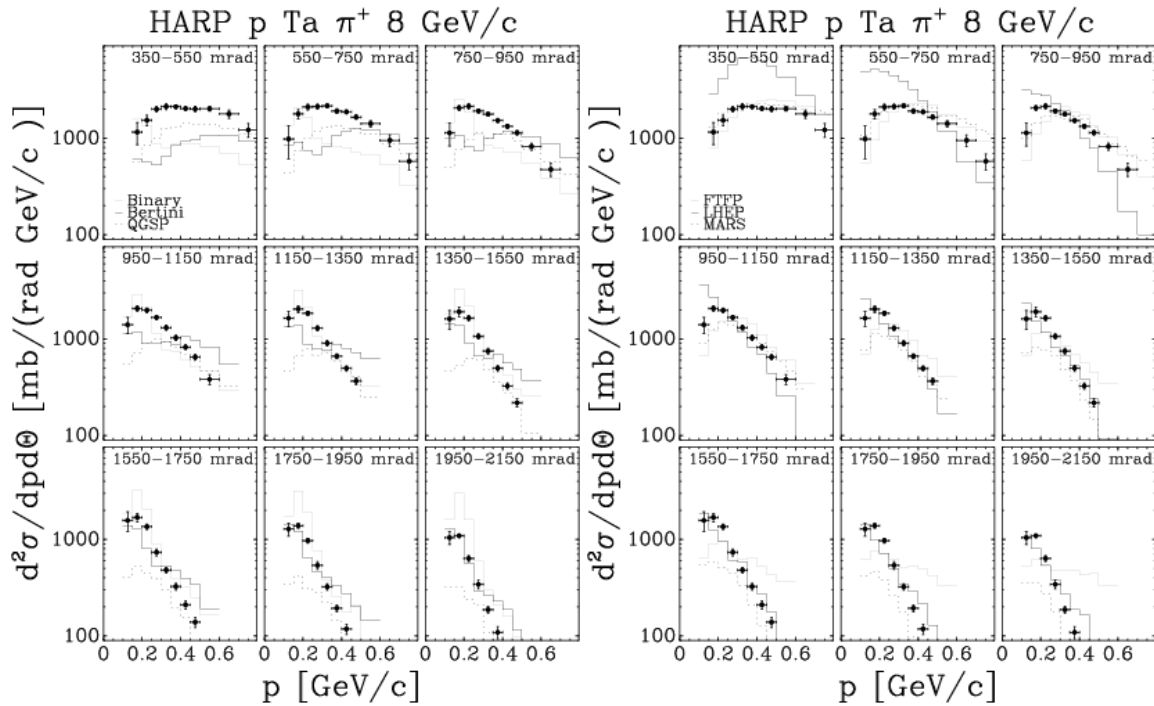


FIG. 31: Comparison of HARP double-differential  $\pi^+$  cross sections for p-Ta at 8 GeV/c with GEANT4 and MARS MC predictions, using several generator models (see text for details).

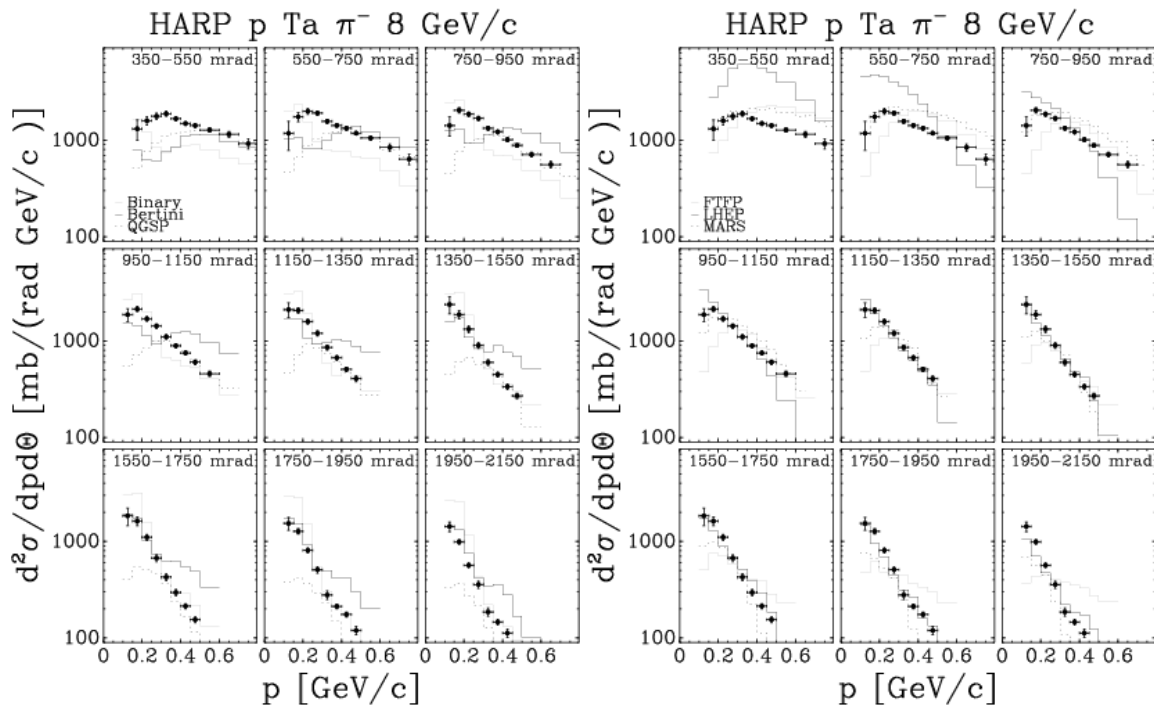


FIG. 32: Comparison of HARP double-differential  $\pi^-$  cross sections for p-Ta at 8 GeV/c with GEANT4 and MARS MC predictions, using several generator models (see text for details).

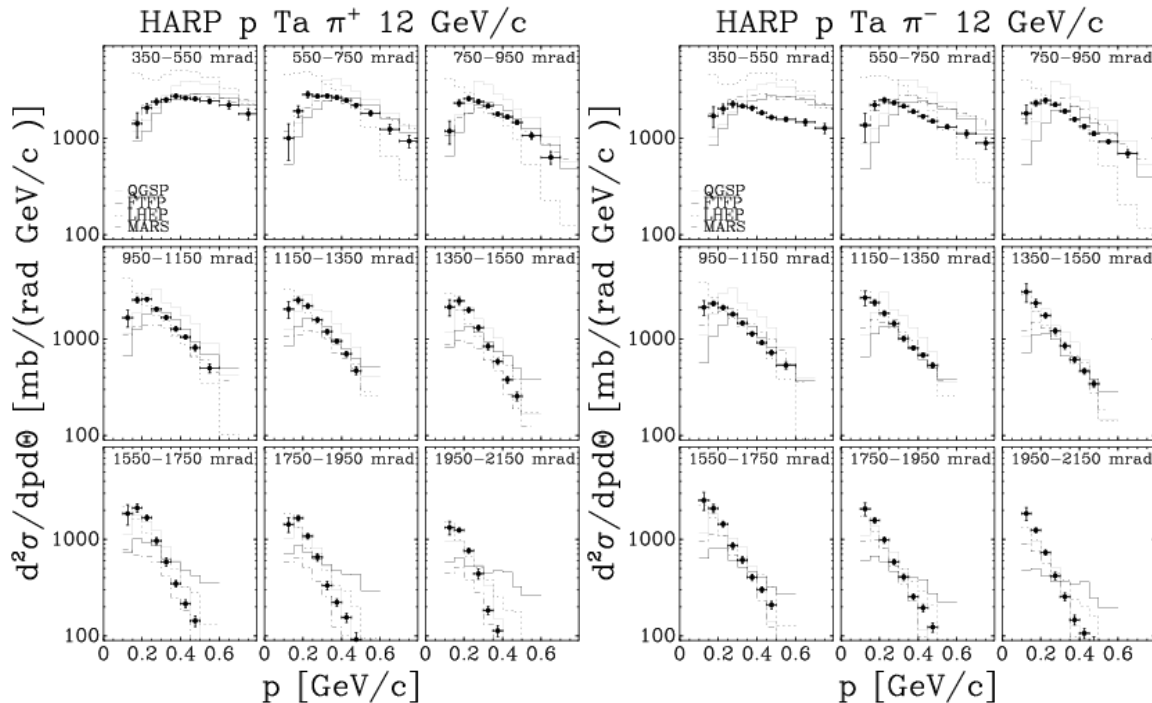


FIG. 33: Comparison of HARP double-differential  $\pi^\pm$  cross sections for p-Ta at 12 GeV/c with GEANT4 and MARS MC predictions, using several generator models (see text for details).

## V. SUMMARY AND CONCLUSIONS

An analysis of the production of pions at large angles with respect to the beam direction for protons of 3 GeV/c, 5 GeV/c, 8 GeV/c, 8.9 GeV/c (Be only), 12 GeV/c and 12.9 GeV/c (Al only) beam momentum impinging on thin (5% interaction length) beryllium, carbon, aluminium, copper, tin, tantalum and lead targets is described. The secondary pion yield is measured in a large angular and momentum range and double-differential cross-sections are obtained. A detailed error estimation has been discussed. Results on the dependence from atomic number A of pion production are also presented.

The data taken with the lead and tantalum targets are relevant for the optimization of the targetry of a Neutrino Factory. The pion yield increases with momentum and in our kinematic range the optimum is between 5 GeV/c and 8 GeV/c.

The use of a single detector for a range of beam momenta makes it possible to measure the dependence of the pion yield on the secondary particle momentum and emission angle  $\theta$  with high precision. The  $A$ -dependence of the cross-section can be studied, using data from a single experiment. Very few pion production measurements in this energy range are reported in the literature. The only comparable results found in the literature agrees with the analysis described in this paper. Hadronic production models describing this energy range have now been compared with our new results.

## VI. ACKNOWLEDGEMENTS

We gratefully acknowledge the help and support of the PS beam staff and of the numerous technical collaborators who contributed to the detector design, construction, commissioning and operation. In particular, we would like to thank G. Barichello, R. Brocard, K. Burin, V. Carassiti, F. Chignoli, D. Conventi, G. Decreuse, M. Delattre, C. Detraz, A. Domeniconi, M. Dwuznik, F. Evangelisti, B. Friend, A. Iaciofano, I. Krasin, D. Lacroix, J.-C. Legrand, M. Lobello, M. Lollo, J. Loquet, F. Marinilli, R. Mazza, J. Mulon, L. Musa, R. Nicholson, A. Pepato, P. Petev, X. Pons, I. Rusinov, M. Scandurra, E. Usenko, and R. van

der Vlugt, for their support in the construction of the detector. The collaboration acknowledges the major contributions and advice of M. Baldo-Ceolin, L. Linssen, M.T. Muciaccia and A. Pullia during the construction of the experiment. The collaboration is indebted to V. Ableev, P. Arce, F. Bergsma, P. Binko, E. Boter, C. Buttar, M. Calvi, M. Campanelli, C. Cavion, A. Chukanov, A. De Min, M. Doucet, D. Düllmann, R. Engel, V. Ermilova, W. Flegel, P. Gruber, Y. Hayato, P. Hodgson, A. Ichikawa, I. Kato, O. Klimov, T. Kobayashi, D. Kustov, M. Laveder, M. Mass, H. Meinhard, T. Nakaya, K. Nishikawa, M. Paganoni, F. Paleari, M. Pasquali, J. Pasternak, C. Pattison, M. Placentino, S. Robbins, G. Santin, S. Simone, A. Tornero, S. Troquereau, S. Ueda, A. Valassi, F. Vannucci and K. Zuber for their contributions to the experiment and to P. Dini for help in MC production.

We acknowledge the contributions of V. Ammosov, G. Chelkov, D. Dedovich, F. Dyak, M. Gostkin, A. Guskov, D. Khartchenko, V. Koreshev, Z. Kroumchtein, I. Nefedov, A. Semak, J. Wotschack, V. Zaets and A. Zhemchugov to the work described in this paper.

The experiment was made possible by grants from the Institut Interuniversitaire des Sciences Nucléaires and the Interuniversitair Instituut voor Kernwetenschappen (Belgium), Ministerio de Educacion y Ciencia, Grant FPA2003-06921-c02-02 and Generalitat Valenciana, grant GV00-054-1, CERN (Geneva, Switzerland), the German Bundesministerium für Bildung und Forschung (Germany), the Istituto Nazionale di Fisica Nucleare (Italy), INR RAS (Moscow) and the Particle Physics and Astronomy Research Council (UK). We gratefully acknowledge their support. This work was supported in part by the Swiss National Science Foundation and the Swiss Agency for Development and Cooperation in the framework of the programme SCOPES - Scientific co-operation between Eastern Europe and Switzerland.

#### **APPENDIX A: CROSS-SECTION DATA**

Results on double differential cross section for protons impinging on thin beryllium, carbon, aluminium, copper, tin, tantalum and lead targets are reported here.

TABLE III: HARP results for the double-differential  $\pi^+$  production cross-section in the laboratory system,  $d^2\sigma^{\pi^+}/(dpd\theta)$  for p–Be interactions. Each row refers to a different ( $p_{\min} \leq p < p_{\max}$ ,  $\theta_{\min} \leq \theta < \theta_{\max}$ ) bin, where  $p$  and  $\theta$  are the pion momentum and polar angle, respectively. The central value as well as the square-root of the diagonal elements of the covariance matrix are given.

$\theta_{\min}$ (rad)	$\theta_{\max}$ (rad)	$p_{\min}$ (GeV/c)	$p_{\max}$ (GeV/c)	$d^2\sigma^{\pi^+}/(dpd\theta)$ barn/(rad GeV/c)				
				<b>3 GeV/c    5 GeV/c    8 GeV/c    8.9 GeV/c    12 GeV/c</b>				
				3	5	8	8.9	12
0.35	0.55	0.15	0.20	0.062±0.011	0.107±0.015	0.122±0.017	0.140±0.017	0.137±0.020
		0.20	0.25	0.079±0.010	0.138±0.013	0.162±0.013	0.184±0.013	0.199±0.013
		0.25	0.30	0.117±0.014	0.187±0.018	0.217±0.020	0.231±0.017	0.240±0.020
		0.30	0.35	0.156±0.017	0.204±0.017	0.241±0.017	0.249±0.020	0.269±0.018
		0.35	0.40	0.164±0.014	0.238±0.017	0.258±0.021	0.269±0.016	0.251±0.014
		0.40	0.45	0.165±0.011	0.223±0.012	0.264±0.012	0.284±0.012	0.297±0.022
		0.45	0.50	0.164±0.011	0.230±0.014	0.271±0.014	0.300±0.016	0.319±0.016
		0.50	0.60	0.162±0.013	0.230±0.013	0.284±0.016	0.292±0.017	0.324±0.016
		0.60	0.70	0.121±0.018	0.214±0.021	0.282±0.027	0.250±0.025	0.271±0.029
		0.70	0.80	0.068±0.016	0.157±0.028	0.210±0.032	0.182±0.029	0.211±0.033
0.55	0.75	0.10	0.15	0.047±0.013	0.080±0.017	0.082±0.019	0.088±0.016	0.085±0.019
		0.15	0.20	0.111±0.012	0.136±0.013	0.145±0.012	0.141±0.010	0.145±0.010
		0.20	0.25	0.146±0.015	0.182±0.014	0.218±0.016	0.205±0.015	0.201±0.018
		0.25	0.30	0.161±0.013	0.198±0.016	0.220±0.016	0.229±0.015	0.237±0.015
		0.30	0.35	0.171±0.017	0.211±0.017	0.226±0.013	0.239±0.013	0.252±0.017
		0.35	0.40	0.173±0.011	0.213±0.011	0.219±0.011	0.231±0.010	0.258±0.012
		0.40	0.45	0.145±0.011	0.172±0.009	0.224±0.011	0.218±0.008	0.237±0.010
		0.45	0.50	0.130±0.010	0.171±0.009	0.206±0.010	0.211±0.009	0.210±0.009
		0.50	0.60	0.089±0.012	0.150±0.012	0.187±0.013	0.179±0.013	0.186±0.012
		0.60	0.70	0.051±0.010	0.099±0.015	0.129±0.019	0.128±0.018	0.138±0.019
0.75	0.95	0.10	0.15	0.082±0.013	0.073±0.014	0.093±0.014	0.092±0.013	0.101±0.015
		0.15	0.20	0.138±0.015	0.161±0.013	0.158±0.011	0.163±0.011	0.163±0.013
		0.20	0.25	0.156±0.014	0.175±0.012	0.181±0.014	0.195±0.012	0.197±0.012
		0.25	0.30	0.154±0.012	0.169±0.010	0.185±0.011	0.214±0.011	0.197±0.012
		0.30	0.35	0.126±0.010	0.148±0.010	0.192±0.012	0.189±0.008	0.197±0.010
		0.35	0.40	0.120±0.009	0.139±0.008	0.165±0.008	0.165±0.006	0.172±0.007
		0.40	0.45	0.098±0.009	0.125±0.007	0.136±0.007	0.140±0.005	0.143±0.006
		0.45	0.50	0.071±0.008	0.109±0.008	0.118±0.006	0.123±0.006	0.128±0.007
		0.50	0.60	0.047±0.006	0.072±0.009	0.099±0.008	0.092±0.009	0.096±0.009
		0.60	0.70	0.025±0.006	0.039±0.008	0.063±0.010	0.055±0.009	0.057±0.010
0.95	1.15	0.10	0.15	0.097±0.012	0.087±0.013	0.089±0.013	0.094±0.012	0.094±0.013
		0.15	0.20	0.127±0.013	0.144±0.011	0.153±0.011	0.154±0.009	0.175±0.012
		0.20	0.25	0.145±0.011	0.180±0.014	0.160±0.009	0.168±0.008	0.177±0.010
		0.25	0.30	0.120±0.010	0.154±0.011	0.148±0.008	0.159±0.008	0.157±0.007
		0.30	0.35	0.097±0.009	0.107±0.006	0.125±0.007	0.123±0.006	0.126±0.006
		0.35	0.40	0.058±0.006	0.089±0.006	0.102±0.006	0.107±0.005	0.108±0.005
		0.40	0.45	0.045±0.004	0.071±0.005	0.080±0.005	0.081±0.005	0.090±0.005
		0.45	0.50	0.033±0.004	0.055±0.005	0.062±0.005	0.062±0.005	0.069±0.006
		0.50	0.60	0.018±0.003	0.034±0.005	0.040±0.005	0.041±0.005	0.043±0.006

$\theta_{\min}$ (rad)	$\theta_{\max}$ (rad)	$p_{\min}$ (GeV/c)	$p_{\max}$ (GeV/c)	$d^2\sigma^{\pi^+}/(dpd\theta)$ barn/(rad GeV/c)				
				<b>3 GeV/c</b>	<b>5 GeV/c</b>	<b>8 GeV/c</b>	<b>8.9 GeV/c</b>	<b>12 GeV/c</b>
1.15	1.35	0.10	0.15	0.093±0.012	0.084±0.011	0.099±0.012	0.101±0.013	0.099±0.013
		0.15	0.20	0.121±0.013	0.131±0.010	0.157±0.010	0.151±0.008	0.134±0.009
		0.20	0.25	0.120±0.010	0.126±0.008	0.133±0.007	0.141±0.006	0.137±0.006
		0.25	0.30	0.078±0.008	0.106±0.008	0.102±0.006	0.106±0.005	0.115±0.006
		0.30	0.35	0.048±0.007	0.071±0.005	0.081±0.006	0.078±0.003	0.078±0.005
		0.35	0.40	0.031±0.003	0.051±0.004	0.067±0.004	0.065±0.003	0.066±0.003
		0.40	0.45	0.025±0.003	0.038±0.004	0.050±0.004	0.046±0.004	0.049±0.004
		0.45	0.50	0.016±0.003	0.025±0.003	0.035±0.004	0.032±0.003	0.035±0.004
1.35	1.55	0.10	0.15	0.086±0.011	0.102±0.012	0.082±0.011	0.101±0.011	0.096±0.012
		0.15	0.20	0.118±0.012	0.119±0.009	0.139±0.011	0.135±0.007	0.136±0.009
		0.20	0.25	0.084±0.009	0.120±0.008	0.116±0.007	0.110±0.006	0.108±0.006
		0.25	0.30	0.062±0.007	0.078±0.007	0.081±0.007	0.081±0.005	0.082±0.005
		0.30	0.35	0.036±0.005	0.048±0.005	0.055±0.004	0.054±0.003	0.056±0.004
		0.35	0.40	0.021±0.003	0.034±0.003	0.040±0.003	0.039±0.003	0.040±0.003
		0.40	0.45	0.012±0.002	0.022±0.003	0.026±0.003	0.026±0.002	0.028±0.003
		0.45	0.50	0.008±0.002	0.013±0.002	0.015±0.003	0.019±0.003	0.018±0.003
1.55	1.75	0.10	0.15	0.070±0.012	0.080±0.010	0.085±0.012	0.085±0.011	0.095±0.011
		0.15	0.20	0.093±0.009	0.118±0.009	0.116±0.007	0.115±0.005	0.106±0.006
		0.20	0.25	0.054±0.007	0.076±0.007	0.076±0.005	0.086±0.005	0.084±0.005
		0.25	0.30	0.035±0.005	0.050±0.005	0.057±0.004	0.056±0.003	0.051±0.005
		0.30	0.35	0.020±0.004	0.029±0.003	0.037±0.003	0.037±0.003	0.030±0.002
		0.35	0.40	0.010±0.002	0.019±0.002	0.026±0.003	0.023±0.002	0.023±0.002
		0.40	0.45	0.008±0.002	0.011±0.002	0.015±0.002	0.014±0.002	0.014±0.002
		0.45	0.50	0.004±0.001	0.006±0.001	0.008±0.002	0.009±0.001	0.008±0.002
1.75	1.95	0.10	0.15	0.060±0.009	0.090±0.011	0.086±0.011	0.081±0.009	0.073±0.010
		0.15	0.20	0.096±0.011	0.096±0.007	0.096±0.006	0.099±0.004	0.099±0.006
		0.20	0.25	0.060±0.009	0.047±0.005	0.065±0.005	0.062±0.004	0.056±0.005
		0.25	0.30	0.020±0.005	0.036±0.004	0.036±0.004	0.041±0.003	0.033±0.002
		0.30	0.35	0.011±0.002	0.018±0.003	0.023±0.002	0.026±0.002	0.024±0.002
		0.35	0.40	0.006±0.002	0.011±0.002	0.013±0.002	0.015±0.002	0.015±0.002
		0.40	0.45	0.003±0.001	0.005±0.001	0.006±0.001	0.007±0.001	0.007±0.002
		0.45	0.50	0.001±0.001	0.003±0.001	0.003±0.001	0.004±0.001	0.004±0.001
1.95	2.15	0.10	0.15	0.063±0.011	0.060±0.008	0.063±0.008	0.068±0.007	0.055±0.007
		0.15	0.20	0.063±0.008	0.082±0.006	0.080±0.006	0.070±0.004	0.073±0.005
		0.20	0.25	0.033±0.005	0.041±0.005	0.044±0.004	0.047±0.003	0.047±0.005
		0.25	0.30	0.013±0.003	0.020±0.003	0.027±0.003	0.027±0.002	0.026±0.003
		0.30	0.35	0.008±0.002	0.009±0.001	0.014±0.002	0.016±0.001	0.013±0.002
		0.35	0.40	0.004±0.002	0.009±0.002	0.007±0.001	0.008±0.001	0.008±0.001
		0.40	0.45	0.002±0.001	0.004±0.001	0.004±0.001	0.004±0.001	0.004±0.001
		0.45	0.50		0.002±0.001	0.002±0.001	0.002±0.001	0.002±0.001

TABLE IV: HARP results for the double-differential  $\pi^-$  production cross-section in the laboratory system,  $d^2\sigma^{\pi^-}/(dpd\theta)$  for p–Be interactions. Each row refers to a different ( $p_{\min} \leq p < p_{\max}$ ,  $\theta_{\min} \leq \theta < \theta_{\max}$ ) bin, where  $p$  and  $\theta$  are the pion momentum and polar angle, respectively. The central value as well as the square-root of the diagonal elements of the covariance matrix are given.

$\theta_{\min}$ (rad)	$\theta_{\max}$ (rad)	$p_{\min}$ (GeV/c)	$p_{\max}$ (GeV/c)	$d^2\sigma^{\pi^-}/(dpd\theta)$ barn/(rad GeV/c)				
				<b>3 GeV/c    5 GeV/c    8 GeV/c    8.9 GeV/c    12 GeV/c</b>				
				3	5	8	8.9	12
0.35	0.55	0.15	0.20	0.048±0.009	0.084±0.013	0.114±0.015	0.124±0.015	0.124±0.020
		0.20	0.25	0.068±0.009	0.095±0.008	0.139±0.011	0.147±0.009	0.170±0.011
		0.25	0.30	0.060±0.008	0.134±0.013	0.160±0.012	0.170±0.011	0.182±0.012
		0.30	0.35	0.079±0.010	0.129±0.009	0.154±0.011	0.171±0.009	0.186±0.013
		0.35	0.40	0.069±0.007	0.111±0.007	0.162±0.010	0.163±0.008	0.184±0.010
		0.40	0.45	0.066±0.007	0.116±0.010	0.155±0.008	0.165±0.009	0.168±0.008
		0.45	0.50	0.057±0.006	0.121±0.008	0.148±0.008	0.164±0.008	0.162±0.008
		0.50	0.60	0.053±0.005	0.129±0.008	0.159±0.010	0.160±0.009	0.172±0.010
		0.60	0.70	0.051±0.006	0.101±0.012	0.157±0.013	0.152±0.013	0.170±0.013
		0.70	0.80	0.039±0.007	0.084±0.011	0.143±0.018	0.128±0.014	0.155±0.018
0.55	0.75	0.10	0.15	0.026±0.008	0.069±0.015	0.070±0.016	0.073±0.015	0.092±0.020
		0.15	0.20	0.058±0.009	0.093±0.009	0.111±0.010	0.123±0.006	0.131±0.008
		0.20	0.25	0.057±0.007	0.126±0.009	0.161±0.012	0.148±0.010	0.135±0.011
		0.25	0.30	0.062±0.008	0.119±0.009	0.152±0.008	0.153±0.009	0.160±0.009
		0.30	0.35	0.077±0.008	0.113±0.009	0.134±0.008	0.150±0.008	0.159±0.009
		0.35	0.40	0.076±0.007	0.111±0.007	0.144±0.010	0.146±0.007	0.151±0.007
		0.40	0.45	0.059±0.006	0.107±0.006	0.146±0.008	0.137±0.006	0.148±0.007
		0.45	0.50	0.052±0.005	0.105±0.007	0.127±0.006	0.129±0.005	0.140±0.006
		0.50	0.60	0.049±0.005	0.095±0.007	0.111±0.006	0.120±0.006	0.131±0.007
		0.60	0.70	0.041±0.006	0.076±0.007	0.100±0.008	0.098±0.010	0.111±0.011
0.75	0.95	0.10	0.15	0.044±0.008	0.056±0.009	0.070±0.010	0.069±0.009	0.079±0.011
		0.15	0.20	0.091±0.011	0.107±0.010	0.120±0.010	0.130±0.008	0.134±0.010
		0.20	0.25	0.078±0.008	0.114±0.008	0.144±0.010	0.139±0.007	0.136±0.008
		0.25	0.30	0.073±0.008	0.111±0.007	0.119±0.006	0.135±0.007	0.141±0.008
		0.30	0.35	0.063±0.006	0.096±0.006	0.110±0.007	0.123±0.005	0.132±0.008
		0.35	0.40	0.060±0.006	0.084±0.005	0.109±0.006	0.108±0.004	0.115±0.005
		0.40	0.45	0.048±0.005	0.080±0.005	0.091±0.004	0.099±0.003	0.099±0.004
		0.45	0.50	0.036±0.004	0.074±0.004	0.087±0.005	0.091±0.003	0.091±0.004
		0.50	0.60	0.033±0.004	0.060±0.005	0.075±0.005	0.078±0.004	0.080±0.005
		0.60	0.70	0.023±0.004	0.042±0.006	0.060±0.006	0.058±0.006	0.062±0.006
0.95	1.15	0.10	0.15	0.038±0.007	0.066±0.009	0.070±0.009	0.077±0.008	0.072±0.009
		0.15	0.20	0.069±0.008	0.120±0.011	0.109±0.009	0.131±0.008	0.119±0.008
		0.20	0.25	0.065±0.008	0.107±0.008	0.117±0.008	0.126±0.006	0.122±0.007
		0.25	0.30	0.061±0.006	0.090±0.008	0.116±0.007	0.114±0.005	0.114±0.006
		0.30	0.35	0.065±0.007	0.076±0.005	0.097±0.005	0.098±0.004	0.096±0.004
		0.35	0.40	0.049±0.006	0.062±0.004	0.088±0.004	0.079±0.003	0.084±0.004
		0.40	0.45	0.034±0.004	0.055±0.004	0.068±0.005	0.068±0.003	0.070±0.004
		0.45	0.50	0.025±0.004	0.043±0.004	0.054±0.003	0.058±0.002	0.059±0.003
		0.50	0.60	0.018±0.003	0.029±0.003	0.044±0.003	0.044±0.003	0.046±0.003

$\theta_{\min}$ (rad)	$\theta_{\max}$ (rad)	$p_{\min}$ (GeV/c)	$p_{\max}$ (GeV/c)	$d^2\sigma^{\pi^-}/(dpd\theta)$ barn/(rad GeV/c)				
				<b>3 GeV/c</b>	<b>5 GeV/c</b>	<b>8 GeV/c</b>	<b>8.9 GeV/c</b>	<b>12 GeV/c</b>
1.15	1.35	0.10	0.15	0.039±0.007	0.073±0.010	0.085±0.008	0.075±0.007	0.085±0.009
		0.15	0.20	0.067±0.009	0.101±0.007	0.105±0.007	0.122±0.008	0.117±0.008
		0.20	0.25	0.088±0.010	0.089±0.006	0.100±0.006	0.109±0.004	0.112±0.006
		0.25	0.30	0.059±0.008	0.077±0.005	0.087±0.005	0.091±0.004	0.092±0.005
		0.30	0.35	0.034±0.005	0.050±0.005	0.072±0.004	0.069±0.003	0.075±0.004
		0.35	0.40	0.022±0.003	0.036±0.003	0.055±0.004	0.055±0.002	0.057±0.003
		0.40	0.45	0.015±0.002	0.034±0.003	0.043±0.003	0.044±0.002	0.043±0.003
		0.45	0.50	0.012±0.002	0.031±0.003	0.036±0.002	0.035±0.002	0.034±0.002
1.35	1.55	0.10	0.15	0.057±0.009	0.073±0.009	0.061±0.007	0.080±0.008	0.078±0.009
		0.15	0.20	0.061±0.007	0.098±0.008	0.106±0.009	0.109±0.006	0.110±0.009
		0.20	0.25	0.063±0.007	0.077±0.006	0.102±0.006	0.095±0.004	0.097±0.006
		0.25	0.30	0.034±0.005	0.060±0.005	0.077±0.005	0.070±0.004	0.074±0.005
		0.30	0.35	0.027±0.004	0.043±0.005	0.051±0.004	0.050±0.002	0.049±0.003
		0.35	0.40	0.019±0.003	0.027±0.003	0.036±0.003	0.037±0.002	0.038±0.002
		0.40	0.45	0.015±0.002	0.022±0.002	0.026±0.002	0.029±0.002	0.029±0.003
		0.45	0.50	0.010±0.002	0.019±0.002	0.020±0.002	0.021±0.002	0.021±0.002
1.55	1.75	0.10	0.15	0.042±0.007	0.068±0.008	0.072±0.009	0.073±0.008	0.084±0.010
		0.15	0.20	0.067±0.009	0.085±0.007	0.090±0.006	0.095±0.005	0.090±0.006
		0.20	0.25	0.052±0.009	0.073±0.006	0.072±0.005	0.078±0.004	0.078±0.005
		0.25	0.30	0.016±0.003	0.057±0.005	0.055±0.005	0.055±0.003	0.054±0.004
		0.30	0.35	0.012±0.002	0.035±0.005	0.038±0.003	0.037±0.002	0.041±0.003
		0.35	0.40	0.014±0.003	0.020±0.003	0.032±0.003	0.027±0.002	0.027±0.003
		0.40	0.45	0.009±0.002	0.012±0.002	0.021±0.002	0.020±0.001	0.018±0.002
		0.45	0.50	0.006±0.002	0.008±0.001	0.015±0.002	0.013±0.001	0.014±0.001
1.75	1.95	0.10	0.15	0.038±0.007	0.053±0.006	0.063±0.008	0.063±0.006	0.060±0.008
		0.15	0.20	0.052±0.007	0.067±0.006	0.081±0.006	0.086±0.004	0.085±0.006
		0.20	0.25	0.029±0.006	0.053±0.005	0.054±0.004	0.061±0.003	0.063±0.004
		0.25	0.30	0.020±0.004	0.037±0.004	0.038±0.003	0.039±0.003	0.041±0.003
		0.30	0.35	0.013±0.004	0.019±0.003	0.027±0.002	0.024±0.002	0.031±0.002
		0.35	0.40	0.006±0.002	0.013±0.002	0.018±0.002	0.017±0.001	0.019±0.003
		0.40	0.45	0.004±0.001	0.008±0.001	0.012±0.001	0.012±0.001	0.010±0.002
		0.45	0.50	0.003±0.001	0.005±0.001	0.008±0.001	0.009±0.001	0.007±0.001
1.95	2.15	0.10	0.15	0.049±0.008	0.047±0.007	0.062±0.007	0.055±0.006	0.047±0.005
		0.15	0.20	0.038±0.006	0.068±0.006	0.061±0.005	0.067±0.003	0.068±0.006
		0.20	0.25	0.023±0.005	0.048±0.005	0.046±0.004	0.049±0.002	0.044±0.005
		0.25	0.30	0.009±0.003	0.026±0.003	0.025±0.003	0.029±0.002	0.023±0.002
		0.30	0.35	0.005±0.002	0.015±0.002	0.017±0.002	0.017±0.001	0.019±0.002
		0.35	0.40	0.001±0.001	0.009±0.001	0.012±0.001	0.013±0.001	0.012±0.001
		0.40	0.45		0.006±0.001	0.009±0.002	0.008±0.001	0.009±0.001
		0.45	0.50		0.003±0.001	0.005±0.001	0.005±0.001	0.006±0.001

TABLE V: HARP results for the double-differential  $\pi^+$  production cross-section in the laboratory system,  $d^2\sigma^{\pi^+}/(dpd\theta)$  for p–C interactions. Each row refers to a different ( $p_{\min} \leq p < p_{\max}$ ,  $\theta_{\min} \leq \theta < \theta_{\max}$ ) bin, where  $p$  and  $\theta$  are the pion momentum and polar angle, respectively. The central value as well as the square-root of the diagonal elements of the covariance matrix are given.

$\theta_{\min}$ (rad)	$\theta_{\max}$ (rad)	$p_{\min}$ (GeV/c)	$p_{\max}$ (GeV/c)	$d^2\sigma^{\pi^+}/(dpd\theta)$				
				$\text{barn}/(\text{rad GeV}/c)$				
				<b>3 GeV/c</b>	<b>5 GeV/c</b>	<b>8 GeV/c</b>	<b>12 GeV/c</b>	
0.35	0.55	0.15	0.20	0.05±0.02	0.12±0.03	0.15±0.03	0.14±0.03	
		0.20	0.25	0.10±0.02	0.18±0.02	0.20±0.02	0.22±0.02	
		0.25	0.30	0.15±0.02	0.23±0.02	0.28±0.03	0.28±0.02	
		0.30	0.35	0.16±0.02	0.25±0.03	0.30±0.02	0.35±0.03	
		0.35	0.40	0.18±0.02	0.29±0.02	0.33±0.03	0.37±0.02	
		0.40	0.45	0.19±0.01	0.29±0.02	0.35±0.02	0.35±0.02	
		0.45	0.50	0.19±0.01	0.29±0.01	0.36±0.02	0.39±0.02	
		0.50	0.60	0.18±0.01	0.28±0.01	0.36±0.02	0.38±0.02	
		0.60	0.70	0.13±0.02	0.25±0.02	0.33±0.03	0.33±0.03	
		0.70	0.80	0.07±0.02	0.18±0.03	0.26±0.04	0.26±0.04	
0.55	0.75	0.10	0.15	0.09±0.03	0.09±0.03	0.10±0.03	0.10±0.03	
		0.15	0.20	0.13±0.02	0.18±0.02	0.19±0.02	0.17±0.02	
		0.20	0.25	0.20±0.02	0.22±0.02	0.26±0.02	0.26±0.02	
		0.25	0.30	0.22±0.02	0.27±0.02	0.31±0.03	0.30±0.02	
		0.30	0.35	0.24±0.02	0.26±0.01	0.29±0.02	0.32±0.02	
		0.35	0.40	0.21±0.02	0.26±0.01	0.30±0.02	0.32±0.01	
		0.40	0.45	0.18±0.01	0.23±0.01	0.28±0.01	0.30±0.01	
		0.45	0.50	0.18±0.01	0.21±0.01	0.26±0.01	0.28±0.01	
		0.50	0.60	0.11±0.02	0.17±0.01	0.22±0.01	0.24±0.01	
		0.60	0.70	0.08±0.01	0.12±0.01	0.17±0.02	0.18±0.02	
0.75	0.95	0.10	0.15	0.09±0.02	0.12±0.02	0.12±0.02	0.12±0.02	
		0.15	0.20	0.17±0.02	0.22±0.02	0.21±0.02	0.20±0.02	
		0.20	0.25	0.21±0.02	0.25±0.02	0.24±0.02	0.28±0.02	
		0.25	0.30	0.19±0.02	0.23±0.01	0.25±0.02	0.27±0.01	
		0.30	0.35	0.20±0.02	0.21±0.01	0.24±0.01	0.24±0.01	
		0.35	0.40	0.14±0.02	0.17±0.01	0.22±0.01	0.24±0.01	
		0.40	0.45	0.10±0.01	0.15±0.01	0.18±0.01	0.20±0.01	
		0.45	0.50	0.08±0.01	0.13±0.01	0.16±0.01	0.17±0.01	
		0.50	0.60	0.05±0.01	0.09±0.01	0.12±0.01	0.13±0.01	
		0.60	0.70	0.03±0.01	0.05±0.01	0.07±0.01	0.07±0.01	
0.95	1.15	0.10	0.15	0.14±0.02	0.13±0.02	0.12±0.02	0.15±0.02	
		0.15	0.20	0.22±0.02	0.20±0.02	0.23±0.02	0.23±0.02	
		0.20	0.25	0.19±0.01	0.21±0.01	0.24±0.01	0.23±0.01	
		0.25	0.30	0.16±0.01	0.18±0.01	0.22±0.01	0.21±0.01	
		0.30	0.35	0.10±0.01	0.15±0.01	0.16±0.01	0.17±0.01	
		0.35	0.40	0.07±0.01	0.12±0.01	0.13±0.01	0.14±0.01	
		0.40	0.45	0.06±0.01	0.09±0.01	0.11±0.01	0.11±0.01	
		0.45	0.50	0.04±0.01	0.07±0.01	0.09±0.01	0.09±0.01	
		0.50	0.60	0.02±0.01	0.04±0.01	0.06±0.01	0.05±0.01	

$\theta_{\min}$ (rad)	$\theta_{\max}$ (rad)	$p_{\min}$ (GeV/c)	$p_{\max}$ (GeV/c)	$d^2\sigma^{\pi^+}/(dpd\theta)$			
				barn/(rad GeV/c)			
				<b>3 GeV/c</b>	<b>5 GeV/c</b>	<b>8 GeV/c</b>	<b>12 GeV/c</b>
1.15	1.35	0.10	0.15	0.14±0.02	0.15±0.02	0.14±0.02	0.14±0.02
		0.15	0.20	0.18±0.02	0.20±0.01	0.21±0.01	0.21±0.01
		0.20	0.25	0.16±0.01	0.17±0.01	0.20±0.01	0.18±0.01
		0.25	0.30	0.09±0.01	0.13±0.01	0.15±0.01	0.16±0.01
		0.30	0.35	0.07±0.01	0.10±0.01	0.12±0.01	0.11±0.01
		0.35	0.40	0.06±0.01	0.07±0.01	0.08±0.01	0.09±0.01
		0.40	0.45	0.03±0.01	0.05±0.01	0.06±0.01	0.07±0.01
		0.45	0.50	0.02±0.01	0.03±0.01	0.04±0.01	0.05±0.01
1.35	1.55	0.10	0.15	0.13±0.02	0.14±0.02	0.14±0.02	0.14±0.02
		0.15	0.20	0.19±0.02	0.18±0.01	0.20±0.01	0.20±0.01
		0.20	0.25	0.14±0.01	0.15±0.01	0.15±0.01	0.15±0.01
		0.25	0.30	0.10±0.01	0.12±0.01	0.10±0.01	0.12±0.01
		0.30	0.35	0.05±0.01	0.07±0.01	0.08±0.01	0.08±0.01
		0.35	0.40	0.03±0.01	0.04±0.01	0.06±0.01	0.06±0.01
		0.40	0.45	0.02±0.01	0.03±0.01	0.04±0.01	0.04±0.01
		0.45	0.50	0.01±0.01	0.02±0.01	0.02±0.01	0.02±0.01
1.55	1.75	0.10	0.15	0.14±0.02	0.13±0.02	0.13±0.02	0.13±0.02
		0.15	0.20	0.18±0.02	0.15±0.01	0.16±0.01	0.17±0.01
		0.20	0.25	0.09±0.01	0.11±0.01	0.12±0.01	0.11±0.01
		0.25	0.30	0.05±0.01	0.07±0.01	0.07±0.01	0.08±0.01
		0.30	0.35	0.04±0.01	0.04±0.01	0.05±0.01	0.05±0.01
		0.35	0.40	0.02±0.01	0.03±0.01	0.03±0.01	0.04±0.01
		0.40	0.45	0.01±0.01	0.01±0.01	0.02±0.01	0.02±0.01
		0.45	0.50		0.01±0.01	0.01±0.01	
1.75	1.95	0.10	0.15	0.12±0.02	0.13±0.01	0.12±0.02	0.12±0.01
		0.15	0.20	0.13±0.01	0.13±0.01	0.14±0.01	0.14±0.01
		0.20	0.25	0.08±0.01	0.09±0.01	0.10±0.01	0.09±0.01
		0.25	0.30	0.03±0.01	0.05±0.01	0.06±0.01	0.06±0.01
		0.30	0.35	0.02±0.01	0.03±0.01	0.03±0.01	0.03±0.01
		0.35	0.40		0.01±0.01	0.02±0.01	0.02±0.01
		0.40	0.45			0.01±0.01	0.01±0.01
		0.45	0.50				
1.95	2.15	0.10	0.15	0.10±0.01	0.10±0.01	0.11±0.01	0.10±0.01
		0.15	0.20	0.10±0.01	0.11±0.01	0.11±0.01	0.11±0.01
		0.20	0.25	0.06±0.01	0.06±0.01	0.06±0.01	0.07±0.01
		0.25	0.30	0.02±0.01	0.03±0.01	0.04±0.01	0.04±0.01
		0.30	0.35	0.01±0.01	0.02±0.01	0.02±0.01	0.02±0.01
		0.35	0.40		0.01±0.01	0.01±0.01	0.01±0.01
		0.40	0.45				
		0.45	0.50				

TABLE VI: HARP results for the double-differential  $\pi^-$  production cross-section in the laboratory system,  $d^2\sigma^{\pi^-}/(dpd\theta)$  for p-C interactions. Each row refers to a different ( $p_{\min} \leq p < p_{\max}$ ,  $\theta_{\min} \leq \theta < \theta_{\max}$ ) bin, where  $p$  and  $\theta$  are the pion momentum and polar angle, respectively. The central value as well as the square-root of the diagonal elements of the covariance matrix are given.

$\theta_{\min}$ (rad)	$\theta_{\max}$ (rad)	$p_{\min}$ (GeV/c)	$p_{\max}$ (GeV/c)	$d^2\sigma^{\pi^-}/(dpd\theta)$				
				$\text{barn}/(\text{rad GeV}/c)$				
				<b>3 GeV/c</b>	<b>5 GeV/c</b>	<b>8 GeV/c</b>	<b>12 GeV/c</b>	
0.35	0.55	0.15	0.20	0.04±0.02	0.08±0.03	0.12±0.03	0.12±0.03	
		0.20	0.25	0.05±0.02	0.12±0.02	0.16±0.02	0.18±0.02	
		0.25	0.30	0.06±0.01	0.13±0.01	0.19±0.01	0.21±0.02	
		0.30	0.35	0.09±0.01	0.13±0.01	0.20±0.01	0.24±0.01	
		0.35	0.40	0.08±0.01	0.14±0.01	0.20±0.01	0.22±0.01	
		0.40	0.45	0.07±0.01	0.13±0.01	0.19±0.01	0.22±0.01	
		0.45	0.50	0.07±0.01	0.12±0.01	0.18±0.01	0.22±0.01	
		0.50	0.60	0.06±0.01	0.13±0.01	0.18±0.01	0.22±0.01	
		0.60	0.70	0.05±0.01	0.12±0.01	0.18±0.01	0.20±0.01	
		0.70	0.80	0.04±0.01	0.10±0.01	0.16±0.02	0.18±0.02	
0.55	0.75	0.10	0.15	0.03±0.02	0.06±0.02	0.06±0.02	0.09±0.03	
		0.15	0.20	0.08±0.02	0.10±0.02	0.15±0.02	0.15±0.02	
		0.20	0.25	0.10±0.01	0.15±0.01	0.17±0.01	0.18±0.01	
		0.25	0.30	0.09±0.01	0.15±0.01	0.18±0.01	0.20±0.01	
		0.30	0.35	0.09±0.01	0.13±0.01	0.17±0.01	0.20±0.01	
		0.35	0.40	0.08±0.01	0.13±0.01	0.17±0.01	0.18±0.01	
		0.40	0.45	0.08±0.01	0.11±0.01	0.17±0.01	0.18±0.01	
		0.45	0.50	0.07±0.01	0.10±0.01	0.15±0.01	0.18±0.01	
		0.50	0.60	0.05±0.01	0.10±0.01	0.14±0.01	0.17±0.01	
		0.60	0.70	0.04±0.01	0.08±0.01	0.12±0.01	0.13±0.01	
0.75	0.95	0.10	0.15	0.04±0.02	0.05±0.01	0.07±0.01	0.09±0.02	
		0.15	0.20	0.08±0.01	0.12±0.01	0.17±0.01	0.17±0.02	
		0.20	0.25	0.09±0.01	0.13±0.01	0.17±0.01	0.18±0.01	
		0.25	0.30	0.08±0.01	0.12±0.01	0.18±0.01	0.18±0.01	
		0.30	0.35	0.07±0.01	0.12±0.01	0.15±0.01	0.17±0.01	
		0.35	0.40	0.07±0.01	0.11±0.01	0.15±0.01	0.15±0.01	
		0.40	0.45	0.05±0.01	0.10±0.01	0.13±0.01	0.13±0.01	
		0.45	0.50	0.04±0.01	0.08±0.01	0.11±0.01	0.12±0.01	
		0.50	0.60	0.03±0.01	0.06±0.01	0.09±0.01	0.10±0.01	
		0.60	0.70	0.02±0.01	0.05±0.01	0.07±0.01	0.07±0.01	
0.95	1.15	0.10	0.15	0.05±0.01	0.07±0.01	0.10±0.01	0.10±0.01	
		0.15	0.20	0.09±0.01	0.14±0.01	0.15±0.01	0.16±0.01	
		0.20	0.25	0.09±0.01	0.12±0.01	0.14±0.01	0.16±0.01	
		0.25	0.30	0.09±0.01	0.12±0.01	0.13±0.01	0.15±0.01	
		0.30	0.35	0.06±0.01	0.09±0.01	0.12±0.01	0.13±0.01	
		0.35	0.40	0.05±0.01	0.07±0.01	0.10±0.01	0.11±0.01	
		0.40	0.45	0.03±0.01	0.06±0.01	0.08±0.01	0.09±0.01	
		0.45	0.50	0.03±0.01	0.05±0.01	0.07±0.01	0.08±0.01	
		0.50	0.60	0.02±0.01	0.04±0.01	0.05±0.01	0.06±0.01	

$\theta_{\min}$ (rad)	$\theta_{\max}$ (rad)	$p_{\min}$ (GeV/c)	$p_{\max}$ (GeV/c)	$d^2\sigma^{\pi^-}/(dpd\theta)$			
				barn/(rad GeV/c)			
				3 GeV/c	5 GeV/c	8 GeV/c	12 GeV/c
1.15	1.35	0.10	0.15	0.07±0.02	0.08±0.01	0.10±0.01	0.11±0.01
		0.15	0.20	0.11±0.01	0.13±0.01	0.15±0.01	0.17±0.01
		0.20	0.25	0.07±0.01	0.12±0.01	0.14±0.01	0.14±0.01
		0.25	0.30	0.06±0.01	0.10±0.01	0.12±0.01	0.12±0.01
		0.30	0.35	0.04±0.01	0.07±0.01	0.09±0.01	0.09±0.01
		0.35	0.40	0.02±0.01	0.05±0.01	0.07±0.01	0.08±0.01
		0.40	0.45	0.02±0.01	0.04±0.01	0.06±0.01	0.06±0.01
		0.45	0.50	0.02±0.01	0.03±0.01	0.04±0.01	0.05±0.01
1.35	1.55	0.10	0.15	0.06±0.01	0.09±0.01	0.10±0.01	0.11±0.01
		0.15	0.20	0.08±0.01	0.12±0.01	0.14±0.01	0.13±0.01
		0.20	0.25	0.05±0.01	0.10±0.01	0.11±0.01	0.11±0.01
		0.25	0.30	0.05±0.01	0.08±0.01	0.08±0.01	0.09±0.01
		0.30	0.35	0.04±0.01	0.05±0.01	0.06±0.01	0.06±0.01
		0.35	0.40	0.03±0.01	0.04±0.01	0.05±0.01	0.05±0.01
		0.40	0.45	0.02±0.01	0.03±0.01	0.04±0.01	0.03±0.01
		0.45	0.50	0.01±0.01	0.02±0.01	0.03±0.01	0.03±0.01
1.55	1.75	0.10	0.15	0.07±0.01	0.08±0.01	0.09±0.01	0.10±0.01
		0.15	0.20	0.09±0.01	0.12±0.01	0.12±0.01	0.13±0.01
		0.20	0.25	0.06±0.01	0.07±0.01	0.09±0.01	0.09±0.01
		0.25	0.30	0.03±0.01	0.05±0.01	0.06±0.01	0.07±0.01
		0.30	0.35	0.01±0.01	0.04±0.01	0.04±0.01	0.05±0.01
		0.35	0.40		0.03±0.01	0.04±0.01	0.03±0.01
		0.40	0.45		0.02±0.01	0.03±0.01	0.02±0.01
		0.45	0.50		0.01±0.01	0.02±0.01	0.02±0.01
1.75	1.95	0.10	0.15	0.07±0.01	0.08±0.01	0.09±0.01	0.08±0.01
		0.15	0.20	0.08±0.01	0.10±0.01	0.10±0.01	0.11±0.01
		0.20	0.25	0.04±0.01	0.07±0.01	0.07±0.01	0.07±0.01
		0.25	0.30	0.03±0.01	0.04±0.01	0.05±0.01	0.05±0.01
		0.30	0.35	0.02±0.01	0.03±0.01	0.03±0.01	0.03±0.01
		0.35	0.40	0.01±0.01	0.02±0.01	0.02±0.01	0.02±0.01
		0.40	0.45		0.01±0.01	0.02±0.01	0.02±0.01
		0.45	0.50		0.01±0.01	0.01±0.01	
1.95	2.15	0.10	0.15	0.04±0.01	0.06±0.01	0.07±0.01	0.07±0.01
		0.15	0.20	0.07±0.01	0.09±0.01	0.08±0.01	0.09±0.01
		0.20	0.25	0.04±0.01	0.05±0.01	0.06±0.01	0.06±0.01
		0.25	0.30	0.01±0.01	0.03±0.01	0.04±0.01	0.04±0.01
		0.30	0.35		0.02±0.01	0.02±0.01	0.02±0.01
		0.35	0.40		0.01±0.01	0.01±0.01	0.01±0.01
		0.40	0.45				0.01±0.01
		0.45	0.50				

TABLE VII: HARP results for the double-differential  $\pi^+$  production cross-section in the laboratory system,  $d^2\sigma^{\pi^+}/(dpd\theta)$  for p-Al interactions. Each row refers to a different ( $p_{\min} \leq p < p_{\max}, \theta_{\min} \leq \theta < \theta_{\max}$ ) bin, where  $p$  and  $\theta$  are the pion momentum and polar angle, respectively. The central value as well as the square-root of the diagonal elements of the covariance matrix are given.

$\theta_{\min}$ (rad)	$\theta_{\max}$ (rad)	$p_{\min}$ (GeV/c)	$p_{\max}$ (GeV/c)	$d^2\sigma^{\pi^+}/(dpd\theta)$				
				$\text{barn}/(\text{rad GeV}/c)$				
				<b>3 GeV/c</b>	<b>5 GeV/c</b>	<b>8 GeV/c</b>	<b>12 GeV/c</b>	<b>12.9 GeV/c</b>
0.35	0.55	0.15	0.20	0.156±0.027	0.296±0.045	0.351±0.048	0.407±0.066	0.424±0.064
		0.20	0.25	0.203±0.025	0.354±0.030	0.488±0.044	0.559±0.038	0.573±0.038
		0.25	0.30	0.226±0.025	0.454±0.038	0.549±0.037	0.667±0.053	0.635±0.042
		0.30	0.35	0.282±0.034	0.503±0.036	0.621±0.043	0.662±0.038	0.716±0.051
		0.35	0.40	0.297±0.024	0.469±0.027	0.615±0.033	0.723±0.047	0.753±0.043
		0.40	0.45	0.308±0.025	0.484±0.027	0.678±0.045	0.758±0.046	0.784±0.034
		0.45	0.50	0.314±0.024	0.515±0.030	0.696±0.033	0.779±0.038	0.747±0.029
		0.50	0.60	0.297±0.027	0.546±0.032	0.644±0.035	0.761±0.044	0.760±0.036
		0.60	0.70	0.199±0.030	0.439±0.048	0.616±0.058	0.739±0.076	0.708±0.072
		0.70	0.80	0.112±0.025	0.315±0.054	0.503±0.074	0.569±0.091	0.555±0.095
0.55	0.75	0.10	0.15	0.189±0.046	0.261±0.061	0.225±0.054	0.298±0.074	0.277±0.070
		0.15	0.20	0.253±0.029	0.372±0.026	0.395±0.036	0.419±0.035	0.447±0.037
		0.20	0.25	0.318±0.031	0.477±0.046	0.570±0.045	0.579±0.041	0.634±0.037
		0.25	0.30	0.377±0.037	0.476±0.027	0.615±0.041	0.621±0.039	0.647±0.040
		0.30	0.35	0.285±0.025	0.465±0.026	0.583±0.027	0.607±0.028	0.639±0.031
		0.35	0.40	0.307±0.032	0.432±0.027	0.580±0.028	0.622±0.038	0.679±0.032
		0.40	0.45	0.305±0.022	0.424±0.021	0.523±0.025	0.646±0.029	0.625±0.021
		0.45	0.50	0.268±0.021	0.407±0.020	0.504±0.024	0.587±0.028	0.577±0.019
		0.50	0.60	0.186±0.024	0.333±0.025	0.485±0.029	0.501±0.035	0.496±0.030
		0.60	0.70	0.116±0.021	0.227±0.030	0.340±0.049	0.361±0.053	0.374±0.049
0.75	0.95	0.10	0.15	0.245±0.038	0.302±0.048	0.276±0.048	0.292±0.047	0.317±0.051
		0.15	0.20	0.337±0.032	0.410±0.028	0.479±0.032	0.469±0.041	0.534±0.035
		0.20	0.25	0.367±0.032	0.443±0.024	0.554±0.035	0.548±0.034	0.620±0.039
		0.25	0.30	0.355±0.027	0.437±0.029	0.542±0.028	0.598±0.038	0.573±0.024
		0.30	0.35	0.253±0.021	0.381±0.021	0.460±0.022	0.519±0.022	0.532±0.019
		0.35	0.40	0.216±0.017	0.347±0.017	0.424±0.020	0.439±0.018	0.489±0.017
		0.40	0.45	0.180±0.017	0.280±0.017	0.362±0.017	0.392±0.018	0.413±0.015
		0.45	0.50	0.137±0.014	0.242±0.014	0.313±0.017	0.346±0.016	0.358±0.017
		0.50	0.60	0.094±0.012	0.180±0.018	0.253±0.021	0.269±0.022	0.287±0.025
		0.60	0.70	0.052±0.010	0.104±0.019	0.165±0.028	0.178±0.029	0.167±0.027
0.95	1.15	0.10	0.15	0.229±0.036	0.319±0.041	0.283±0.037	0.291±0.046	0.323±0.045
		0.15	0.20	0.385±0.033	0.412±0.021	0.494±0.037	0.521±0.043	0.506±0.028
		0.20	0.25	0.324±0.027	0.420±0.031	0.504±0.023	0.519±0.024	0.538±0.028
		0.25	0.30	0.244±0.022	0.354±0.022	0.390±0.020	0.404±0.019	0.456±0.021
		0.30	0.35	0.169±0.019	0.271±0.015	0.346±0.020	0.341±0.017	0.380±0.013
		0.35	0.40	0.128±0.012	0.221±0.012	0.298±0.016	0.288±0.014	0.320±0.010
		0.40	0.45	0.084±0.011	0.171±0.012	0.217±0.015	0.245±0.012	0.259±0.014
		0.45	0.50	0.059±0.009	0.114±0.013	0.173±0.011	0.201±0.014	0.194±0.017
		0.50	0.60	0.037±0.006	0.073±0.010	0.128±0.013	0.137±0.017	0.125±0.014

$\theta_{\min}$ (rad)	$\theta_{\max}$ (rad)	$p_{\min}$ (GeV/c)	$p_{\max}$ (GeV/c)	$d^2\sigma^{\pi^+}/(dpd\theta)$ barn/(rad GeV/c)				
				<b>3 GeV/c</b>	<b>5 GeV/c</b>	<b>8 GeV/c</b>	<b>8.9 GeV/c</b>	<b>12 GeV/c</b>
1.15	1.35	0.10	0.15	0.239±0.034	0.320±0.042	0.320±0.044	0.298±0.041	0.355±0.050
		0.15	0.20	0.328±0.030	0.428±0.024	0.460±0.027	0.474±0.031	0.483±0.022
		0.20	0.25	0.269±0.023	0.344±0.021	0.406±0.019	0.438±0.022	0.438±0.018
		0.25	0.30	0.197±0.020	0.245±0.016	0.332±0.018	0.332±0.017	0.347±0.015
		0.30	0.35	0.128±0.017	0.198±0.011	0.247±0.013	0.260±0.015	0.258±0.012
		0.35	0.40	0.073±0.009	0.140±0.010	0.195±0.012	0.173±0.015	0.199±0.010
		0.40	0.45	0.051±0.006	0.103±0.011	0.142±0.011	0.139±0.009	0.140±0.009
		0.45	0.50	0.033±0.006	0.072±0.008	0.101±0.010	0.104±0.009	0.105±0.010
1.35	1.55	0.10	0.15	0.214±0.030	0.324±0.041	0.357±0.040	0.354±0.049	0.365±0.051
		0.15	0.20	0.334±0.034	0.385±0.024	0.422±0.024	0.433±0.025	0.436±0.020
		0.20	0.25	0.255±0.032	0.283±0.018	0.299±0.016	0.356±0.019	0.364±0.015
		0.25	0.30	0.112±0.013	0.179±0.011	0.232±0.014	0.241±0.014	0.254±0.014
		0.30	0.35	0.076±0.009	0.150±0.010	0.171±0.012	0.178±0.011	0.179±0.009
		0.35	0.40	0.054±0.008	0.087±0.009	0.119±0.009	0.137±0.011	0.129±0.008
		0.40	0.45	0.035±0.007	0.058±0.008	0.078±0.008	0.089±0.010	0.087±0.009
		0.45	0.50	0.021±0.005	0.036±0.006	0.049±0.006	0.058±0.009	0.056±0.008
1.55	1.75	0.10	0.15	0.224±0.033	0.311±0.038	0.310±0.037	0.301±0.039	0.341±0.041
		0.15	0.20	0.304±0.026	0.312±0.019	0.360±0.018	0.370±0.023	0.391±0.017
		0.20	0.25	0.176±0.019	0.234±0.016	0.228±0.013	0.274±0.020	0.260±0.012
		0.25	0.30	0.113±0.013	0.142±0.012	0.171±0.011	0.190±0.013	0.173±0.010
		0.30	0.35	0.052±0.009	0.101±0.008	0.118±0.009	0.101±0.011	0.115±0.006
		0.35	0.40	0.026±0.006	0.063±0.006	0.075±0.007	0.062±0.005	0.086±0.007
		0.40	0.45	0.012±0.004	0.038±0.008	0.047±0.006	0.046±0.005	0.053±0.006
		0.45	0.50	0.005±0.002	0.021±0.004	0.028±0.005	0.029±0.005	0.032±0.005
1.75	1.95	0.10	0.15	0.230±0.032	0.281±0.032	0.306±0.034	0.292±0.036	0.296±0.033
		0.15	0.20	0.235±0.021	0.292±0.017	0.309±0.022	0.332±0.019	0.315±0.014
		0.20	0.25	0.147±0.017	0.193±0.013	0.211±0.014	0.192±0.016	0.207±0.009
		0.25	0.30	0.094±0.012	0.093±0.011	0.117±0.011	0.116±0.010	0.126±0.009
		0.30	0.35	0.046±0.011	0.051±0.006	0.065±0.006	0.063±0.008	0.078±0.006
		0.35	0.40	0.014±0.005	0.034±0.004	0.041±0.005	0.041±0.004	0.049±0.005
		0.40	0.45	0.006±0.002	0.020±0.004	0.024±0.004	0.026±0.004	0.031±0.004
		0.45	0.50	0.004±0.002	0.012±0.003	0.013±0.003	0.016±0.003	0.017±0.002
1.95	2.15	0.10	0.15	0.228±0.027	0.205±0.025	0.268±0.031	0.223±0.028	0.234±0.029
		0.15	0.20	0.189±0.020	0.253±0.016	0.260±0.014	0.246±0.016	0.258±0.011
		0.20	0.25	0.084±0.016	0.121±0.012	0.158±0.018	0.140±0.015	0.156±0.009
		0.25	0.30	0.040±0.008	0.061±0.008	0.072±0.007	0.073±0.006	0.085±0.007
		0.30	0.35	0.015±0.005	0.032±0.004	0.045±0.005	0.046±0.006	0.048±0.004
		0.35	0.40	0.008±0.003	0.022±0.003	0.021±0.004	0.031±0.004	0.028±0.003
		0.40	0.45	0.006±0.003	0.010±0.002	0.012±0.002	0.015±0.004	0.015±0.002
		0.45	0.50	0.003±0.002	0.005±0.002	0.006±0.001	0.007±0.002	0.010±0.002

TABLE VIII: HARP results for the double-differential  $\pi^-$  production cross-section in the laboratory system,  $d^2\sigma^{\pi^-}/(dpd\theta)$  for p-Al interactions. Each row refers to a different ( $p_{\min} \leq p < p_{\max}, \theta_{\min} \leq \theta < \theta_{\max}$ ) bin, where  $p$  and  $\theta$  are the pion momentum and polar angle, respectively. The central value as well as the square-root of the diagonal elements of the covariance matrix are given.

$\theta_{\min}$ (rad)	$\theta_{\max}$ (rad)	$p_{\min}$ (GeV/c)	$p_{\max}$ (GeV/c)	$d^2\sigma^{\pi^-}/(dpd\theta)$ barn/(rad GeV/c)				
				<b>3 GeV/c    5 GeV/c    8 GeV/c    12 GeV/c    12.9 GeV/c</b>				
				0.131±0.030	0.243±0.042	0.338±0.051	0.342±0.053	0.397±0.065
0.35	0.55	0.15	0.20	0.124±0.021	0.258±0.022	0.411±0.037	0.442±0.037	0.492±0.035
		0.25	0.30	0.126±0.022	0.289±0.024	0.479±0.027	0.516±0.032	0.548±0.030
		0.30	0.35	0.170±0.020	0.312±0.024	0.387±0.023	0.470±0.031	0.529±0.020
		0.35	0.40	0.186±0.021	0.293±0.018	0.428±0.034	0.485±0.027	0.468±0.018
		0.40	0.45	0.132±0.017	0.262±0.015	0.463±0.026	0.485±0.025	0.475±0.024
		0.45	0.50	0.112±0.012	0.257±0.015	0.428±0.022	0.440±0.022	0.473±0.020
		0.50	0.60	0.131±0.014	0.246±0.017	0.383±0.022	0.431±0.025	0.458±0.024
		0.60	0.70	0.087±0.013	0.217±0.019	0.377±0.029	0.415±0.034	0.454±0.035
		0.70	0.80	0.061±0.013	0.166±0.025	0.334±0.040	0.398±0.041	0.388±0.049
		0.55	0.75	0.075±0.027	0.176±0.047	0.223±0.060	0.275±0.075	0.270±0.066
0.75	0.95	0.10	0.15	0.115±0.019	0.290±0.024	0.383±0.031	0.353±0.028	0.411±0.030
		0.20	0.25	0.196±0.027	0.273±0.020	0.438±0.028	0.389±0.029	0.456±0.024
		0.25	0.30	0.164±0.018	0.279±0.018	0.429±0.025	0.443±0.030	0.448±0.021
		0.30	0.35	0.153±0.018	0.265±0.016	0.382±0.021	0.447±0.028	0.447±0.020
		0.35	0.40	0.143±0.014	0.231±0.012	0.397±0.024	0.371±0.015	0.422±0.015
		0.40	0.45	0.130±0.013	0.219±0.015	0.361±0.017	0.374±0.020	0.388±0.012
		0.45	0.50	0.119±0.012	0.228±0.014	0.317±0.016	0.374±0.017	0.373±0.013
		0.50	0.60	0.095±0.010	0.201±0.013	0.304±0.017	0.337±0.020	0.348±0.016
		0.60	0.70	0.076±0.011	0.156±0.017	0.269±0.026	0.287±0.027	0.297±0.026
		0.70	0.80	0.055±0.011	0.126±0.020	0.214±0.031	0.240±0.034	0.239±0.034
0.95	1.15	0.10	0.15	0.099±0.025	0.177±0.030	0.243±0.043	0.313±0.054	0.292±0.050
		0.15	0.20	0.200±0.023	0.322±0.022	0.394±0.023	0.404±0.023	0.463±0.023
		0.20	0.25	0.170±0.019	0.286±0.020	0.384±0.025	0.378±0.031	0.412±0.019
		0.25	0.30	0.145±0.015	0.280±0.016	0.350±0.021	0.402±0.021	0.411±0.020
		0.30	0.35	0.134±0.015	0.233±0.013	0.327±0.016	0.339±0.015	0.371±0.014
		0.35	0.40	0.125±0.012	0.220±0.012	0.304±0.015	0.296±0.014	0.330±0.011
		0.40	0.45	0.115±0.012	0.185±0.011	0.267±0.012	0.291±0.013	0.274±0.008
		0.45	0.50	0.094±0.011	0.158±0.009	0.241±0.011	0.249±0.014	0.259±0.009
		0.50	0.60	0.059±0.010	0.120±0.009	0.205±0.013	0.217±0.014	0.219±0.012
		0.60	0.70	0.034±0.006	0.086±0.011	0.158±0.017	0.171±0.018	0.172±0.019

$\theta_{\min}$ (rad)	$\theta_{\max}$ (rad)	$p_{\min}$ (GeV/c)	$p_{\max}$ (GeV/c)	$d^2\sigma^{\pi^-}/(dpd\theta)$ barn/(rad GeV/c)					
				<b>3 GeV/c</b>					<b>8.9 GeV/c</b>
				<b>3 GeV/c</b>	<b>5 GeV/c</b>	<b>8 GeV/c</b>	<b>8.9 GeV/c</b>	<b>12 GeV/c</b>	
1.15	1.35	0.10	0.15	0.123±0.020	0.211±0.025	0.266±0.032	0.266±0.037	0.319±0.033	
		0.15	0.20	0.160±0.018	0.288±0.019	0.346±0.020	0.366±0.023	0.386±0.023	
		0.20	0.25	0.159±0.017	0.239±0.015	0.305±0.017	0.321±0.018	0.344±0.012	
		0.25	0.30	0.132±0.015	0.185±0.013	0.257±0.014	0.243±0.014	0.270±0.009	
		0.30	0.35	0.084±0.011	0.164±0.010	0.181±0.012	0.208±0.012	0.216±0.008	
		0.35	0.40	0.062±0.009	0.114±0.008	0.142±0.008	0.156±0.010	0.162±0.006	
		0.40	0.45	0.036±0.006	0.087±0.007	0.115±0.006	0.126±0.008	0.127±0.006	
		0.45	0.50	0.026±0.004	0.064±0.006	0.094±0.006	0.100±0.007	0.099±0.006	
1.35	1.55	0.10	0.15	0.187±0.027	0.224±0.027	0.251±0.027	0.270±0.033	0.305±0.035	
		0.15	0.20	0.198±0.020	0.247±0.017	0.289±0.017	0.298±0.021	0.341±0.017	
		0.20	0.25	0.130±0.016	0.209±0.014	0.251±0.013	0.273±0.018	0.284±0.012	
		0.25	0.30	0.083±0.011	0.130±0.011	0.190±0.012	0.221±0.014	0.221±0.010	
		0.30	0.35	0.067±0.010	0.107±0.008	0.147±0.009	0.151±0.011	0.160±0.008	
		0.35	0.40	0.035±0.006	0.091±0.007	0.110±0.007	0.115±0.007	0.117±0.007	
		0.40	0.45	0.025±0.005	0.066±0.006	0.089±0.006	0.090±0.007	0.083±0.005	
		0.45	0.50	0.019±0.004	0.044±0.006	0.067±0.006	0.065±0.007	0.062±0.005	
1.55	1.75	0.10	0.15	0.140±0.022	0.224±0.025	0.257±0.033	0.267±0.036	0.285±0.030	
		0.15	0.20	0.151±0.017	0.241±0.015	0.270±0.016	0.300±0.019	0.295±0.014	
		0.20	0.25	0.101±0.013	0.171±0.013	0.208±0.013	0.229±0.014	0.217±0.010	
		0.25	0.30	0.064±0.009	0.102±0.009	0.158±0.011	0.171±0.013	0.157±0.008	
		0.30	0.35	0.046±0.008	0.079±0.006	0.091±0.009	0.095±0.011	0.109±0.007	
		0.35	0.40	0.020±0.006	0.057±0.005	0.060±0.005	0.068±0.005	0.079±0.005	
		0.40	0.45	0.009±0.003	0.040±0.005	0.046±0.004	0.049±0.004	0.056±0.004	
		0.45	0.50	0.006±0.002	0.026±0.004	0.033±0.003	0.040±0.005	0.039±0.003	
1.75	1.95	0.10	0.15	0.118±0.019	0.190±0.019	0.227±0.023	0.261±0.029	0.247±0.026	
		0.15	0.20	0.163±0.018	0.191±0.013	0.235±0.013	0.240±0.015	0.244±0.010	
		0.20	0.25	0.080±0.012	0.136±0.010	0.168±0.010	0.170±0.012	0.181±0.006	
		0.25	0.30	0.053±0.009	0.082±0.008	0.129±0.009	0.102±0.008	0.119±0.007	
		0.30	0.35	0.035±0.007	0.055±0.005	0.070±0.008	0.080±0.006	0.075±0.005	
		0.35	0.40	0.025±0.006	0.044±0.005	0.047±0.004	0.060±0.005	0.054±0.002	
		0.40	0.45	0.013±0.004	0.024±0.005	0.037±0.003	0.038±0.005	0.041±0.003	
		0.45	0.50	0.007±0.003	0.014±0.003	0.026±0.003	0.027±0.004	0.027±0.003	
1.95	2.15	0.10	0.15	0.109±0.017	0.132±0.015	0.197±0.019	0.187±0.020	0.206±0.020	
		0.15	0.20	0.104±0.014	0.173±0.012	0.190±0.012	0.196±0.015	0.187±0.010	
		0.20	0.25	0.053±0.009	0.103±0.009	0.117±0.009	0.130±0.012	0.136±0.006	
		0.25	0.30	0.037±0.008	0.066±0.007	0.064±0.008	0.078±0.007	0.085±0.005	
		0.30	0.35	0.018±0.005	0.038±0.005	0.044±0.004	0.052±0.006	0.052±0.004	
		0.35	0.40	0.010±0.004	0.024±0.004	0.040±0.004	0.029±0.004	0.036±0.003	
		0.40	0.45	0.005±0.003	0.012±0.003	0.025±0.004	0.019±0.003	0.026±0.002	
		0.45	0.50	0.002±0.002	0.008±0.002	0.013±0.003	0.015±0.003	0.018±0.002	

TABLE IX: HARP results for the double-differential  $\pi^+$  production cross-section in the laboratory system,  $d^2\sigma^{\pi^+}/(dpd\theta)$  for p–Cu interactions. Each row refers to a different ( $p_{\min} \leq p < p_{\max}$ ,  $\theta_{\min} \leq \theta < \theta_{\max}$ ) bin, where  $p$  and  $\theta$  are the pion momentum and polar angle, respectively. The central value as well as the square-root of the diagonal elements of the covariance matrix are given.

$\theta_{\min}$ (rad)	$\theta_{\max}$ (rad)	$p_{\min}$ (GeV/c)	$p_{\max}$ (GeV/c)	$d^2\sigma^{\pi^+}/(dpd\theta)$				
				$\text{barn}/(\text{rad GeV}/c)$				
				<b>3 GeV/c</b>	<b>5 GeV/c</b>	<b>8 GeV/c</b>	<b>12 GeV/c</b>	
0.35	0.55	0.15	0.20	0.20±0.05	0.54±0.09	0.76±0.13	0.87±0.15	
		0.20	0.25	0.22±0.05	0.68±0.07	0.94±0.08	1.01±0.08	
		0.25	0.30	0.46±0.07	0.81±0.06	1.09±0.06	1.32±0.10	
		0.30	0.35	0.45±0.05	0.86±0.06	1.11±0.08	1.42±0.08	
		0.35	0.40	0.44±0.05	0.82±0.04	1.20±0.07	1.40±0.07	
		0.40	0.45	0.37±0.04	0.78±0.04	1.25±0.06	1.31±0.05	
		0.45	0.50	0.41±0.05	0.78±0.04	1.17±0.05	1.35±0.08	
		0.50	0.60	0.41±0.04	0.76±0.04	1.13±0.05	1.31±0.07	
		0.60	0.70	0.30±0.05	0.61±0.07	1.00±0.09	1.19±0.11	
		0.70	0.80	0.15±0.04	0.39±0.07	0.77±0.11	0.97±0.13	
0.55	0.75	0.10	0.15	0.40±0.11	0.40±0.12	0.51±0.15	0.58±0.17	
		0.15	0.20	0.44±0.06	0.71±0.07	0.91±0.07	0.92±0.08	
		0.20	0.25	0.46±0.06	0.82±0.05	1.08±0.08	1.28±0.10	
		0.25	0.30	0.47±0.05	0.81±0.06	1.11±0.06	1.33±0.06	
		0.30	0.35	0.53±0.08	0.88±0.06	1.12±0.06	1.24±0.06	
		0.35	0.40	0.58±0.05	0.82±0.04	1.08±0.04	1.25±0.05	
		0.40	0.45	0.44±0.04	0.66±0.04	0.99±0.04	1.18±0.05	
		0.45	0.50	0.36±0.04	0.61±0.03	0.94±0.04	1.07±0.04	
		0.50	0.60	0.26±0.03	0.52±0.04	0.78±0.05	0.88±0.06	
		0.60	0.70	0.13±0.03	0.35±0.04	0.50±0.06	0.64±0.08	
0.75	0.95	0.10	0.15	0.41±0.10	0.51±0.11	0.56±0.13	0.68±0.15	
		0.15	0.20	0.56±0.06	0.83±0.06	0.96±0.06	1.19±0.08	
		0.20	0.25	0.49±0.05	0.82±0.05	1.13±0.08	1.22±0.06	
		0.25	0.30	0.50±0.05	0.71±0.04	1.06±0.06	1.15±0.07	
		0.30	0.35	0.37±0.04	0.70±0.04	0.94±0.04	1.15±0.05	
		0.35	0.40	0.25±0.03	0.58±0.03	0.81±0.03	0.95±0.04	
		0.40	0.45	0.20±0.02	0.45±0.03	0.67±0.03	0.83±0.03	
		0.45	0.50	0.18±0.02	0.38±0.02	0.57±0.03	0.67±0.04	
		0.50	0.60	0.10±0.02	0.27±0.02	0.42±0.03	0.51±0.04	
		0.60	0.70	0.05±0.01	0.16±0.03	0.26±0.03	0.30±0.05	
0.95	1.15	0.10	0.15	0.44±0.09	0.65±0.11	0.66±0.12	0.82±0.16	
		0.15	0.20	0.59±0.06	0.87±0.05	1.08±0.07	1.14±0.07	
		0.20	0.25	0.44±0.04	0.66±0.04	0.95±0.04	1.11±0.06	
		0.25	0.30	0.36±0.04	0.60±0.04	0.80±0.04	0.87±0.05	
		0.30	0.35	0.26±0.03	0.52±0.03	0.62±0.03	0.76±0.04	
		0.35	0.40	0.18±0.02	0.39±0.02	0.52±0.03	0.60±0.03	
		0.40	0.45	0.15±0.02	0.30±0.02	0.42±0.02	0.47±0.03	
		0.45	0.50	0.11±0.02	0.24±0.02	0.32±0.02	0.38±0.03	
		0.50	0.60	0.06±0.01	0.15±0.02	0.22±0.02	0.24±0.03	

$\theta_{\min}$ (rad)	$\theta_{\max}$ (rad)	$p_{\min}$ (GeV/c)	$p_{\max}$ (GeV/c)	$d^2\sigma^{\pi^+}/(dpd\theta)$				
				barn/(rad GeV/c)				
				3 GeV/c	5 GeV/c	8 GeV/c	12 GeV/c	
1.15	1.35	0.10	0.15	0.51±0.10	0.68±0.14	0.72±0.15	0.78±0.16	
		0.15	0.20	0.54±0.06	0.81±0.05	1.01±0.07	1.07±0.08	
		0.20	0.25	0.41±0.04	0.63±0.04	0.87±0.04	1.05±0.05	
		0.25	0.30	0.31±0.04	0.48±0.03	0.58±0.04	0.73±0.04	
		0.30	0.35	0.18±0.02	0.32±0.03	0.41±0.02	0.53±0.03	
		0.35	0.40	0.11±0.02	0.23±0.02	0.33±0.02	0.36±0.02	
		0.40	0.45	0.08±0.01	0.17±0.01	0.25±0.01	0.26±0.02	
		0.45	0.50	0.05±0.01	0.12±0.01	0.18±0.01	0.19±0.02	
1.35	1.55	0.10	0.15	0.52±0.12	0.70±0.15	0.73±0.18	0.83±0.18	
		0.15	0.20	0.47±0.05	0.71±0.06	0.90±0.07	0.99±0.09	
		0.20	0.25	0.30±0.04	0.52±0.04	0.73±0.04	0.84±0.05	
		0.25	0.30	0.18±0.02	0.34±0.03	0.48±0.04	0.51±0.03	
		0.30	0.35	0.13±0.02	0.23±0.02	0.32±0.02	0.38±0.02	
		0.35	0.40	0.07±0.01	0.16±0.01	0.22±0.02	0.29±0.02	
		0.40	0.45	0.04±0.01	0.11±0.01	0.15±0.01	0.20±0.02	
		0.45	0.50	0.03±0.01	0.06±0.01	0.10±0.01	0.11±0.02	
1.55	1.75	0.10	0.15	0.53±0.13	0.67±0.15	0.83±0.19	0.83±0.20	
		0.15	0.20	0.43±0.05	0.72±0.05	0.81±0.06	0.87±0.07	
		0.20	0.25	0.27±0.03	0.46±0.04	0.61±0.04	0.67±0.05	
		0.25	0.30	0.17±0.03	0.24±0.02	0.34±0.02	0.36±0.03	
		0.30	0.35	0.13±0.02	0.15±0.01	0.22±0.02	0.23±0.02	
		0.35	0.40	0.06±0.01	0.12±0.01	0.15±0.01	0.18±0.01	
		0.40	0.45	0.03±0.01	0.08±0.01	0.09±0.01	0.11±0.01	
		0.45	0.50	0.02±0.01	0.04±0.01	0.06±0.01	0.06±0.01	
1.75	1.95	0.10	0.15	0.50±0.10	0.61±0.10	0.70±0.12	0.70±0.12	
		0.15	0.20	0.51±0.05	0.60±0.04	0.69±0.04	0.72±0.04	
		0.20	0.25	0.35±0.05	0.34±0.03	0.44±0.03	0.46±0.03	
		0.25	0.30	0.08±0.02	0.17±0.02	0.21±0.02	0.26±0.02	
		0.30	0.35	0.04±0.01	0.10±0.01	0.12±0.01	0.16±0.02	
		0.35	0.40	0.02±0.01	0.07±0.01	0.09±0.01	0.10±0.01	
		0.40	0.45	0.01±0.01	0.05±0.01	0.06±0.01	0.06±0.01	
		0.45	0.50		0.02±0.01	0.03±0.01	0.03±0.01	
1.95	2.15	0.10	0.15	0.38±0.06	0.49±0.07	0.56±0.08	0.48±0.08	
		0.15	0.20	0.42±0.05	0.44±0.03	0.55±0.02	0.56±0.03	
		0.20	0.25	0.18±0.03	0.26±0.02	0.29±0.02	0.31±0.02	
		0.25	0.30	0.07±0.02	0.11±0.01	0.14±0.01	0.19±0.02	
		0.30	0.35	0.04±0.01	0.07±0.01	0.08±0.01	0.10±0.01	
		0.35	0.40	0.02±0.01	0.04±0.01	0.05±0.01	0.06±0.01	
		0.40	0.45		0.02±0.01	0.03±0.01	0.04±0.01	
		0.45	0.50		0.01±0.01	0.02±0.01	0.02±0.01	

TABLE X: HARP results for the double-differential  $\pi^-$  production cross-section in the laboratory system,  $d^2\sigma^{\pi^-}/(dpd\theta)$  for p–Cu interactions. Each row refers to a different ( $p_{\min} \leq p < p_{\max}$ ,  $\theta_{\min} \leq \theta < \theta_{\max}$ ) bin, where  $p$  and  $\theta$  are the pion momentum and polar angle, respectively. The central value as well as the square-root of the diagonal elements of the covariance matrix are given.

$\theta_{\min}$ (rad)	$\theta_{\max}$ (rad)	$p_{\min}$ (GeV/c)	$p_{\max}$ (GeV/c)	$d^2\sigma^{\pi^-}/(dpd\theta)$				
				$\text{barn}/(\text{rad GeV}/c)$				
				<b>3 GeV/c</b>	<b>5 GeV/c</b>	<b>8 GeV/c</b>	<b>12 GeV/c</b>	
0.35	0.55	0.15	0.20	0.15±0.06	0.43±0.08	0.70±0.11	0.85±0.17	
		0.20	0.25	0.21±0.05	0.48±0.05	0.79±0.07	1.06±0.07	
		0.25	0.30	0.13±0.04	0.49±0.04	0.89±0.06	1.03±0.06	
		0.30	0.35	0.18±0.03	0.49±0.03	0.79±0.04	0.99±0.06	
		0.35	0.40	0.17±0.03	0.47±0.03	0.78±0.04	0.90±0.04	
		0.40	0.45	0.17±0.02	0.43±0.03	0.74±0.03	0.81±0.03	
		0.45	0.50	0.19±0.03	0.39±0.02	0.70±0.03	0.75±0.03	
		0.50	0.60	0.19±0.03	0.41±0.02	0.68±0.03	0.78±0.04	
		0.60	0.70	0.13±0.02	0.36±0.03	0.63±0.04	0.69±0.06	
		0.70	0.80	0.10±0.02	0.29±0.03	0.54±0.06	0.63±0.07	
0.55	0.75	0.10	0.15	0.27±0.08	0.49±0.13	0.53±0.15	0.57±0.18	
		0.15	0.20	0.28±0.06	0.56±0.05	0.74±0.07	0.96±0.09	
		0.20	0.25	0.44±0.06	0.64±0.05	0.81±0.05	1.06±0.06	
		0.25	0.30	0.20±0.03	0.60±0.04	0.85±0.06	1.02±0.05	
		0.30	0.35	0.24±0.03	0.52±0.03	0.78±0.04	0.86±0.04	
		0.35	0.40	0.24±0.03	0.47±0.03	0.67±0.03	0.83±0.04	
		0.40	0.45	0.21±0.03	0.42±0.02	0.62±0.03	0.78±0.03	
		0.45	0.50	0.17±0.02	0.37±0.02	0.61±0.02	0.75±0.03	
		0.50	0.60	0.14±0.02	0.29±0.02	0.54±0.02	0.63±0.04	
		0.60	0.70	0.09±0.02	0.24±0.02	0.44±0.04	0.49±0.04	
0.75	0.95	0.10	0.15	0.32±0.07	0.48±0.09	0.59±0.12	0.63±0.13	
		0.15	0.20	0.33±0.05	0.64±0.05	0.86±0.05	0.98±0.06	
		0.20	0.25	0.24±0.03	0.59±0.04	0.81±0.05	0.92±0.05	
		0.25	0.30	0.22±0.03	0.47±0.03	0.73±0.04	0.90±0.06	
		0.30	0.35	0.21±0.03	0.42±0.02	0.64±0.03	0.82±0.04	
		0.35	0.40	0.23±0.03	0.34±0.02	0.61±0.03	0.73±0.03	
		0.40	0.45	0.18±0.02	0.28±0.02	0.51±0.02	0.59±0.03	
		0.45	0.50	0.14±0.02	0.25±0.01	0.42±0.02	0.48±0.02	
		0.50	0.60	0.10±0.02	0.21±0.01	0.34±0.02	0.40±0.02	
		0.60	0.70	0.06±0.01	0.17±0.02	0.27±0.02	0.32±0.03	
0.95	1.15	0.10	0.15	0.25±0.06	0.55±0.09	0.68±0.11	0.72±0.14	
		0.15	0.20	0.32±0.05	0.65±0.04	0.84±0.05	0.89±0.06	
		0.20	0.25	0.32±0.04	0.51±0.04	0.77±0.04	0.83±0.05	
		0.25	0.30	0.23±0.03	0.43±0.03	0.63±0.03	0.72±0.04	
		0.30	0.35	0.13±0.02	0.36±0.02	0.51±0.03	0.57±0.03	
		0.35	0.40	0.11±0.02	0.27±0.02	0.43±0.02	0.49±0.02	
		0.40	0.45	0.12±0.02	0.22±0.01	0.35±0.02	0.43±0.02	
		0.45	0.50	0.11±0.02	0.19±0.01	0.29±0.01	0.36±0.02	
		0.50	0.60	0.07±0.01	0.14±0.01	0.22±0.02	0.25±0.02	

$\theta_{\min}$ (rad)	$\theta_{\max}$ (rad)	$p_{\min}$ (GeV/c)	$p_{\max}$ (GeV/c)	$d^2\sigma^{\pi^-}/(dpd\theta)$			
				barn/(rad GeV/c)			
				<b>3 GeV/c</b>	<b>5 GeV/c</b>	<b>8 GeV/c</b>	<b>12 GeV/c</b>
1.15	1.35	0.10	0.15	0.30±0.07	0.63±0.11	0.71±0.13	0.79±0.17
		0.15	0.20	0.38±0.05	0.64±0.05	0.75±0.06	0.97±0.07
		0.20	0.25	0.32±0.04	0.48±0.03	0.64±0.04	0.79±0.05
		0.25	0.30	0.16±0.03	0.37±0.02	0.51±0.03	0.58±0.03
		0.30	0.35	0.15±0.02	0.29±0.02	0.38±0.02	0.45±0.02
		0.35	0.40	0.10±0.02	0.20±0.01	0.30±0.01	0.36±0.02
		0.40	0.45	0.06±0.01	0.15±0.01	0.24±0.01	0.28±0.02
		0.45	0.50	0.04±0.01	0.12±0.01	0.19±0.01	0.20±0.02
1.35	1.55	0.10	0.15	0.39±0.09	0.63±0.13	0.72±0.16	0.80±0.19
		0.15	0.20	0.39±0.05	0.57±0.05	0.73±0.06	0.85±0.07
		0.20	0.25	0.27±0.04	0.41±0.03	0.53±0.03	0.69±0.04
		0.25	0.30	0.20±0.03	0.30±0.02	0.37±0.02	0.47±0.03
		0.30	0.35	0.15±0.02	0.20±0.02	0.29±0.02	0.33±0.02
		0.35	0.40	0.09±0.02	0.13±0.01	0.21±0.01	0.24±0.02
		0.40	0.45	0.07±0.01	0.09±0.01	0.16±0.01	0.18±0.01
		0.45	0.50	0.04±0.01	0.06±0.01	0.12±0.01	0.13±0.01
1.55	1.75	0.10	0.15	0.37±0.08	0.56±0.12	0.73±0.17	0.84±0.20
		0.15	0.20	0.27±0.04	0.50±0.04	0.66±0.05	0.71±0.06
		0.20	0.25	0.20±0.03	0.33±0.03	0.44±0.03	0.50±0.04
		0.25	0.30	0.12±0.02	0.19±0.02	0.31±0.02	0.33±0.03
		0.30	0.35	0.07±0.01	0.13±0.01	0.21±0.02	0.23±0.02
		0.35	0.40	0.04±0.01	0.09±0.01	0.14±0.01	0.17±0.01
		0.40	0.45	0.02±0.01	0.06±0.01	0.10±0.01	0.11±0.01
		0.45	0.50	0.01±0.01	0.04±0.01	0.07±0.01	0.08±0.01
1.75	1.95	0.10	0.15	0.26±0.05	0.51±0.08	0.63±0.10	0.66±0.11
		0.15	0.20	0.21±0.03	0.42±0.03	0.51±0.03	0.64±0.04
		0.20	0.25	0.19±0.03	0.28±0.02	0.35±0.02	0.40±0.03
		0.25	0.30	0.08±0.02	0.15±0.02	0.22±0.02	0.24±0.02
		0.30	0.35	0.06±0.01	0.09±0.01	0.14±0.01	0.14±0.01
		0.35	0.40	0.05±0.01	0.06±0.01	0.10±0.01	0.11±0.01
		0.40	0.45	0.02±0.01	0.04±0.01	0.07±0.01	0.07±0.01
		0.45	0.50	0.01±0.01	0.03±0.01	0.05±0.01	0.05±0.01
1.95	2.15	0.10	0.15	0.26±0.05	0.42±0.06	0.52±0.07	0.55±0.08
		0.15	0.20	0.20±0.03	0.31±0.02	0.42±0.02	0.47±0.03
		0.20	0.25	0.13±0.03	0.17±0.01	0.25±0.01	0.28±0.02
		0.25	0.30	0.06±0.02	0.11±0.01	0.16±0.01	0.15±0.02
		0.30	0.35	0.02±0.01	0.07±0.01	0.09±0.01	0.10±0.01
		0.35	0.40	0.02±0.01	0.05±0.01	0.05±0.01	0.07±0.01
		0.40	0.45	0.01±0.01	0.03±0.01	0.04±0.01	0.06±0.01
		0.45	0.50	0.02±0.01	0.03±0.01	0.04±0.01	0.04±0.01

TABLE XI: HARP results for the double-differential  $\pi^+$  production cross-section in the laboratory system,  $d^2\sigma^{\pi^+}/(dpd\theta)$  for p–Sn interactions. Each row refers to a different ( $p_{\min} \leq p < p_{\max}$ ,  $\theta_{\min} \leq \theta < \theta_{\max}$ ) bin, where  $p$  and  $\theta$  are the pion momentum and polar angle, respectively. The central value as well as the square-root of the diagonal elements of the covariance matrix are given.

$\theta_{\min}$ (rad)	$\theta_{\max}$ (rad)	$p_{\min}$ (GeV/c)	$p_{\max}$ (GeV/c)	$d^2\sigma^{\pi^+}/(dpd\theta)$				
				$\text{barn}/(\text{rad GeV}/c)$				
				<b>3 GeV/c</b>	<b>5 GeV/c</b>	<b>8 GeV/c</b>	<b>12 GeV/c</b>	
0.35	0.55	0.15	0.20	0.28±0.11	0.74±0.14	1.20±0.18	1.55±0.25	
		0.20	0.25	0.41±0.10	0.78±0.09	1.42±0.12	1.81±0.16	
		0.25	0.30	0.55±0.06	1.05±0.10	1.59±0.11	2.18±0.14	
		0.30	0.35	0.53±0.05	1.00±0.05	1.67±0.11	2.14±0.14	
		0.35	0.40	0.56±0.05	1.05±0.08	1.64±0.07	2.14±0.07	
		0.40	0.45	0.50±0.04	1.10±0.06	1.55±0.08	2.21±0.14	
		0.45	0.50	0.47±0.04	1.10±0.05	1.53±0.06	2.15±0.07	
		0.50	0.60	0.44±0.04	0.94±0.06	1.45±0.07	2.20±0.12	
		0.60	0.70	0.36±0.04	0.80±0.08	1.27±0.13	2.12±0.18	
		0.70	0.80	0.26±0.04	0.47±0.08	0.93±0.16	1.78±0.21	
0.55	0.75	0.10	0.15	0.33±0.12	0.76±0.17	0.87±0.21	1.26±0.30	
		0.15	0.20	0.49±0.08	1.02±0.10	1.53±0.10	1.77±0.14	
		0.20	0.25	0.59±0.09	1.23±0.09	1.72±0.12	2.19±0.17	
		0.25	0.30	0.60±0.05	1.11±0.07	1.61±0.10	2.15±0.17	
		0.30	0.35	0.56±0.05	1.12±0.07	1.54±0.07	2.13±0.10	
		0.35	0.40	0.46±0.04	1.03±0.05	1.47±0.07	2.08±0.07	
		0.40	0.45	0.46±0.04	0.87±0.04	1.27±0.05	1.98±0.06	
		0.45	0.50	0.37±0.04	0.80±0.04	1.21±0.05	1.76±0.07	
		0.50	0.60	0.27±0.03	0.61±0.05	1.03±0.06	1.53±0.09	
		0.60	0.70	0.17±0.03	0.38±0.05	0.71±0.10	1.21±0.11	
0.75	0.95	0.10	0.15	0.47±0.10	0.80±0.13	1.07±0.17	1.16±0.20	
		0.15	0.20	0.63±0.07	1.17±0.07	1.69±0.11	1.95±0.12	
		0.20	0.25	0.76±0.06	1.22±0.07	1.64±0.09	1.94±0.11	
		0.25	0.30	0.57±0.05	0.95±0.05	1.45±0.07	1.92±0.11	
		0.30	0.35	0.57±0.04	0.93±0.06	1.31±0.06	1.78±0.08	
		0.35	0.40	0.46±0.04	0.73±0.04	1.17±0.05	1.40±0.05	
		0.40	0.45	0.36±0.03	0.60±0.04	0.99±0.04	1.27±0.05	
		0.45	0.50	0.30±0.03	0.50±0.03	0.80±0.05	1.11±0.05	
		0.50	0.60	0.19±0.03	0.35±0.03	0.56±0.05	0.85±0.06	
		0.60	0.70	0.09±0.02	0.20±0.03	0.32±0.05	0.55±0.06	
0.95	1.15	0.10	0.15	0.45±0.09	0.80±0.11	1.13±0.14	1.14±0.17	
		0.15	0.20	0.68±0.07	1.12±0.07	1.55±0.09	1.82±0.11	
		0.20	0.25	0.51±0.04	1.01±0.06	1.40±0.09	1.72±0.08	
		0.25	0.30	0.43±0.04	0.77±0.04	1.16±0.05	1.48±0.07	
		0.30	0.35	0.29±0.02	0.59±0.04	0.92±0.07	1.20±0.06	
		0.35	0.40	0.27±0.03	0.50±0.03	0.72±0.04	0.97±0.05	
		0.40	0.45	0.19±0.03	0.41±0.03	0.65±0.03	0.79±0.05	
		0.45	0.50	0.14±0.02	0.30±0.02	0.49±0.04	0.64±0.04	
		0.50	0.60	0.08±0.01	0.20±0.02	0.30±0.03	0.46±0.04	

$\theta_{\min}$ (rad)	$\theta_{\max}$ (rad)	$p_{\min}$ (GeV/c)	$p_{\max}$ (GeV/c)	$d^2\sigma^{\pi^+}/(dpd\theta)$			
				barn/(rad GeV/c)			
				<b>3 GeV/c</b>	<b>5 GeV/c</b>	<b>8 GeV/c</b>	<b>12 GeV/c</b>
1.15	1.35	0.10	0.15	0.57±0.09	0.76±0.10	1.06±0.14	1.10±0.18
		0.15	0.20	0.64±0.05	1.09±0.08	1.39±0.10	1.74±0.11
		0.20	0.25	0.47±0.04	0.85±0.05	1.22±0.07	1.43±0.07
		0.25	0.30	0.40±0.04	0.65±0.04	0.93±0.05	1.09±0.06
		0.30	0.35	0.25±0.03	0.46±0.03	0.67±0.05	0.86±0.05
		0.35	0.40	0.15±0.02	0.32±0.03	0.48±0.02	0.69±0.04
		0.40	0.45	0.10±0.01	0.23±0.02	0.38±0.02	0.51±0.04
		0.45	0.50	0.08±0.01	0.18±0.02	0.28±0.03	0.34±0.03
1.35	1.55	0.10	0.15	0.72±0.12	0.86±0.14	1.26±0.21	1.30±0.23
		0.15	0.20	0.70±0.06	1.11±0.09	1.44±0.10	1.77±0.16
		0.20	0.25	0.44±0.04	0.83±0.06	1.11±0.09	1.29±0.09
		0.25	0.30	0.33±0.03	0.52±0.04	0.74±0.05	0.92±0.06
		0.30	0.35	0.19±0.03	0.37±0.03	0.52±0.03	0.63±0.05
		0.35	0.40	0.11±0.01	0.26±0.02	0.36±0.02	0.48±0.03
		0.40	0.45	0.07±0.01	0.16±0.02	0.24±0.02	0.37±0.03
		0.45	0.50	0.04±0.01	0.09±0.01	0.17±0.02	0.21±0.03
1.55	1.75	0.10	0.15	0.65±0.12	0.99±0.16	1.27±0.20	1.29±0.23
		0.15	0.20	0.71±0.06	1.00±0.08	1.40±0.10	1.57±0.11
		0.20	0.25	0.41±0.04	0.68±0.05	0.95±0.07	1.04±0.08
		0.25	0.30	0.24±0.03	0.45±0.04	0.57±0.04	0.67±0.04
		0.30	0.35	0.13±0.02	0.23±0.02	0.36±0.03	0.46±0.03
		0.35	0.40	0.08±0.01	0.18±0.02	0.24±0.02	0.31±0.02
		0.40	0.45	0.04±0.01	0.09±0.01	0.16±0.02	0.20±0.02
		0.45	0.50	0.03±0.01	0.06±0.01	0.10±0.02	0.12±0.02
1.75	1.95	0.10	0.15	0.60±0.09	0.88±0.10	0.99±0.11	1.01±0.13
		0.15	0.20	0.56±0.05	0.77±0.05	1.00±0.05	1.13±0.06
		0.20	0.25	0.28±0.03	0.48±0.03	0.62±0.05	0.73±0.04
		0.25	0.30	0.15±0.03	0.26±0.03	0.34±0.03	0.40±0.03
		0.30	0.35	0.07±0.01	0.15±0.02	0.22±0.02	0.24±0.02
		0.35	0.40	0.03±0.01	0.08±0.01	0.14±0.02	0.15±0.02
		0.40	0.45	0.01±0.01	0.05±0.01	0.08±0.01	0.10±0.01
		0.45	0.50		0.02±0.01	0.05±0.01	0.06±0.01
1.95	2.15	0.10	0.15	0.51±0.07	0.63±0.07	0.75±0.07	0.73±0.08
		0.15	0.20	0.45±0.04	0.65±0.04	0.72±0.04	0.90±0.04
		0.20	0.25	0.22±0.03	0.36±0.03	0.43±0.03	0.52±0.04
		0.25	0.30	0.11±0.02	0.17±0.02	0.24±0.02	0.24±0.03
		0.30	0.35	0.05±0.01	0.10±0.01	0.14±0.01	0.17±0.01
		0.35	0.40	0.02±0.01	0.05±0.01	0.09±0.01	0.11±0.01
		0.40	0.45	0.01±0.01	0.03±0.01	0.05±0.01	0.06±0.01
		0.45	0.50		0.02±0.01	0.02±0.01	0.04±0.01

TABLE XII: HARP results for the double-differential  $\pi^-$  production cross-section in the laboratory system,  $d^2\sigma^{\pi^-}/(dpd\theta)$  for p–Sn interactions. Each row refers to a different ( $p_{\min} \leq p < p_{\max}, \theta_{\min} \leq \theta < \theta_{\max}$ ) bin, where  $p$  and  $\theta$  are the pion momentum and polar angle, respectively. The central value as well as the square-root of the diagonal elements of the covariance matrix are given.

$\theta_{\min}$ (rad)	$\theta_{\max}$ (rad)	$p_{\min}$ (GeV/c)	$p_{\max}$ (GeV/c)	$d^2\sigma^{\pi^-}/(dpd\theta)$				
				$\text{barn}/(\text{rad GeV}/c)$				
				3 GeV/c	5 GeV/c	8 GeV/c	12 GeV/c	
0.35	0.55	0.15	0.20	0.33±0.12	0.74±0.13	1.30±0.19	1.62±0.24	
		0.20	0.25	0.39±0.08	0.74±0.09	1.41±0.11	1.75±0.16	
		0.25	0.30	0.35±0.06	0.76±0.07	1.36±0.09	1.88±0.12	
		0.30	0.35	0.36±0.04	0.78±0.05	1.35±0.07	1.78±0.08	
		0.35	0.40	0.25±0.03	0.66±0.04	1.28±0.06	1.65±0.06	
		0.40	0.45	0.34±0.04	0.61±0.03	1.16±0.05	1.48±0.05	
		0.45	0.50	0.29±0.03	0.56±0.03	1.07±0.04	1.42±0.06	
		0.50	0.60	0.23±0.02	0.50±0.03	0.96±0.05	1.34±0.06	
		0.60	0.70	0.19±0.03	0.46±0.04	0.86±0.06	1.31±0.09	
		0.70	0.80	0.13±0.03	0.36±0.05	0.68±0.08	1.16±0.12	
0.55	0.75	0.10	0.15	0.30±0.12	0.58±0.15	1.07±0.22	1.21±0.31	
		0.15	0.20	0.38±0.07	0.97±0.10	1.54±0.10	1.67±0.14	
		0.20	0.25	0.43±0.06	0.92±0.06	1.35±0.08	1.76±0.13	
		0.25	0.30	0.39±0.04	0.78±0.05	1.32±0.08	1.66±0.07	
		0.30	0.35	0.32±0.03	0.67±0.04	1.28±0.06	1.53±0.06	
		0.35	0.40	0.29±0.03	0.63±0.03	1.09±0.05	1.38±0.06	
		0.40	0.45	0.27±0.03	0.59±0.03	1.00±0.04	1.27±0.05	
		0.45	0.50	0.23±0.02	0.52±0.03	0.94±0.04	1.15±0.04	
		0.50	0.60	0.17±0.02	0.44±0.03	0.77±0.04	1.05±0.05	
		0.60	0.70	0.13±0.02	0.37±0.03	0.61±0.05	0.88±0.07	
0.75	0.95	0.10	0.15	0.30±0.08	0.70±0.11	1.07±0.14	1.18±0.18	
		0.15	0.20	0.51±0.07	1.00±0.07	1.55±0.09	1.83±0.12	
		0.20	0.25	0.45±0.05	0.79±0.05	1.36±0.07	1.66±0.08	
		0.25	0.30	0.37±0.04	0.78±0.05	1.20±0.06	1.51±0.07	
		0.30	0.35	0.31±0.03	0.70±0.04	1.05±0.05	1.32±0.05	
		0.35	0.40	0.28±0.03	0.56±0.03	0.88±0.04	1.15±0.04	
		0.40	0.45	0.20±0.03	0.47±0.02	0.77±0.03	0.97±0.04	
		0.45	0.50	0.16±0.02	0.39±0.02	0.63±0.03	0.88±0.04	
		0.50	0.60	0.13±0.02	0.32±0.02	0.54±0.03	0.73±0.04	
		0.60	0.70	0.09±0.01	0.24±0.03	0.39±0.04	0.56±0.05	
0.95	1.15	0.10	0.15	0.43±0.07	0.69±0.09	1.01±0.12	1.16±0.14	
		0.15	0.20	0.50±0.05	0.83±0.05	1.30±0.07	1.63±0.09	
		0.20	0.25	0.37±0.04	0.75±0.05	1.20±0.07	1.39±0.08	
		0.25	0.30	0.32±0.03	0.70±0.04	1.07±0.05	1.23±0.05	
		0.30	0.35	0.28±0.03	0.55±0.03	0.80±0.04	1.04±0.05	
		0.35	0.40	0.21±0.02	0.42±0.03	0.66±0.03	0.84±0.04	
		0.40	0.45	0.13±0.02	0.31±0.02	0.53±0.03	0.69±0.03	
		0.45	0.50	0.08±0.01	0.27±0.02	0.44±0.02	0.57±0.03	
		0.50	0.60	0.05±0.01	0.21±0.02	0.32±0.02	0.44±0.03	

$\theta_{\min}$ (rad)	$\theta_{\max}$ (rad)	$p_{\min}$ (GeV/c)	$p_{\max}$ (GeV/c)	$d^2\sigma^{\pi^-}/(dpd\theta)$				
				barn/(rad GeV/c)				
				<b>3 GeV/c</b>	<b>5 GeV/c</b>	<b>8 GeV/c</b>	<b>12 GeV/c</b>	
1.15	1.35	0.10	0.15	0.48±0.08	0.68±0.09	1.00±0.12	1.21±0.19	
		0.15	0.20	0.37±0.04	0.89±0.06	1.26±0.07	1.59±0.10	
		0.20	0.25	0.37±0.04	0.76±0.04	1.00±0.05	1.23±0.06	
		0.25	0.30	0.29±0.03	0.56±0.04	0.83±0.05	0.97±0.05	
		0.30	0.35	0.19±0.02	0.39±0.03	0.62±0.04	0.76±0.04	
		0.35	0.40	0.16±0.02	0.31±0.02	0.48±0.03	0.65±0.03	
		0.40	0.45	0.10±0.02	0.24±0.02	0.38±0.02	0.49±0.03	
		0.45	0.50	0.07±0.01	0.18±0.02	0.28±0.02	0.36±0.02	
1.35	1.55	0.10	0.15	0.45±0.08	0.81±0.13	1.06±0.17	1.45±0.26	
		0.15	0.20	0.50±0.05	0.98±0.07	1.33±0.09	1.64±0.11	
		0.20	0.25	0.38±0.04	0.68±0.05	0.93±0.06	1.20±0.07	
		0.25	0.30	0.24±0.03	0.48±0.04	0.76±0.05	0.86±0.06	
		0.30	0.35	0.18±0.02	0.32±0.02	0.52±0.05	0.60±0.04	
		0.35	0.40	0.12±0.02	0.24±0.02	0.34±0.02	0.43±0.03	
		0.40	0.45	0.07±0.01	0.15±0.01	0.26±0.02	0.32±0.02	
		0.45	0.50	0.04±0.01	0.10±0.01	0.19±0.02	0.24±0.02	
1.55	1.75	0.10	0.15	0.46±0.08	0.74±0.11	0.91±0.14	1.37±0.23	
		0.15	0.20	0.55±0.05	0.87±0.06	1.28±0.09	1.43±0.10	
		0.20	0.25	0.33±0.03	0.56±0.04	0.77±0.06	0.95±0.06	
		0.25	0.30	0.17±0.03	0.35±0.03	0.53±0.04	0.64±0.05	
		0.30	0.35	0.10±0.01	0.25±0.02	0.37±0.03	0.47±0.04	
		0.35	0.40	0.06±0.01	0.16±0.02	0.25±0.02	0.31±0.02	
		0.40	0.45	0.04±0.01	0.10±0.01	0.17±0.01	0.22±0.02	
		0.45	0.50	0.02±0.01	0.08±0.01	0.12±0.01	0.16±0.01	
1.75	1.95	0.10	0.15	0.41±0.05	0.60±0.07	0.81±0.09	0.94±0.12	
		0.15	0.20	0.35±0.03	0.58±0.04	0.89±0.04	1.01±0.05	
		0.20	0.25	0.22±0.03	0.40±0.03	0.55±0.03	0.62±0.04	
		0.25	0.30	0.14±0.02	0.24±0.02	0.36±0.03	0.40±0.03	
		0.30	0.35	0.09±0.02	0.16±0.01	0.26±0.02	0.27±0.02	
		0.35	0.40	0.06±0.01	0.09±0.01	0.18±0.01	0.18±0.01	
		0.40	0.45	0.03±0.01	0.07±0.01	0.12±0.01	0.15±0.01	
		0.45	0.50	0.02±0.01	0.05±0.01	0.08±0.01	0.10±0.01	
1.95	2.15	0.10	0.15	0.33±0.04	0.58±0.05	0.72±0.05	0.80±0.07	
		0.15	0.20	0.32±0.04	0.50±0.04	0.67±0.04	0.73±0.04	
		0.20	0.25	0.16±0.02	0.25±0.02	0.39±0.02	0.46±0.02	
		0.25	0.30	0.08±0.02	0.15±0.02	0.26±0.02	0.31±0.02	
		0.30	0.35	0.04±0.01	0.11±0.01	0.15±0.02	0.19±0.02	
		0.35	0.40	0.02±0.01	0.07±0.01	0.10±0.01	0.11±0.01	
		0.40	0.45	0.01±0.01	0.04±0.01	0.08±0.01	0.08±0.01	
		0.45	0.50	0.03±0.01	0.07±0.01	0.05±0.01		

TABLE XIII: HARP results for the double-differential  $\pi^+$  production cross-section in the laboratory system,  $d^2\sigma^{\pi^+}/(dpd\theta)$  for p-Ta interactions. Each row refers to a different ( $p_{\min} \leq p < p_{\max}, \theta_{\min} \leq \theta < \theta_{\max}$ ) bin, where  $p$  and  $\theta$  are the pion momentum and polar angle, respectively. The central value as well as the square-root of the diagonal elements of the covariance matrix are given.

$\theta_{\min}$ (rad)	$\theta_{\max}$ (rad)	$p_{\min}$ (GeV/c)	$p_{\max}$ (GeV/c)	$d^2\sigma^{\pi^+}/(dpd\theta)$				
				$\text{barn}/(\text{rad GeV}/c)$				
				3 GeV/c	5 GeV/c	8 GeV/c	12 GeV/c	
0.35	0.55	0.15	0.20	0.14±0.09	0.60±0.20	1.16±0.30	1.42±0.41	
		0.20	0.25	0.39±0.10	0.93±0.15	1.54±0.19	2.06±0.23	
		0.25	0.30	0.54±0.06	1.16±0.11	2.00±0.14	2.39±0.18	
		0.30	0.35	0.55±0.08	1.27±0.09	2.13±0.16	2.50±0.13	
		0.35	0.40	0.69±0.06	1.24±0.08	2.12±0.10	2.72±0.16	
		0.40	0.45	0.68±0.06	1.23±0.07	2.03±0.08	2.60±0.10	
		0.45	0.50	0.66±0.05	1.22±0.06	2.01±0.13	2.56±0.09	
		0.50	0.60	0.55±0.05	1.15±0.06	2.02±0.11	2.42±0.13	
		0.60	0.70	0.30±0.06	0.91±0.09	1.78±0.18	2.20±0.21	
		0.70	0.80	0.18±0.04	0.57±0.10	1.22±0.20	1.79±0.24	
0.55	0.75	0.10	0.15	0.29±0.13	0.73±0.26	0.98±0.37	1.00±0.41	
		0.15	0.20	0.51±0.11	0.99±0.16	1.79±0.19	1.91±0.26	
		0.20	0.25	0.71±0.08	1.34±0.13	2.10±0.15	2.84±0.21	
		0.25	0.30	0.67±0.07	1.35±0.09	2.13±0.13	2.72±0.13	
		0.30	0.35	0.61±0.06	1.30±0.08	2.17±0.09	2.74±0.13	
		0.35	0.40	0.67±0.05	1.19±0.06	1.91±0.11	2.64±0.11	
		0.40	0.45	0.54±0.05	1.06±0.05	1.87±0.09	2.46±0.09	
		0.45	0.50	0.47±0.04	0.96±0.05	1.65±0.09	2.19±0.09	
		0.50	0.60	0.28±0.04	0.78±0.06	1.41±0.10	1.82±0.12	
		0.60	0.70	0.16±0.03	0.48±0.07	0.95±0.13	1.24±0.14	
0.75	0.95	0.10	0.15	0.53±0.13	1.05±0.22	1.13±0.30	1.19±0.32	
		0.15	0.20	0.75±0.08	1.42±0.11	2.06±0.12	2.31±0.19	
		0.20	0.25	0.77±0.06	1.49±0.11	2.15±0.14	2.57±0.14	
		0.25	0.30	0.72±0.06	1.31±0.08	1.92±0.09	2.39±0.12	
		0.30	0.35	0.61±0.05	1.05±0.06	1.78±0.08	2.16±0.09	
		0.35	0.40	0.46±0.04	0.96±0.05	1.53±0.08	1.78±0.08	
		0.40	0.45	0.40±0.04	0.82±0.05	1.33±0.06	1.66±0.07	
		0.45	0.50	0.31±0.03	0.63±0.04	1.14±0.06	1.45±0.07	
		0.50	0.60	0.19±0.03	0.43±0.04	0.82±0.07	1.06±0.08	
		0.60	0.70	0.06±0.02	0.25±0.04	0.48±0.07	0.63±0.09	
0.95	1.15	0.10	0.15	0.69±0.14	1.08±0.18	1.40±0.27	1.65±0.33	
		0.15	0.20	0.81±0.06	1.42±0.10	2.06±0.13	2.53±0.18	
		0.20	0.25	0.75±0.06	1.32±0.07	1.98±0.11	2.57±0.11	
		0.25	0.30	0.61±0.05	1.06±0.06	1.67±0.08	2.03±0.09	
		0.30	0.35	0.40±0.04	0.79±0.05	1.30±0.08	1.66±0.08	
		0.35	0.40	0.34±0.03	0.63±0.03	1.02±0.07	1.27±0.07	
		0.40	0.45	0.27±0.03	0.49±0.03	0.82±0.05	1.04±0.05	
		0.45	0.50	0.17±0.03	0.34±0.03	0.65±0.04	0.81±0.06	
		0.50	0.60	0.09±0.02	0.21±0.02	0.38±0.04	0.50±0.05	

$\theta_{\min}$ (rad)	$\theta_{\max}$ (rad)	$p_{\min}$ (GeV/c)	$p_{\max}$ (GeV/c)	$d^2\sigma^{\pi^+}/(dpd\theta)$			
				barn/(rad GeV/c)			
				<b>3 GeV/c</b>	<b>5 GeV/c</b>	<b>8 GeV/c</b>	<b>12 GeV/c</b>
1.15	1.35	0.10	0.15	0.71±0.15	1.08±0.20	1.64±0.29	2.02±0.39
		0.15	0.20	0.87±0.07	1.35±0.10	2.03±0.17	2.51±0.20
		0.20	0.25	0.68±0.05	1.17±0.07	1.84±0.10	2.19±0.13
		0.25	0.30	0.43±0.04	0.84±0.05	1.29±0.08	1.57±0.10
		0.30	0.35	0.31±0.04	0.65±0.04	0.90±0.06	1.18±0.07
		0.35	0.40	0.22±0.02	0.48±0.03	0.66±0.04	0.94±0.05
		0.40	0.45	0.14±0.02	0.33±0.03	0.49±0.03	0.70±0.04
		0.45	0.50	0.08±0.01	0.23±0.03	0.36±0.03	0.47±0.04
1.35	1.55	0.10	0.15	0.62±0.15	1.15±0.24	1.61±0.35	2.13±0.41
		0.15	0.20	0.86±0.10	1.41±0.13	1.91±0.21	2.47±0.24
		0.20	0.25	0.72±0.06	1.11±0.09	1.64±0.11	1.98±0.13
		0.25	0.30	0.41±0.04	0.67±0.05	1.06±0.07	1.31±0.09
		0.30	0.35	0.26±0.02	0.43±0.03	0.75±0.05	0.83±0.07
		0.35	0.40	0.16±0.02	0.28±0.03	0.50±0.04	0.58±0.04
		0.40	0.45	0.09±0.01	0.18±0.02	0.32±0.03	0.38±0.03
		0.45	0.50	0.05±0.01	0.11±0.01	0.22±0.02	0.25±0.03
1.55	1.75	0.10	0.15	0.68±0.15	1.05±0.22	1.57±0.37	1.85±0.44
		0.15	0.20	0.78±0.08	1.31±0.12	1.69±0.17	2.12±0.21
		0.20	0.25	0.62±0.06	1.00±0.07	1.36±0.09	1.68±0.11
		0.25	0.30	0.33±0.04	0.57±0.05	0.74±0.06	0.97±0.08
		0.30	0.35	0.18±0.02	0.35±0.03	0.48±0.03	0.58±0.06
		0.35	0.40	0.09±0.02	0.19±0.02	0.32±0.03	0.35±0.03
		0.40	0.45	0.05±0.01	0.10±0.01	0.21±0.02	0.22±0.02
		0.45	0.50	0.03±0.01	0.06±0.01	0.14±0.02	0.14±0.02
1.75	1.95	0.10	0.15	0.78±0.12	1.03±0.19	1.28±0.20	1.43±0.25
		0.15	0.20	0.65±0.05	1.09±0.06	1.39±0.08	1.66±0.10
		0.20	0.25	0.44±0.04	0.71±0.05	0.97±0.06	1.08±0.07
		0.25	0.30	0.20±0.03	0.38±0.04	0.54±0.05	0.66±0.06
		0.30	0.35	0.09±0.01	0.21±0.02	0.32±0.03	0.33±0.03
		0.35	0.40	0.06±0.01	0.12±0.02	0.19±0.02	0.22±0.02
		0.40	0.45	0.06±0.03	0.08±0.01	0.12±0.01	0.16±0.02
		0.45	0.50	0.01±0.01	0.04±0.01	0.07±0.01	0.09±0.02
1.95	2.15	0.10	0.15	0.72±0.12	0.92±0.14	1.04±0.16	1.33±0.21
		0.15	0.20	0.55±0.05	0.80±0.05	1.09±0.05	1.25±0.06
		0.20	0.25	0.28±0.03	0.51±0.03	0.64±0.05	0.76±0.04
		0.25	0.30	0.13±0.02	0.26±0.03	0.34±0.04	0.44±0.05
		0.30	0.35	0.06±0.01	0.13±0.02	0.19±0.02	0.18±0.02
		0.35	0.40	0.03±0.01	0.07±0.01	0.11±0.02	0.11±0.01
		0.40	0.45	0.02±0.01	0.05±0.01	0.05±0.01	0.07±0.01
		0.45	0.50	0.01±0.01	0.02±0.01	0.03±0.01	0.04±0.01

TABLE XIV: HARP results for the double-differential  $\pi^-$  production cross-section in the laboratory system,  $d^2\sigma^{\pi^-}/(dpd\theta)$  for p-Ta interactions. Each row refers to a different ( $p_{\min} \leq p < p_{\max}, \theta_{\min} \leq \theta < \theta_{\max}$ ) bin, where  $p$  and  $\theta$  are the pion momentum and polar angle, respectively. The central value as well as the square-root of the diagonal elements of the covariance matrix are given.

$\theta_{\min}$ (rad)	$\theta_{\max}$ (rad)	$p_{\min}$ (GeV/c)	$p_{\max}$ (GeV/c)	$d^2\sigma^{\pi^-}/(dpd\theta)$				
				barn/(rad GeV/c)				
				3 GeV/c	5 GeV/c	8 GeV/c	12 GeV/c	
0.35	0.55	0.15	0.20	0.33±0.12	0.80±0.23	1.31±0.31	1.70±0.41	
		0.20	0.25	0.34±0.08	0.89±0.13	1.59±0.16	2.02±0.23	
		0.25	0.30	0.41±0.07	1.10±0.12	1.77±0.14	2.26±0.17	
		0.30	0.35	0.47±0.05	0.94±0.07	1.88±0.11	2.15±0.10	
		0.35	0.40	0.47±0.05	0.88±0.06	1.67±0.08	2.05±0.10	
		0.40	0.45	0.38±0.04	0.77±0.04	1.49±0.07	1.83±0.07	
		0.45	0.50	0.30±0.03	0.72±0.05	1.42±0.06	1.64±0.08	
		0.50	0.60	0.25±0.03	0.74±0.04	1.28±0.07	1.57±0.09	
		0.60	0.70	0.22±0.03	0.64±0.05	1.15±0.08	1.47±0.13	
		0.70	0.80	0.18±0.03	0.46±0.07	0.92±0.11	1.27±0.15	
0.55	0.75	0.10	0.15	0.37±0.16	0.82±0.27	1.18±0.39	1.37±0.45	
		0.15	0.20	0.54±0.09	1.27±0.16	1.74±0.18	2.21±0.25	
		0.20	0.25	0.46±0.05	1.18±0.09	1.99±0.14	2.48±0.16	
		0.25	0.30	0.52±0.06	1.07±0.08	1.91±0.10	2.33±0.09	
		0.30	0.35	0.37±0.04	0.97±0.06	1.57±0.08	2.15±0.09	
		0.35	0.40	0.30±0.03	0.89±0.05	1.43±0.07	1.89±0.07	
		0.40	0.45	0.35±0.05	0.75±0.04	1.33±0.06	1.69±0.06	
		0.45	0.50	0.38±0.03	0.65±0.03	1.18±0.05	1.50±0.06	
		0.50	0.60	0.25±0.03	0.56±0.03	1.05±0.05	1.31±0.06	
		0.60	0.70	0.16±0.02	0.44±0.04	0.84±0.08	1.12±0.10	
0.75	0.95	0.10	0.15	0.54±0.13	0.99±0.20	1.42±0.32	1.81±0.39	
		0.15	0.20	0.71±0.07	1.29±0.10	2.04±0.13	2.32±0.16	
		0.20	0.25	0.65±0.06	1.12±0.08	1.87±0.10	2.46±0.16	
		0.25	0.30	0.55±0.05	0.99±0.05	1.68±0.08	2.22±0.10	
		0.30	0.35	0.38±0.04	0.82±0.05	1.33±0.06	1.90±0.09	
		0.35	0.40	0.33±0.03	0.72±0.04	1.22±0.06	1.57±0.07	
		0.40	0.45	0.27±0.03	0.64±0.03	1.01±0.05	1.33±0.05	
		0.45	0.50	0.19±0.02	0.57±0.03	0.88±0.04	1.12±0.05	
		0.50	0.60	0.14±0.02	0.46±0.03	0.71±0.04	0.92±0.05	
		0.60	0.70	0.09±0.01	0.30±0.04	0.56±0.05	0.69±0.07	
0.95	1.15	0.10	0.15	0.74±0.12	1.30±0.21	1.86±0.29	2.12±0.36	
		0.15	0.20	0.65±0.06	1.39±0.08	2.13±0.13	2.32±0.13	
		0.20	0.25	0.55±0.05	1.02±0.07	1.69±0.09	2.11±0.12	
		0.25	0.30	0.48±0.04	0.87±0.05	1.42±0.08	1.80±0.08	
		0.30	0.35	0.37±0.03	0.69±0.04	1.10±0.06	1.45±0.07	
		0.35	0.40	0.29±0.03	0.54±0.03	0.89±0.04	1.13±0.06	
		0.40	0.45	0.22±0.02	0.43±0.02	0.75±0.03	0.91±0.05	
		0.45	0.50	0.14±0.02	0.35±0.02	0.60±0.03	0.72±0.04	
		0.50	0.60	0.08±0.01	0.26±0.02	0.46±0.03	0.53±0.04	

$\theta_{\min}$ (rad)	$\theta_{\max}$ (rad)	$p_{\min}$ (GeV/c)	$p_{\max}$ (GeV/c)	$d^2\sigma^{\pi^-}/(dpd\theta)$			
				barn/(rad GeV/c)			
				<b>3 GeV/c</b>	<b>5 GeV/c</b>	<b>8 GeV/c</b>	<b>12 GeV/c</b>
1.15	1.35	0.10	0.15	0.86±0.15	1.36±0.23	2.11±0.36	2.66±0.46
		0.15	0.20	0.67±0.06	1.28±0.09	2.07±0.14	2.37±0.17
		0.20	0.25	0.50±0.04	0.96±0.06	1.58±0.09	1.84±0.11
		0.25	0.30	0.36±0.04	0.73±0.05	1.20±0.08	1.44±0.08
		0.30	0.35	0.22±0.02	0.56±0.04	0.85±0.05	1.00±0.06
		0.35	0.40	0.18±0.02	0.43±0.03	0.67±0.04	0.80±0.04
		0.40	0.45	0.12±0.02	0.30±0.02	0.51±0.03	0.68±0.04
		0.45	0.50	0.07±0.01	0.22±0.02	0.41±0.03	0.53±0.04
1.35	1.55	0.10	0.15	0.73±0.15	1.31±0.25	2.37±0.47	3.06±0.66
		0.15	0.20	0.61±0.07	1.14±0.12	1.87±0.18	2.34±0.22
		0.20	0.25	0.42±0.04	0.82±0.07	1.32±0.10	1.74±0.12
		0.25	0.30	0.29±0.03	0.62±0.05	0.90±0.07	1.21±0.08
		0.30	0.35	0.19±0.02	0.42±0.04	0.60±0.04	0.85±0.07
		0.35	0.40	0.12±0.02	0.29±0.02	0.45±0.03	0.61±0.04
		0.40	0.45	0.08±0.01	0.21±0.02	0.34±0.02	0.46±0.03
		0.45	0.50	0.05±0.01	0.14±0.01	0.27±0.02	0.34±0.03
1.55	1.75	0.10	0.15	0.80±0.16	1.34±0.27	1.84±0.38	2.54±0.53
		0.15	0.20	0.56±0.07	1.06±0.10	1.62±0.16	2.10±0.21
		0.20	0.25	0.35±0.04	0.73±0.05	1.11±0.08	1.44±0.10
		0.25	0.30	0.19±0.02	0.49±0.04	0.67±0.05	0.86±0.07
		0.30	0.35	0.13±0.02	0.31±0.03	0.43±0.04	0.61±0.05
		0.35	0.40	0.09±0.01	0.22±0.02	0.30±0.02	0.41±0.03
		0.40	0.45	0.05±0.01	0.14±0.01	0.21±0.01	0.30±0.02
		0.45	0.50	0.04±0.01	0.10±0.01	0.15±0.01	0.21±0.02
1.75	1.95	0.10	0.15	0.79±0.11	1.28±0.20	1.54±0.23	2.07±0.31
		0.15	0.20	0.48±0.05	0.95±0.06	1.27±0.08	1.58±0.11
		0.20	0.25	0.25±0.03	0.53±0.04	0.81±0.05	0.99±0.07
		0.25	0.30	0.14±0.02	0.32±0.03	0.51±0.04	0.58±0.04
		0.30	0.35	0.11±0.02	0.22±0.02	0.28±0.03	0.41±0.03
		0.35	0.40	0.08±0.01	0.14±0.02	0.21±0.01	0.26±0.02
		0.40	0.45	0.05±0.01	0.09±0.01	0.18±0.01	0.20±0.02
		0.45	0.50	0.03±0.01	0.06±0.01	0.12±0.01	0.12±0.01
1.95	2.15	0.10	0.15	0.59±0.11	1.12±0.16	1.43±0.17	1.85±0.29
		0.15	0.20	0.50±0.05	0.80±0.06	0.99±0.05	1.24±0.07
		0.20	0.25	0.21±0.03	0.39±0.03	0.57±0.03	0.73±0.05
		0.25	0.30	0.09±0.02	0.23±0.02	0.36±0.03	0.42±0.04
		0.30	0.35	0.04±0.01	0.14±0.02	0.19±0.02	0.25±0.02
		0.35	0.40	0.03±0.01	0.09±0.01	0.15±0.01	0.15±0.02
		0.40	0.45	0.02±0.01	0.05±0.01	0.11±0.01	0.11±0.01
		0.45	0.50	0.02±0.01	0.03±0.01	0.07±0.01	0.09±0.01

TABLE XV: HARP results for the double-differential  $\pi^+$  production cross-section in the laboratory system,  $d^2\sigma^{\pi^+}/(dpd\theta)$  for p–Pb interactions. Each row refers to a different ( $p_{\min} \leq p < p_{\max}, \theta_{\min} \leq \theta < \theta_{\max}$ ) bin, where  $p$  and  $\theta$  are the pion momentum and polar angle, respectively. The central value as well as the square-root of the diagonal elements of the covariance matrix are given.

$\theta_{\min}$ (rad)	$\theta_{\max}$ (rad)	$p_{\min}$ (GeV/c)	$p_{\max}$ (GeV/c)	$d^2\sigma^{\pi^+}/(dpd\theta)$				
				barn/(rad GeV/c)				
				3 GeV/c	5 GeV/c	8 GeV/c	12 GeV/c	
0.35	0.55	0.15	0.20	0.31±0.11	0.85±0.22	1.15±0.32	1.38±0.41	
		0.20	0.25	0.29±0.08	0.87±0.15	1.75±0.20	2.04±0.26	
		0.25	0.30	0.49±0.10	1.18±0.13	2.13±0.15	2.66±0.25	
		0.30	0.35	0.76±0.08	1.27±0.11	2.19±0.13	2.61±0.17	
		0.35	0.40	0.67±0.07	1.34±0.09	2.21±0.10	2.84±0.18	
		0.40	0.45	0.76±0.07	1.38±0.10	2.20±0.09	2.53±0.13	
		0.45	0.50	0.65±0.06	1.42±0.08	1.99±0.08	2.40±0.12	
		0.50	0.60	0.48±0.06	1.27±0.08	1.96±0.09	2.53±0.16	
		0.60	0.70	0.26±0.04	0.99±0.10	1.71±0.16	2.19±0.22	
		0.70	0.80	0.18±0.03	0.67±0.12	1.12±0.18	1.76±0.23	
0.55	0.75	0.10	0.15	0.35±0.15	0.69±0.25	0.84±0.35	1.02±0.46	
		0.15	0.20	0.56±0.09	1.31±0.17	1.75±0.22	2.19±0.29	
		0.20	0.25	0.70±0.09	1.46±0.11	2.31±0.15	2.87±0.22	
		0.25	0.30	0.73±0.07	1.46±0.11	2.21±0.13	3.13±0.20	
		0.30	0.35	0.60±0.05	1.31±0.09	2.16±0.12	2.79±0.14	
		0.35	0.40	0.61±0.07	1.08±0.08	2.07±0.11	2.65±0.13	
		0.40	0.45	0.62±0.06	1.16±0.09	1.87±0.08	2.58±0.14	
		0.45	0.50	0.44±0.05	1.17±0.07	1.63±0.08	2.41±0.12	
		0.50	0.60	0.31±0.04	0.86±0.08	1.33±0.08	1.96±0.14	
		0.60	0.70	0.18±0.03	0.48±0.08	0.93±0.11	1.39±0.14	
0.75	0.95	0.10	0.15	0.52±0.13	0.83±0.21	1.20±0.31	1.29±0.39	
		0.15	0.20	0.87±0.09	1.54±0.14	2.25±0.14	2.78±0.20	
		0.20	0.25	0.86±0.08	1.40±0.10	2.25±0.14	2.91±0.19	
		0.25	0.30	0.67±0.06	1.20±0.12	1.98±0.11	2.69±0.15	
		0.30	0.35	0.59±0.05	1.14±0.07	1.83±0.08	2.39±0.13	
		0.35	0.40	0.47±0.05	0.97±0.06	1.65±0.07	2.06±0.11	
		0.40	0.45	0.37±0.04	0.79±0.05	1.38±0.06	1.92±0.10	
		0.45	0.50	0.29±0.03	0.66±0.04	1.17±0.05	1.61±0.10	
		0.50	0.60	0.19±0.03	0.44±0.05	0.81±0.07	1.10±0.10	
		0.60	0.70	0.11±0.02	0.25±0.04	0.47±0.07	0.70±0.09	
0.95	1.15	0.10	0.15	0.55±0.13	1.02±0.20	1.40±0.25	1.55±0.36	
		0.15	0.20	0.92±0.08	1.56±0.11	2.31±0.17	3.00±0.20	
		0.20	0.25	0.68±0.07	1.43±0.09	2.01±0.13	2.68±0.16	
		0.25	0.30	0.71±0.07	1.12±0.10	1.56±0.10	2.07±0.13	
		0.30	0.35	0.48±0.05	0.84±0.07	1.31±0.09	1.74±0.11	
		0.35	0.40	0.32±0.04	0.72±0.05	1.07±0.06	1.62±0.10	
		0.40	0.45	0.25±0.03	0.55±0.04	0.85±0.05	1.33±0.08	
		0.45	0.50	0.16±0.02	0.45±0.04	0.65±0.04	0.96±0.08	
		0.50	0.60	0.09±0.02	0.24±0.03	0.44±0.05	0.59±0.07	

$\theta_{\min}$ (rad)	$\theta_{\max}$ (rad)	$p_{\min}$ (GeV/c)	$p_{\max}$ (GeV/c)	$d^2\sigma^{\pi^+}/(dpd\theta)$			
				barn/(rad GeV/c)			
				<b>3 GeV/c</b>	<b>5 GeV/c</b>	<b>8 GeV/c</b>	<b>12 GeV/c</b>
1.15	1.35	0.10	0.15	0.67±0.14	1.27±0.21	1.68±0.28	1.75±0.35
		0.15	0.20	0.90±0.08	1.49±0.10	2.32±0.15	2.88±0.23
		0.20	0.25	0.64±0.06	1.17±0.08	1.96±0.10	2.53±0.15
		0.25	0.30	0.51±0.05	0.92±0.06	1.32±0.07	1.87±0.13
		0.30	0.35	0.32±0.04	0.64±0.05	0.91±0.07	1.27±0.09
		0.35	0.40	0.21±0.03	0.45±0.04	0.74±0.04	0.89±0.06
		0.40	0.45	0.15±0.02	0.32±0.03	0.55±0.04	0.65±0.05
		0.45	0.50	0.10±0.02	0.22±0.03	0.37±0.03	0.43±0.05
1.35	1.55	0.10	0.15	0.79±0.15	1.39±0.27	1.74±0.35	1.83±0.40
		0.15	0.20	0.90±0.08	1.46±0.11	2.08±0.17	2.51±0.20
		0.20	0.25	0.72±0.06	1.02±0.07	1.68±0.09	2.01±0.14
		0.25	0.30	0.36±0.05	0.66±0.05	1.01±0.06	1.53±0.11
		0.30	0.35	0.21±0.03	0.47±0.05	0.71±0.05	0.89±0.08
		0.35	0.40	0.13±0.02	0.32±0.03	0.53±0.04	0.63±0.06
		0.40	0.45	0.07±0.01	0.21±0.02	0.40±0.03	0.43±0.04
		0.45	0.50	0.05±0.01	0.14±0.02	0.23±0.03	0.27±0.03
1.55	1.75	0.10	0.15	0.80±0.17	1.21±0.23	1.62±0.32	1.93±0.42
		0.15	0.20	0.73±0.07	1.38±0.11	1.83±0.12	2.28±0.16
		0.20	0.25	0.52±0.05	0.96±0.07	1.38±0.09	1.71±0.12
		0.25	0.30	0.29±0.04	0.56±0.05	0.81±0.05	1.00±0.09
		0.30	0.35	0.17±0.02	0.38±0.04	0.54±0.04	0.65±0.06
		0.35	0.40	0.11±0.02	0.25±0.02	0.37±0.03	0.46±0.04
		0.40	0.45	0.06±0.01	0.16±0.02	0.23±0.02	0.31±0.04
		0.45	0.50	0.04±0.01	0.11±0.01	0.15±0.02	0.18±0.03
1.75	1.95	0.10	0.15	0.81±0.13	1.02±0.17	1.47±0.21	1.64±0.28
		0.15	0.20	0.67±0.06	1.23±0.08	1.60±0.08	1.97±0.12
		0.20	0.25	0.36±0.04	0.75±0.07	1.03±0.07	1.29±0.10
		0.25	0.30	0.16±0.03	0.36±0.04	0.56±0.04	0.62±0.07
		0.30	0.35	0.09±0.02	0.22±0.03	0.32±0.03	0.40±0.04
		0.35	0.40	0.07±0.02	0.14±0.02	0.20±0.02	0.21±0.03
		0.40	0.45	0.04±0.01	0.09±0.01	0.13±0.02	0.12±0.02
		0.45	0.50	0.02±0.01	0.06±0.01	0.06±0.01	0.07±0.01
1.95	2.15	0.10	0.15	0.88±0.13	0.81±0.12	1.13±0.17	1.41±0.22
		0.15	0.20	0.64±0.06	0.93±0.06	1.19±0.06	1.40±0.11
		0.20	0.25	0.36±0.05	0.56±0.05	0.74±0.06	1.04±0.09
		0.25	0.30	0.15±0.03	0.25±0.05	0.39±0.04	0.44±0.06
		0.30	0.35	0.07±0.02	0.13±0.02	0.19±0.02	0.24±0.03
		0.35	0.40	0.03±0.01	0.10±0.01	0.11±0.01	0.16±0.02
		0.40	0.45	0.02±0.01	0.06±0.01	0.06±0.01	0.09±0.02
		0.45	0.50	0.02±0.01	0.03±0.01	0.04±0.01	0.06±0.02

TABLE XVI: HARP results for the double-differential  $\pi^-$  production cross-section in the laboratory system,  $d^2\sigma^{\pi^-}/(dpd\theta)$  for p–Pb interactions. Each row refers to a different ( $p_{\min} \leq p < p_{\max}, \theta_{\min} \leq \theta < \theta_{\max}$ ) bin, where  $p$  and  $\theta$  are the pion momentum and polar angle, respectively. The central value as well as the square-root of the diagonal elements of the covariance matrix are given.

$\theta_{\min}$ (rad)	$\theta_{\max}$ (rad)	$p_{\min}$ (GeV/c)	$p_{\max}$ (GeV/c)	$d^2\sigma^{\pi^-}/(dpd\theta)$				
				$\text{barn}/(\text{rad GeV}/c)$				
				<b>3 GeV/c</b>	<b>5 GeV/c</b>	<b>8 GeV/c</b>	<b>12 GeV/c</b>	
0.35	0.55	0.15	0.20	0.20±0.10	0.72±0.24	1.47±0.32	1.90±0.46	
		0.20	0.25	0.33±0.09	0.78±0.16	1.85±0.21	2.36±0.26	
		0.25	0.30	0.37±0.06	0.94±0.10	2.02±0.12	2.67±0.23	
		0.30	0.35	0.34±0.05	1.01±0.11	1.87±0.10	2.40±0.14	
		0.35	0.40	0.39±0.05	1.07±0.07	1.67±0.08	2.04±0.12	
		0.40	0.45	0.34±0.04	0.80±0.06	1.58±0.07	1.74±0.09	
		0.45	0.50	0.35±0.04	0.72±0.05	1.42±0.06	1.66±0.12	
		0.50	0.60	0.30±0.04	0.75±0.05	1.34±0.06	1.58±0.11	
		0.60	0.70	0.18±0.03	0.67±0.07	1.22±0.09	1.45±0.13	
		0.70	0.80	0.15±0.03	0.46±0.08	1.03±0.11	1.51±0.17	
0.55	0.75	0.10	0.15	0.43±0.15	0.93±0.32	1.26±0.41	1.72±0.54	
		0.15	0.20	0.39±0.09	1.37±0.16	1.91±0.20	2.38±0.30	
		0.20	0.25	0.49±0.08	1.19±0.10	2.14±0.13	2.36±0.15	
		0.25	0.30	0.53±0.06	1.20±0.08	2.06±0.11	2.55±0.21	
		0.30	0.35	0.44±0.05	1.00±0.08	1.87±0.10	2.26±0.11	
		0.35	0.40	0.42±0.05	1.02±0.07	1.52±0.08	2.01±0.10	
		0.40	0.45	0.32±0.04	0.84±0.06	1.33±0.06	1.81±0.09	
		0.45	0.50	0.30±0.03	0.68±0.05	1.25±0.06	1.57±0.08	
		0.50	0.60	0.25±0.03	0.58±0.04	1.10±0.05	1.42±0.08	
		0.60	0.70	0.16±0.03	0.47±0.05	0.88±0.07	1.17±0.10	
0.75	0.95	0.10	0.15	0.64±0.14	1.19±0.23	1.77±0.36	1.78±0.40	
		0.15	0.20	0.62±0.07	1.45±0.10	2.24±0.13	2.83±0.24	
		0.20	0.25	0.55±0.07	1.15±0.08	2.07±0.10	2.69±0.15	
		0.25	0.30	0.47±0.05	1.11±0.09	1.79±0.09	2.20±0.15	
		0.30	0.35	0.35±0.04	0.98±0.07	1.52±0.07	2.14±0.11	
		0.35	0.40	0.34±0.04	0.76±0.05	1.21±0.06	1.74±0.09	
		0.40	0.45	0.23±0.03	0.59±0.05	1.08±0.05	1.48±0.08	
		0.45	0.50	0.19±0.02	0.47±0.03	0.93±0.04	1.27±0.07	
		0.50	0.60	0.16±0.02	0.40±0.03	0.76±0.04	0.99±0.07	
		0.60	0.70	0.11±0.02	0.32±0.03	0.59±0.06	0.70±0.09	
0.95	1.15	0.10	0.15	0.62±0.12	1.40±0.22	2.14±0.32	2.43±0.39	
		0.15	0.20	0.70±0.07	1.46±0.11	2.29±0.13	3.02±0.20	
		0.20	0.25	0.56±0.06	1.09±0.08	1.85±0.10	2.66±0.16	
		0.25	0.30	0.40±0.04	0.96±0.08	1.49±0.07	2.10±0.12	
		0.30	0.35	0.30±0.03	0.83±0.06	1.15±0.06	1.73±0.10	
		0.35	0.40	0.29±0.03	0.63±0.05	0.96±0.05	1.38±0.08	
		0.40	0.45	0.28±0.03	0.47±0.04	0.78±0.04	1.06±0.07	
		0.45	0.50	0.20±0.03	0.36±0.03	0.66±0.03	0.81±0.06	
		0.50	0.60	0.10±0.02	0.25±0.02	0.50±0.03	0.60±0.04	

$\theta_{\min}$ (rad)	$\theta_{\max}$ (rad)	$p_{\min}$ (GeV/c)	$p_{\max}$ (GeV/c)	$d^2\sigma^{\pi^-}/(dpd\theta)$			
				barn/(rad GeV/c)			
				3 GeV/c	5 GeV/c	8 GeV/c	12 GeV/c
1.15	1.35	0.10	0.15	0.63±0.12	1.51±0.24	2.39±0.37	3.18±0.51
		0.15	0.20	0.68±0.07	1.47±0.09	2.20±0.15	2.97±0.21
		0.20	0.25	0.54±0.05	1.01±0.08	1.70±0.10	2.28±0.14
		0.25	0.30	0.33±0.04	0.77±0.06	1.25±0.07	1.61±0.11
		0.30	0.35	0.21±0.03	0.58±0.05	0.94±0.06	1.12±0.08
		0.35	0.40	0.15±0.02	0.42±0.03	0.70±0.04	0.89±0.05
		0.40	0.45	0.13±0.02	0.33±0.03	0.55±0.03	0.74±0.05
		0.45	0.50	0.09±0.02	0.27±0.02	0.45±0.03	0.60±0.05
1.35	1.55	0.10	0.15	0.95±0.20	1.51±0.27	2.36±0.46	3.78±0.67
		0.15	0.20	0.68±0.06	1.29±0.10	2.09±0.13	2.84±0.18
		0.20	0.25	0.44±0.05	0.89±0.07	1.50±0.09	1.89±0.13
		0.25	0.30	0.27±0.04	0.54±0.05	1.03±0.07	1.27±0.09
		0.30	0.35	0.15±0.02	0.37±0.03	0.68±0.05	0.89±0.07
		0.35	0.40	0.15±0.02	0.30±0.02	0.50±0.03	0.72±0.05
		0.40	0.45	0.09±0.02	0.25±0.02	0.37±0.03	0.57±0.05
		0.45	0.50	0.05±0.01	0.19±0.02	0.26±0.02	0.40±0.04
1.55	1.75	0.10	0.15	1.05±0.16	1.36±0.25	2.14±0.39	3.43±0.65
		0.15	0.20	0.57±0.06	1.17±0.09	1.78±0.10	2.48±0.15
		0.20	0.25	0.41±0.05	0.75±0.06	1.13±0.07	1.38±0.10
		0.25	0.30	0.28±0.04	0.44±0.04	0.81±0.06	0.93±0.07
		0.30	0.35	0.14±0.03	0.34±0.03	0.51±0.04	0.67±0.05
		0.35	0.40	0.09±0.01	0.24±0.03	0.35±0.03	0.48±0.04
		0.40	0.45	0.07±0.01	0.15±0.02	0.25±0.02	0.33±0.03
		0.45	0.50	0.05±0.01	0.10±0.01	0.19±0.01	0.23±0.03
1.75	1.95	0.10	0.15	0.85±0.13	1.19±0.19	1.78±0.25	2.61±0.45
		0.15	0.20	0.48±0.05	1.06±0.06	1.42±0.07	1.89±0.12
		0.20	0.25	0.32±0.04	0.64±0.06	0.83±0.05	1.15±0.08
		0.25	0.30	0.18±0.03	0.30±0.03	0.56±0.04	0.67±0.06
		0.30	0.35	0.09±0.02	0.23±0.02	0.33±0.03	0.39±0.05
		0.35	0.40	0.09±0.02	0.17±0.02	0.24±0.01	0.28±0.03
		0.40	0.45	0.06±0.02	0.12±0.02	0.20±0.01	0.23±0.02
		0.45	0.50	0.03±0.01	0.08±0.01	0.14±0.01	0.17±0.02
1.95	2.15	0.10	0.15	0.74±0.13	0.97±0.17	1.56±0.21	2.02±0.31
		0.15	0.20	0.44±0.05	0.74±0.05	1.16±0.05	1.37±0.09
		0.20	0.25	0.18±0.03	0.40±0.05	0.65±0.04	0.93±0.08
		0.25	0.30	0.10±0.02	0.23±0.03	0.39±0.03	0.53±0.06
		0.30	0.35	0.07±0.02	0.14±0.03	0.22±0.03	0.30±0.04
		0.35	0.40	0.03±0.01	0.08±0.01	0.14±0.01	0.23±0.03
		0.40	0.45	0.02±0.01	0.09±0.01	0.10±0.01	0.15±0.02
		0.45	0.50	0.01±0.01	0.08±0.01	0.08±0.01	0.09±0.02

- 
- [1] M.G. Catanesi *et al.*, HARP Collaboration, “Proposal to study hadron production for the neutrino factory and for the atmospheric neutrino flux”, CERN-SPSC/99-35 (1999).
- [2] G. Ambrosini *et al.*, NA56 Collaboration, Eur. Phys. J. C10 (1999), 605  
G. Ambrosini *et al.*, NA56 Collaboration, Phys. Lett. B420 (1998), 225  
G. Ambrosini *et al.*, NA56 Collaboration, Phys. Lett. B425 (1998), 208.
- [3] H.W. Atherton *et al.*, CERN 80-07, August 1980.
- [4] A. Blondel *et al.*, CERN-2004-002, ECFA/04/230;  
M. M.Alsharoa *et al.*, Phys. Rev. ST. Accel. Beams 6,081001 (2003).
- [5] G. Battistoni, Nucl. Phys. Proc. Suppl. **B100** (2001) 101.
- [6] T. Stanev, Rapporteur’s talk at the 26th Int. Cosmic Ray Conference (Salt Lake City, Utah, USA; eds. B.L. Dingus *et al.*, AIP Conf. Proceedings 516, (2000) 247).
- [7] T.K. Gaisser, Nucl. Phys. Proc. Suppl. **B87** (2000) 145.
- [8] R. Engel, T.K. Gaisser and T. Stanev, Phys. Lett. **B472** (2000) 113.
- [9] M. Honda, Nucl. Phys. **B77** (1999) 140.
- [10] M. Bonesini and A. Guglielmi, Phys. Rep. **433** (2006) 66.
- [11] M.H. Ahn *et al.*, K2K Collaboration, Phys. Rev. Lett. **90** (2003) 041801.
- [12] M. H. Ahn *et al.*, K2K Collaboration, Phys. Rev. **D74** (2006) 072003, arXiv:hep-ex/0606032.
- [13] A. A. Aguilar-Arevalo, The MiniBooNE Collaboration, “A Search for Electron Neutrino Appearance at the  $\Delta m^2 \sim 1 \text{ eV}^2$  Scale”, arXiv:0704.1500.  
E. Church *et al.*, BooNe Collaboration, “A proposal for an experiment to measure muon-neutrino  $\rightarrow$  electron-neutrino oscillations and muon-neutrino disappearance at the Fermilab Booster: BooNE”, FERMILAB-PROPOSAL-0898, (1997).
- [14] A. A. Aguilar-Arevalo *et al.*, SciBooNE Collaboration, “Bringing the SciBar detector to the Booster neutrino beam,” FERMILAB-PROPOSAL-0954, (2006), arXiv:hep-ex/0601022.
- [15] M.G. Catanesi *et al.*, HARP Collaboration, Eur. Phys. J. **C51**(2007) 787, arXiv:0706.1600.
- [16] M.G. Catanesi *et al.*, HARP Collaboration, Eur. Phys. J. **C53**(2008) 177, arXiv:0709.3464
- [17] M.G. Catanesi *et al.*, HARP Collaboration, Eur. Phys. J. **C54** (2008) 37, arXiv:0709.3458.
- [18] M. G. Catanesi *et al.*, HARP Collaboration, Nucl. Phys. **B732** (2006) 1, arXiv:hep-ex/0510039.
- [19] M. G. Catanesi *et al.*, HARP Collaboration, Astr. Physics **29**, 257 (2008), arXiv:0802.0657.
- [20] M. G. Catanesi *et al.*, HARP Collaboration, Eur. Phys. J. **C52** (2007) 29, arXiv:hep-ex/0702024.
- [21] M.G. Catanesi *et al.*, HARP Collaboration, Nucl. Instrum. Meth. **A571** (2007) 527; **A571** (2007) 564.
- [22] M. Anfreville *et al.*, Nucl. Instrum. Meth. **A481** (2002) 339.
- [23] M. Baldo-Ceolin *et al.*, Nucl. Instrum. Meth. **A532** (2004) 548;  
M. Bonesini *et al.*, IEEE Trans. Nucl. Sci. **50** (2003) 1053.
- [24] E. Radicioni, presented at NSS2004, IEEE Transaction on Nuclear Science, Vol 52, N 6 (2005) 2986.
- [25] M. Bogomilov *et al.*, Nucl. Instrum. Methods **A508** (2003) 152;  
G. Barr *et al.*, Nucl. Instrum. Methods **A533** (2004) 214;  
M. Bogomilov *et al.*, IEEE Transaction on Nuclear Science **54** (2007) 342.
- [26] L. Durieu, A. Mueller and M. Martini, PAC-2001-TPAH142 *Presented at IEEE Particle Accelerator Conference (PAC2001), Chicago, Illinois, 18-22 Jun 2001*;  
L. Durieu *et al.*, Proceedings of PAC’97, Vancouver, (1997);  
L. Durieu, O. Fernando, CERN PS/PA Note 96-38.
- [27] G. D’Agostini, Nucl. Instrum. Meth. **A362** (1995) 487.
- [28] S. Agostinelli *et al.*, GEANT4 Collaboration, Nucl. Instrum. Meth. **A506**, (2003) 250.
- [29] M. G. Catanesi *et al.*, HARP Collaboration, “Momentum scale in the HARP TPC”, 2008 JINST 3 P04007, arXiv:0709.1600.
- [30] I. Chemakin *et al.*, E910 Collaboration, Phys. Rev. **C65** (2002) 024904.
- [31] K. Long, Nucl. Phys. B (Proc. Suppl.), **154** (2006) 111; ISS/2005/01, “An international scoping study of a Neutrino Factory and super-beam facility”, [http://www.hep.ph.ic.ac.uk/iss/issnotes/ISS\\_Doc1\\_v02\\_13-7-2005.pdf](http://www.hep.ph.ic.ac.uk/iss/issnotes/ISS_Doc1_v02_13-7-2005.pdf).
- [32] R.C. Fernow and J. Gallardo, private communication; S.J. Brooks, private communication.
- [33] S.J. Brooks and K.A Walaton, Nucl. Phys. B (Proc. Suppl.), **155** (2006) 295.
- [34] D.H. Wright *et al.*, AIP Conf. Proc. 867 (2006) 479.
- [35] G. Folger, V. Ivanchenko and H.P. Wellisch, Eur. Phys. J. A21 (2004) 407.
- [36] D.H. Wright *et al.*, AIP Conf. Proc. 896 (2007) 11.
- [37] A. Heikkinen *et al.* e-print physics/0306008.
- [38] H.W. Bertini, P. Guthrie, Nucl. Phys. **A169** (1971).
- [39] G. Folger and H.P. Wellisch, e-print physics/0306007.
- [40] N.V. Mokhov, S.I. Striganov, “MARS overview”, FERMILAB-CONF-07-008-AD, 2007.
- [41] S.G. Mashnik *et al.*, LANL report LA-UR-05-7321, 2005.
- [42] H. Fesefeld, Technical report PITHA 85-02, Aachen, 1985.

- [43] We do not make a correction for the attenuation of the proton beam in the target, so that strictly speaking the cross-sections are valid for a  $\lambda_I = 5\%$  target.
- [44] The migration matrix is calculated without prior knowledge of the cross-sections, while the unfolding procedure determined the unfolding matrix from the migration matrix and the distributions found in the data.